Quantum optomechanics

Markus Aspelmeyer, Pierre Meystre, and Keith Schwab

Aided by optical cavities and superconducting circuits, researchers are coaxing ever-larger objects to wiggle, shake, and flex in ways that are distinctly quantum mechanical.

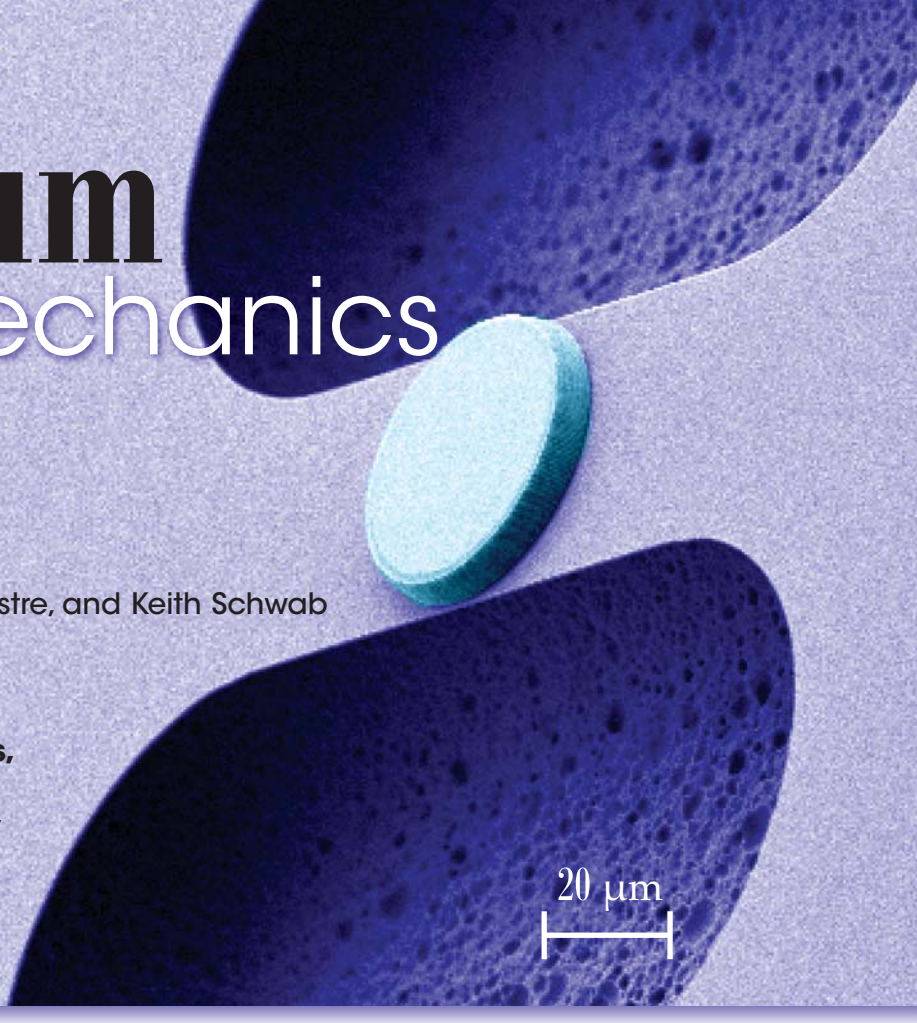

VIENNA CENTER FOR QUANTUM SCIENCE AND TECHNOLOGY AND ARKITEK STUDIOS

Give me a place to stand and with a lever I will move the whole world. —Archimedes

Over two millennia ago, scholars from antiquity had already come to understand the power of simple mechanical elements. And from that understanding they formulated an enduring, common-sense notion of the nature of reality, described thusly in Plato's *The Republic*:

> The same thing cannot ever act or be acted upon in two opposite ways, or be two opposite things, at the same time, in respect of the same part of itself, and in relation to the same object.

Today researchers at the cutting edge of physics are still exploiting simple mechanical elements as tools with which to carefully probe our world. But unlike their predecessors, they are preparing those elements deeply in the quantum regime and, in the process, challenging ancient notions of reality. Ironically, today's devices, though similar in many ways to those of antiquity, steer us to a completely different worldview—one in which an object, possibly even a macroscopic one, can indeed act in two ways at the same time.

Two key developments, born of two converging perspectives on the physical world, have enabled the advance. From the top-down perspective, nanoscience and the semiconductor industries have developed advanced materials and processing techniques, which in turn have given rise to ultrasensitive micromechanical and nanomechanical devices. Such devices can probe extremely tiny forces, often with spatial resolution at atomic scales, as exemplified by the recent measurements of the Casimir force (see the article by Steve Lamoreaux, PHYSICS TODAY, February 2007, page 40) and the mechanical detection and imaging of a single electron spin (see PHYSICS TODAY, October 2004, page 22). From the bottom-up perspective, quantum optics and atomic physics have yielded an exquisite understanding of the mechanical aspects of light–matter interaction, including how quantum mechanics limits the ultimate sensitivity of measurements and how back-action—the influence a quantum measurement necessarily exerts on the object being measured—can be harnessed to control quantum states of mechanical systems.

Quantum optomechanics combines the two perspectives: By pairing optical or microwave cavities with mechanical resonators to form a cavity optomechanical system, one acquires a means to achieve quantum control over mechanical motion or, conversely, mechanical control over optical or microwave fields. The laws of quantum physics can then be made to reveal themselves in the motion of objects ranging in size from nanometers to

Markus Aspelmeyer is a professor of physics at the University of Vienna. **Pierre Meystre** is Regents Professor of Physics and Optical Sciences at the University of Arizona in Tucson. **Keith Schwab** is a professor of applied physics at the California Institute of Technology in Pasadena.

LIGO LABORATORY

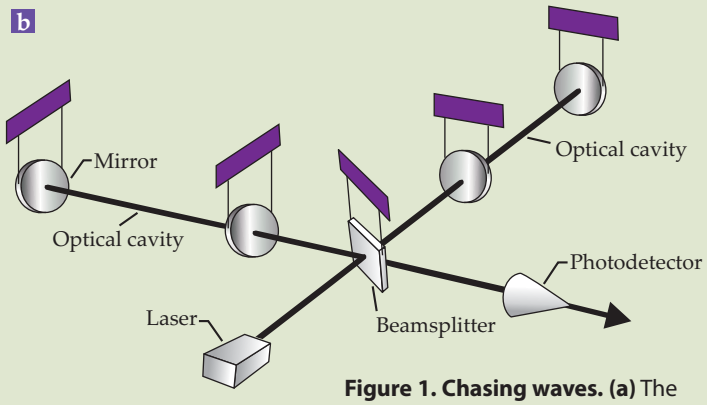

HARALD LÜCK, MAX PLANCK INSTITUTE FOR GRAVITATIONAL PHYSICS

Figure 1. Chasing waves. (a) The Laser Interferometer Gravitational-Wave Observatory in Livingston, Louisiana, and similar gravitational-wave detectors were among the first cavity optomechanical systems. **(b)** They typically consist of massive mirrors suspended to form a pair of optical cavities, each some kilometers long. The cavities make up the arms of a Michelson interferometer and together can detect changes in distance as small as 10^{-21} relative to the cavity length. **(c)** Mirrors used in the gravitational-wave detector GEO600, located near Sarstedt, Germany.

centimeters, from femtograms to kilograms. Cavity optomechanical systems hold promise as a means to both observe and control the quantum states of macroscopic objects and to measure feeble forces and fields with a sensitivity, precision, and accuracy approaching the quantum limit[1] (see the article by Keith Schwab and Michael Roukes, PHYSICS TODAY, July 2005, page 36).

Early optomechanics

Put simply, a cavity optomechanical system is an optical or microwave cavity that contains a mechanical element, a moving part that can support collective oscillation modes whose quanta of excitation are known as phonons. The system could be as simple as an optical cavity in which one of the end mirrors oscillates as if attached to a spring.

Among the first well-understood cavity optomechanical systems were the early gravitational-wave detectors developed in the late 1970s and early 1980s, with major contributions by Vladimir Braginsky, Kip Thorne, Carlton Caves, William Unruh, and others.[2] Such detectors are essentially giant interferometers, with each arm being a kilometers-long optical cavity bounded by mirrors several kilograms in mass (see figure 1). In theory, a ripple in the local curvature of spacetime due to a passing gravitational wave should alter each cavity's optical path length, modulate its resonance frequency, and, in turn, alter the optical transmission to a photodetector. The Laser Interferometer Gravitational-Wave Observatory, currently the gold standard of gravitational-wave detectors, can achieve displacement sensitivities as high as 10^{-19} m $Hz^{-1/2}$. In other words, it can detect a displacement of about 1/1000 of a proton radius based on a one-second measurement.

A related approach to detecting gravitational waves calls for using a massive, multiton cylinder as a gravitational-wave antenna. In theory, the cylinder should undergo bending oscillations in the presence of a passing gravitational wave. Provided the cylinder is integrated into a high-quality superconducting microwave cavity, that bending should detectably modulate the cavity's resonance frequency. Although the interferometer and bar-antenna approaches to gravitational-wave detection deploy very different technologies, both rely on the underlying concept that mechanical motion can be harnessed to modulate an electromagnetic resonance.

Thirty years after the first deep studies of the limits of gravitational wave detectors, it's evident to us that Braginsky, Caves, and their contemporaries had two very exciting things to say: First, gravitational-wave astronomy might be possible, and second, so might the measurement and manipulation of macroscopic objects at their quantum limits.[3] The second message has motivated an increasing number of mostly young researchers trained in areas as diverse as solid-state physics, quantum information, and computation to look for and exploit the quantum behavior of large mechanical objects in tabletop experiments.

Getting to zero

Quantum effects in any system are most pronounced when the influence of thermal fluctuations can be ignored. So, ideally, a mechanical quantum experiment would start with the mechanical element in its quantum ground state of motion, in which all thermal quanta have been removed. In practice, however, one settles for cooling the element such that for a given mechanical mode the time-averaged number of thermal phonons, the so-called occupation number N, is less than one. Put another way, the mean thermal energy $k_B T$ should be less than the quantum of mechanical energy $\hbar\omega_m$, so that $N \approx k_B T/\hbar\omega_m < 1$. Here k_B is Boltzmann's constant, $\hbar$ is the reduced Planck's constant, T is the

temperature, and ω_m is the frequency of the vibrational mode of the mechanical element.

Removing thermal phonons from the mechanical element is a key experimental challenge. Interestingly, the ideas and methods for doing so were theoretically developed as early as the 1960s. The main idea is to exploit the intracavity radiation pressure, the force due to momentum transfer associated with photon scattering. In particular, Braginsky realized that the finite time delay between a change in position of the mechanical element and the response of the intracavity field allows the radiation field to extract work from or perform work on the mechanical system.

The process is best illustrated for the case of a basic Fabry–Perot resonator (see figure 2). When both of the resonator's mirrors are held fixed, the optical transmission is sharply peaked near the cavity resonance frequencies $\omega_p = p\pi c/L$, where L is the mirror separation, p is a positive integer, and c is the speed of light. The resonances result from the constructive interferences between the partial waves propagating back and forth inside the cavity. The higher the quality of the mirror, the more roundtrips light takes before exiting the cavity, and the sharper are the resonance peaks.

If one end mirror is mounted on a spring to form a simple harmonic oscillator, a pump laser of frequency ω_L will be modulated by the mechanical frequency and form sidebands with frequencies $\omega_L \pm \omega_m$. From a quantum mechanical perspective, the process is analogous to the generation of Stokes and anti-Stokes sidebands in Raman scattering: The upper sideband is a result of pump-laser photons acquiring energy by annihilating thermal phonons in the mechanical element; the lower sideband results from photons depositing phonons and shedding energy. The first process occurs at a rate proportional to the occupation factor N of the mechanical mode of interest; the second, at a rate proportional to $N + 1$.

By carefully detuning the frequency of the pump field relative to a specific cavity resonance ω_c, one can resonantly enhance one of the processes. In particular, red-detuning from the cavity resonance enhances the upper sideband and promotes extraction of energy from the mechanical element. As long as the up-converted photons leave the cavity sufficiently fast, carrying with them their newly acquired energy, the process can cool the motion of the mechanical element to well below the temperature of its surroundings. Although the quantum noise of the optical source imposes a fundamental cooling limit, it is nonetheless theoretically possible to cool the mechanical mode arbitrarily close to the quantum ground state, $N = 0$. Furthermore, the coherent interaction between photons and phonons allows manipulations in the quantum regime, as pointed out early on by one of us (Meystre), Peter Knight, Paolo Tombesi, and Claude Fabre.

The technique, a form of sideband cooling, was first demonstrated in experiments by Braginsky and by David Blair in the microwave regime as a way to reduce noise in gravitational-wave antennas.[4] Since 2004, several laboratories around the world have used the method to cool nano- and micromechanical levers, in both the optical and microwave domains. Today, high-quality optomechanical devices produce couplings strong enough to cool low-mass levers—ranging from a few picograms to hundreds of nanograms—to their ground state of motion.

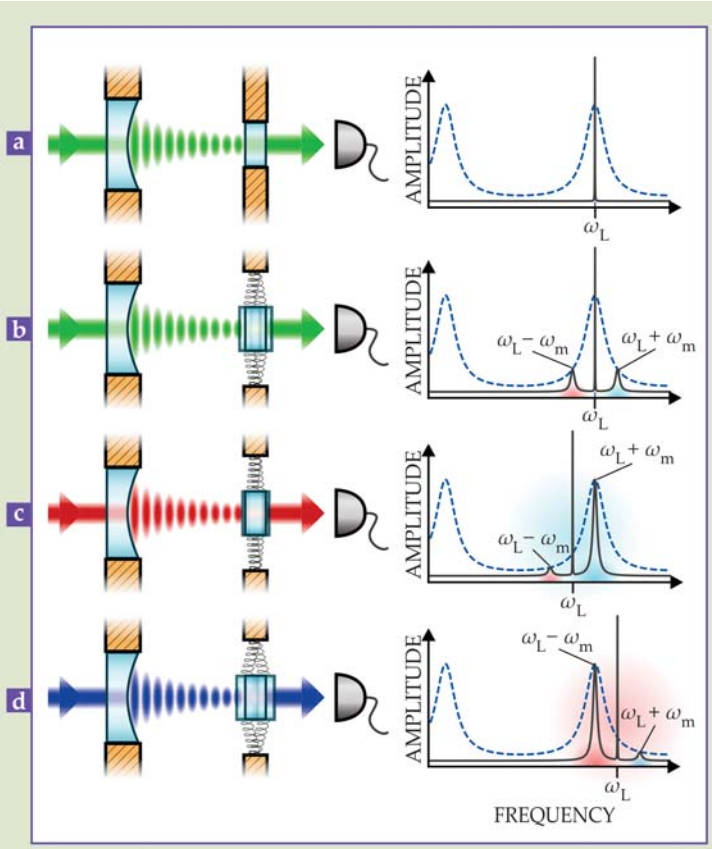

Figure 2. Quantum optomechanics: the basics. (a) If both end mirrors of a Fabry–Perot cavity are fixed in place, pump-laser photons having frequency ω_L tuned to a cavity resonance arrive at a detector with no frequency modulation. (The total transmission to the detector is indicated in the plot at right by the solid line; the cavity transmission spectrum is indicated by the dashed line.) **(b)** However, if one mirror is allowed to oscillate harmonically, pump photons are modulated by the oscillation frequency ω_m: A pump beam tuned to a cavity resonance will yield sidebands of equal amplitude at frequencies $\omega_L \pm \omega_m$. Each photon in the upper sideband acquires energy by extracting a phonon from the oscillator, and each photon in the lower sideband sheds energy by depositing a phonon. **(c)** By red-detuning the pump laser, one can enhance the upper sideband and thereby cool the oscillating mirror. **(d)** By blue-detuning the pump laser, one enhances the lower sideband and amplifies the mirror oscillations. (Figure prepared by Jonas Schmöle.)

The methods used in cavity optomechanics are in many ways analogous to the conventional laser-cooling techniques developed for quantum information processing with trapped ions (see the article by Ignacio Cirac and Peter Zoller, PHYSICS TODAY, March 2004, page 38). There, the collective normal-mode oscillations of a string of ions modify the response of the pump laser that drives their internal state. The resulting optomechanical coupling between the ions' motional and internal degrees of freedom allows one

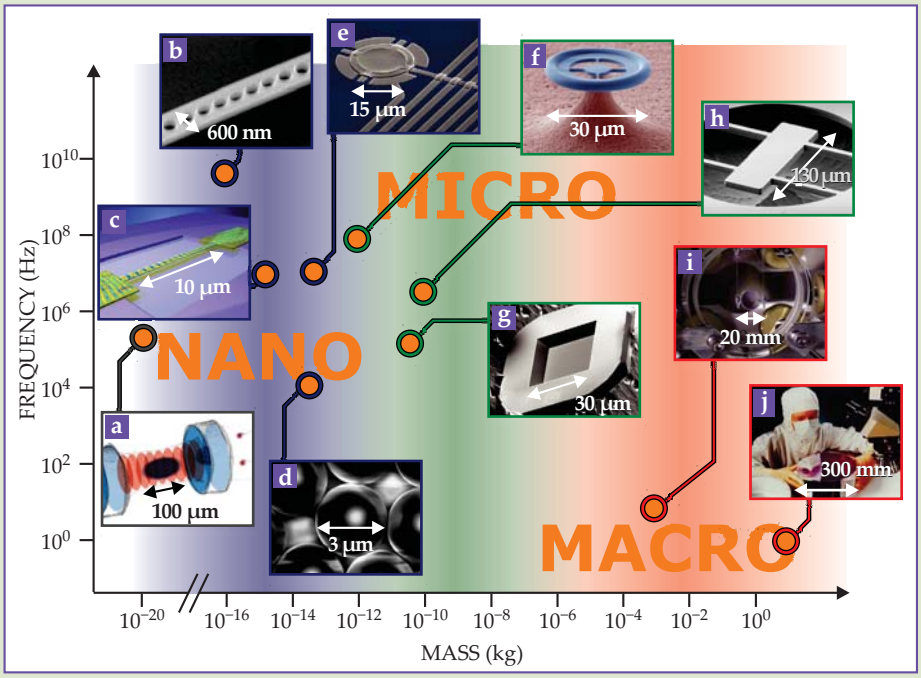

Figure 3. Cavity optomechanical devices range from nanometer-sized structures of as little as 10^7 atoms and 10^{-20} kg to micromechanical structures of 10^{14} atoms and 10^{-11} kg to macroscopic, centimeter-sized mirrors comprising more than 10^{20} atoms and weighing several kilograms. They include **(a)** gases of ultracold atoms, **(d)** microspheres, and **(g)** microscale membranes, all of which have mechanical resonances that can couple with the light inside an optical cavity; **(b, c)** flexible, nanoscale waveguides that have both optical and mechanical resonances; **(e)** superconducting membranes that exhibit drum-like vibrations and can be integrated into microwave cavities; **(f)** microtoroidal waveguides having both optical and mechanical resonances; and mechanically compliant mirrors, which can range from the microscopic **(h)** to the macroscopic **(i, j)** and which introduce mechanical degrees of freedom to an optical cavity when incorporated as an end mirror. (Figure prepared by Jonas Schmöle. Images courtesy of (a) Ferdinand Brennecke, ETH Zürich; (d) the Vienna Center for Quantum Science and Technology; (i) Christopher Wipf; and (j) LIGO Laboratory. Other images adapted from (b) ref. 8, J. Chan et al.; (c) M. Li et al., *Nature* **456**, 80, 2008; (e) ref. 7; (f) ref. 10, E. Verhagen et al.; (g) J. D. Thompson et al., *Nature* **452**, 72, 2008; and (h) G. D. Cole et al., *Nat. Commun.* **2**, 231, 2011.)

to cool the ions or prepare other quantum states of interest.[5] However, cavity optomechanics differs in an important and attractive aspect: Whereas conventional laser cooling relies on the fixed internal resonances of materials to enhance light–matter interactions, cavity optomechanical cooling allows one to engineer the resonance-enhancing structure. That structure could be an optical cavity with a series of narrow resonances or a microwave cavity such as a superconducting *LC* circuit.

A tale of few phonons

Until recently, the pioneering developments in optomechanical coupling went largely unnoticed outside of the experimental gravitation and quantum optics communities. Michael Roukes, who realized nearly two decades ago that high-frequency nanoscale mechanical devices could be chilled to the quantum regime, is a notable exception. Advances in materials science and nanofabrication—particularly the rise of nano- and microelectromechanical systems and optical microcavities—have since opened the possibility of coupling quantum optical modes with mechanical devices in tabletop experiments.[6] The original ideas of optomechanical coupling were extended in many new directions and realized in widely varied optomechanical systems (see figure 3). In the past year, those efforts have culminated in the cooling of at least three different micromechanical systems to within a fraction of a phonon of their ground state of vibrational motion. (Here and below, unless otherwise specified, mechanical cooling refers to cooling of the center-of-mass motion.)

In a NIST experiment led by John Teufel and Ray Simmonds,[7] the mechanical resonator was a circular aluminum membrane, 15 μm across and 100 nm thick, that underwent drum-like vibrations with a resonance frequency of 10 MHz (see figure 3e). The membrane was tightly coupled to a superconducting microwave cavity and chilled in a cryostat to 20 mK, at which the phonon occupation N was about 40. Sideband cooling was then used to cool the membrane to $N \approx 0.3$.

At Caltech, Oskar Painter and colleagues were similarly successful using a 15-μm-long, 600-nm-wide, and 100-nm-thick silicon beam as the optomechanical system (see figure 3b).[8] Clamped at both ends to a silicon wafer, the suspended beam acts simultaneously as a mechanical resonator and an optical cavity. The mechanical mode of interest was a breathing mode, a periodic widening and narrowing that is most pronounced near the beam's midpoint and has a remarkably high quality factor of 10^5. (On average, a phonon survives 10^5 oscillations before being lost to the environment.) And periodic perforations patterned into the beam create a photonic crystal cavity that confines light to the same region around the beam's midpoint.

The co-localization of light and vibrational motion in such a small volume facilitates large optomechanical coupling. Thus, after cryogenically chilling the structure to 20 K, at which $N \approx 100$, the researchers could use sideband cooling to remove the remaining phonons and cool the beam to $N \approx 0.8$. At that point, the group was able to observe another genuine quantum feature: Near the ground state, a mechanical resonator is significantly more likely to absorb phonons than to emit them, and that asymmetry reveals itself experimentally as a preferential sideband scattering of blue-detuned

light over red-detuned light. (See figure 4.)

The next challenge is to control the quantum state of the mechanical resonator. A group led by Andrew Cleland at the University of California, Santa Barbara, took an important first step in that direction by coupling an acoustic resonator to a qubit, a two-state quantum system.[9] The resonator was a 300-nm-thick sheet of aluminum nitride, 40 μm long and 20 μm wide, whose thickness oscillates at a frequency of 6 GHz. At such high oscillation frequencies, the phonon energy $\hbar\omega_m$ is large, and therefore a conventional dilution refrigerator—which can reach temperatures near 25 mK—sufficed to cool the resonator to an occupation factor $N < 0.07$.

Exploiting the piezoelectric nature of AlN, the Santa Barbara team then coupled the resonator to the qubit, a superconducting Josephson junction, which could in turn detect the presence of a single phonon. A null result meant the mechanical resonator was in the ground state. The technique is analogous to those that have been developed over the years in cavity and circuit quantum electrodynamics, except that the photons are replaced by phonons.

Not only did the resonator–qubit coupling allow observation of the energy quantization and other quantum features of the resonator, it also enabled controlled manipulation of the mechanical resonator at the few-phonon level. The Santa Barbara group was able to observe a few coherent oscillations of a single quantum exchanged between the qubit and the resonator—a first demonstration of coherent control over single quantum excitations in a micromechanical resonator. Recent experiments at Caltech and Harvard University and in Grenoble, France, have made important further steps by coupling mechanical devices to a variety of other qubits.

Single-quantum or few-quanta control can occur only in a strong-coupling regime, where energy is exchanged between the mechanical resonator and the qubit or optical mode with very little dissipation; loss of photons and phonons to the environment must be minimal. That regime has now been reached with several micromechanical devices in addition to the one used in the Santa Barbara experiment.[10] Eventually, such strong optomechanical coupling will allow high-fidelity transfer of quantum states between light and mechanical systems. It should even be possible to generate entanglement between photons and phonons. Conversely, phonon fields can be mapped onto an optical mode to take advantage of the reliable, high-efficiency detection schemes available in optics.

Promise in the field

The lure of quantum optomechanics goes far beyond simply adding another class of objects—mechanical resonators—to the list of "tamed" quantum systems. Rather, the promise is that just as we've learned to couple mechanical elements with the photons in an optical cavity, we can functionalize those same elements to couple with, say, the spins in a magnetic material or the charges at a conducting surface. That way, a mechanical element would serve as a universal transducer, an intermediary between otherwise incompatible systems. Flying photons could be linked with stationary, nonoptical qubits, for instance. Only recently, a group led by Philipp Treutlein at the University of Basel, Switzerland, has demonstrated a hybrid optomechanical system coupling ultracold atoms to a micromechanical membrane. Such hybrid quantum systems may be important in classical and quantum information processing, for which the ability to convert information from one form to another is crucial. In fact, several laboratories are now working to couple single mechanical elements to both optical and microwave frequency resonators, with the goal of connecting superconducting microwave circuits and qubits to optical fields.

The connection between optomechanics and atomic physics is particularly interesting. Not only did laser cooling of atoms inspire and enable the rapid progress in quantum optomechanics, it also led to the discovery of other phenomena such as optomechanically induced transparency, the analogue to electromagnetically induced transparency. The effect, which exploits optical interference between a mechanical resonator's excitation paths to control the cavity transmission, may allow storage

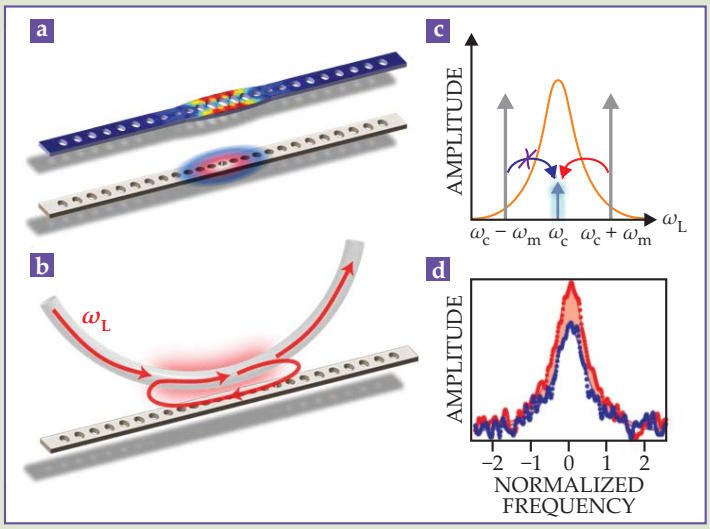

Figure 4. Quantum signatures near the ground state. **(a)** The nanoscale beam shown here undergoes breathing-mode oscillations—successive expansions and contractions—that are strongest near the center, as indicated in the simulated image at top. The perforations along the beam's length form a photonic cavity that confines light to the same region, as indicated in the bottom image. **(b)** A laser field at an appropriately detuned frequency ω_L can be coupled to the waveguide via a tapered optical fiber and used to cool the breathing-mode oscillations to near the ground state. **(c)** At that point, red-detuned photons are less likely to extract phonons and shift upward in frequency (blue arrow) than are blue-detuned photons to create phonons and shift downward (red arrow). (Here, ω_c is the cavity resonance frequency and ω_m is the breathing-mode frequency.) **(d)** The asymmetry is detectable in experiments: With roughly three phonons residing in the beam, the upper sideband (blue) generated from a red-detuned laser is significantly smaller than the lower sideband (red) generated from an equivalently blue-detuned laser. (Panels a–c courtesy of Oskar Painter and colleagues. Panel d adapted from ref. 8, H. Safavi-Naeini et al.)

of light in arrays of cavity optomechanical devices.[11]

Atomic systems can also serve as mechanical elements in cavity optomechanical systems.[12] After trapping 10^5 ultracold rubidium atoms inside an optical cavity, Dan Stamper-Kurn and colleagues at the University of California, Berkeley, coupled the cloud of atoms with a pump laser that was detuned by the resonance frequency of the atoms' collective motion, about 40 kHz. By blue-detuning the pump laser so that it deposited phonons into the cloud, the group was able to observe the back-action exerted on the atoms by the quantum fluctuations of the optical field.

The generation and manipulation of mechanical quantum states is also a challenging and important goal for quantum metrology and sensing applications. To date, the force sensitivity of atomic force microscopes and other classical mechanical devices already exceeds 10^{-18} N $Hz^{-1/2}$. In other words, in less than a second, one can measure a force as small as the gravitational attraction between a person in Los Angeles and another in New York. Still, we haven't reached the ultimate limit. Current implementations suffer from thermal noise and, eventually, from noise associated with quantum uncertainty.

Fortunately, quantum physics provides a way around thermal and quantum noise by way of what are known as quantum nondemolition measurements. Such measurements, first posited in the 1970s by Braginsky and coworkers, typically call for generating a squeezed state—that is, confining the unwanted but unavoidable quantum noise to a variable that is complementary to the variable of interest.

Heisenberg's uncertainty principle states that certain pairs of physical properties—say, the amplitude and phase of an electromagnetic wave—cannot simultaneously be known with arbitrary precision. But a measurement of the wave's amplitude can be performed in such a way that most of the uncertainty is carried by the phase, or vice versa. Such squeezed states of light have recently been shown to enhance the sensitivity of gravitational-wave detectors[13] (see PHYSICS TODAY, November 2011, page 11).

In principle, it is also possible to prepare mechanical squeezed states in which nearly all of the quantum uncertainty is confined to either the position or the momentum. In fact, the classical squeezing of micromechanical oscillators below the thermal noise limit was first demonstrated several years ago by Daniel Rugar and colleagues at IBM.[14] However, squeezing below the standard quantum limit—the precision limit for the case when quantum uncertainty is distributed evenly among complementary properties—has yet to be achieved. A number of strategies based on Braginsky's original schemes, which can be readily implemented in optomechanical systems, are being actively pursued.

> Today's devices, though similar in many ways to those of antiquity, steer us to a completely different worldview—one in which an object, possibly even a macroscopic one, can indeed act in two ways at the same time.

Macroscale quantum mechanics

Although still speculative, micromechanical oscillators could offer a route to new tests of quantum theory at unprecedented size and mass scales. Since fundamental particles behave quantum mechanically, one would by induction expect that large collections of particles should also behave quantum mechanically. But that conclusion certainly seems contrary to our everyday classical experience with ordinary matter. Even large quantum condensates—a cupful of superfluid helium, for instance—which do display quantum properties such as frictionless, quantized flow, do not display macroscopic superposition states.

To explain the so-called quantum measurement problem, also notoriously known as Schrödinger's cat, some theorists propose that standard quantum mechanics breaks down for macroscopic objects in such a way that their superposition is forbidden. In one such theory, gravitation, which is always unshieldable, ultimately causes massive objects to decohere, or transition from quantum to classical behavior. In another theory, objects couple to a stochastic background field that localizes the object at a rate that scales with the number of particles.

Quantum optomechanics offers a promising way to produce spatial superpositions in massive objects such as mechanical levers or quartz nanospheres and to directly test theories of how they decohere.[15] Ongoing work in that direction builds on optical-trapping and optical-cooling techniques originally proposed by Arthur Ashkin[16] and should eventually allow a single trapped particle to be prepared in a quantum superposition of two distinct center-of-mass states.

Approaching the problem from the opposite direction—from the bottom up—researchers in Vienna used conventional molecular-beam techniques to produce matter-wave interferences with large, 430-atom molecules.[17] Ultimately, it may be possible to conduct similar quantum experiments with even more massive mechanical systems. A group led by Nergis Mavalvala of MIT recently took a first step in that direction by cooling a kilogram-size oscillator to within about 200 phonons of the quantum ground state.[18]

Macroscale mechanical quantum experiments will have to overcome a number of daunting technical issues. Some of those issues—identifying gravity's role in decoherence, for example—might be resolved by conducting experiments in free fall, perhaps aboard a satellite. (Last year's Caltech experiment, in which a phonon occupancy of less than one was achieved at a bath temperature of 20 K, shows that ground-state cooling is now within the range of commercial cryocoolers that can be flown on satellites.) We are confident that coming experiments will lead to a more profound understanding of quantum mechanics, establish limits to its validity, or confirm what we, and likely many others, believe—that technical issues such as environmental decoherence, and not the appearance of new physical principles, establish the transition from the quantum world to the classical. We have never been so close to being able to truly address those profound questions and to challenge Plato's commonsense notion of reality in the laboratory.

References

1. For recent reviews, see T. J. Kippenberg, K. J. Vahala, *Science* **321**, 1172 (2008); M. Aspelmeyer et al., *J. Opt. Soc. Am. B* **27**, A189 (2010); F. Marquardt, S. M. Girvin, *Physics* **2**, 40 (2009).
2. V. B. Braginsky, Y. I. Vorontsov, K. S. Thorne, *Science* **209**, 547 (1980); C. M. Caves et al., *Rev. Mod. Phys.* **52**, 341 (1980). For a historical perspective, see P. Meystre, M. O. Scully, eds., *Quantum Optics, Experimental Gravitation, and Measurement Theory*, Plenum Press, New York (1983).
3. V. B. Braginsky, F. Y. Khalili, *Quantum Measurement*, Cambridge U. Press, New York (1992); C. M. Caves, *Phys. Rev. Lett.* **45**, 75 (1980).
4. V. Braginsky, A. Manukin, *Sov. Phys. JETP* **25**, 653 (1967); D. G. Blair et al., *Phys. Rev. Lett.* **74**, 1908 (1995).
5. R. Blatt, D. Wineland, *Nature* **453**, 1008 (2008); D. Leibfried et al., *Rev. Mod. Phys.* **75**, 281 (2003); J. D. Jost et al., *Nature* **459**, 683 (2009).
6. H. Rokhsari et al., *Opt. Exp.* **13**, 5293 (2005); T. Carmon et al., *Phys. Rev. Lett.* **94**, 223902 (2005); T. J. Kippenberg et al., *Phys. Rev. Lett.* **95**, 033901 (2005).
7. J. D. Teufel et al., *Nature* **475**, 359 (2011).
8. J. Chan et al., *Nature* **478**, 89 (2011); A. H. Safavi-Naeini et al., *Phys. Rev. Lett.* **108**, 033602 (2012).
9. A. D. O'Connell et al., *Nature* **464**, 697 (2010).
10. S. Gröblacher et al., *Nature* **460**, 724 (2009); J. D. Teufel et al., *Nature* **471**, 204 (2011); E. Verhagen et al., *Nature* **482**, 63 (2012).
11. S. Weis et al., *Science* **330**, 1520 (2010); A. H. Safavi-Naeini et al., *Nature* **472**, 69 (2011).
12. K. W. Murch et al., *Nat. Phys.* **4**, 561 (2008); F. Brennecke et al., *Science* **322**, 235 (2008); M. Schleier-Smith et al., *Phys. Rev. Lett.* **107**, 143005 (2011).
13. J. Abadie et al. (LIGO Scientific Collaboration), *Nat. Phys.* **7**, 962 (2011).
14. D. Rugar, P. Grütter, *Phys. Rev. Lett.* **67**, 699 (1991); J. Suh et al., *Nano Lett.* **10**, 3990 (2010).
15. W. Marshall et al., *Phys. Rev. Lett.* **91**, 130401 (2003); O. Romero-Isart et al., *Phys. Rev. Lett.* **107**, 020405 (2011); O. Romero-Isart, *Phys. Rev. A* **84**, 052121 (2011).
16. A. Ashkin, *Phys. Rev. Lett.* **24**, 156 (1970); O. Romero-Isart et al., *New J. Phys.* **12**, 033015 (2010); D. E. Chang et al., *Proc. Natl. Acad. Sci. USA* **107**, 1005 (2010); P. F. Barker, M. N. Shneider, *Phys. Rev. A* **81**, 023826 (2010).
17. S. Gerlich et al., *Nat. Commun.* **2**, 263 (2011).
18. B. Abbott et al., *New J. Phys.* **11**, 073032 (2009). ■

Effective Field Theory Approach to Gravitationally Induced Decoherence

M. P. Blencowe*

Department of Physics and Astronomy, Dartmouth College, Hanover, New Hampshire 03755, USA

(Received 27 November 2012; revised manuscript received 10 April 2013; published 12 July 2013)

Adopting the viewpoint that the standard perturbative quantization of general relativity provides an effective description of quantum gravity that is valid at ordinary energies, we show that gravity as an environment induces the rapid decoherence of stationary matter superposition states when the energy differences in the superposition exceed the Planck energy scale.

DOI: 10.1103/PhysRevLett.111.021302 PACS numbers: 04.60.Bc, 03.65.Ta, 03.65.Yz

Introduction.—The emergence of the macroscopic classical world from the microscopic quantum world is commonly understood to be a consequence of the fact that any given quantum system is open, unavoidably interacting with unobserved environmental degrees of freedom that will cause initial quantum superposition states of the system to decohere, resulting in classical mixtures of either-or alternatives [1–3]. Consider, for example, a system consisting of a vibrating micrometer scale silicon wire in ultrahigh vacuum at dilution fridge temperatures (~ 10 mK). Assuming a realizable quality factor $Q \sim 10^5$ that is limited by clamping radiation loss [4] and elastic strain-coupled two level system defects within the wire [5], an initial center of mass coherent state superposition with separation $\Delta x \sim 1$ nm will decohere in about a picosecond, rapidly enforcing classicality in the dynamics of the vibrating wire. Suppose, however, that the common sources of decoherence are removed through levitating the silicon mass by optical [6,7] or other means [8,9]. Can the coherence times of center of mass superposition states be increased without bound by removing the effects of clamping and defect loss in this way and minimizing the interaction with the electromagnetic environment? More generally, can systems of arbitrarily increasing mass energy be placed in nonclassical states, such as center of mass quantum superposition states?

Gravity has been invoked in various ways as playing a possible fundamental role in enforcing classicality of matter systems beyond a certain scale [10–34]. Certainly, one environment that cannot be avoided is the stochastic gravitational radiation background arising from the big bang and other sources [27,35]. A clue as to the possible effect this environment might have on a low energy quantum matter system comes from the fact that the space-time metric in Einstein's equations couples to the system via its energy-momentum tensor. For a stationary system, only its rest energy should be relevant for the decoherence dynamics of an initial quantum superposition state. Consider for the moment a model oscillator system coupled via its energy to an oscillator environment, described by the Hamiltonian

$$H = \hbar\omega_0 a^\dagger a\left(1 + \sum_i \lambda_i \frac{q_i}{\Delta_i}\right) + \sum_i \left(\frac{p_i^2}{2m_i} + \frac{1}{2} m_i \omega_i^2 q_i^2\right), \tag{1}$$

where ω_0 is the system oscillator's frequency and $\Delta_i = \sqrt{\hbar/(2m_i\omega_i)}$ is the ith bath oscillator's zero-point uncertainty. Assuming an Ohmic bath spectral density $J(\omega)/(\hbar\omega_0)^2 = \pi\sum_i \lambda_i^2 \delta(\omega - \omega_i) = C\omega/\omega_0^2$, for weak system-bath dimensionless coupling C in the high temperature limit, we obtain the following time evolution of the system density matrix in the Born-Markov approximation:

$$\rho_{n\tilde{n}}(t) = e^{-i\omega_0(n-\tilde{n})t - C(k_B T/\hbar)(n-\tilde{n})^2 t}\rho_{n\tilde{n}}(0), \tag{2}$$

where T is the oscillator bath temperature. Notice that the thermal oscillator environment induces decoherence of initial superpositions of different Fock states $|n\rangle$, $|\tilde{n}\rangle$ into mixtures of these states. By analogy, and with the aid of dimensional analysis, we might therefore expect that a stochastic gravitational environment will similarly decohere a matter system initially in a superposition of say two different rest energy states E and $\tilde{E}$ with a rate given by

$$\Gamma_{\text{decohere}} \sim \frac{k_B T}{\hbar}\left(\frac{E - \tilde{E}}{E_P}\right)^2, \tag{3}$$

where $E_P = \sqrt{\hbar c^5/G}$ is the Planck energy and we assume for simplicity a thermal graviton environment at temperature T.

In the following, we shall derive Eq. (3)—including the missing dimensionless numerical factor—by applying standard perturbative quantum field theory techniques to gravity [36–38]. The justification for such an approach follows from the fact that we are considering laboratory scale systems, where the matter is localized to regions of small curvature. As with other low energy effects, such as the quantum gravity correction to the Newtonian potential between two ordinary masses [36], it should be possible to quantitatively evaluate gravitationally induced decoherence rates by employing standard perturbative quantum gravity as an effective field theory [36,39]; whatever the final form the eventual correct quantum theory of gravity

takes, it must converge in its predictions with the effective field theory description at low energies.

Effective field theory derivation.—In order to be able to construct matter system states starting from a generally covariant field theory, we will adopt as a simple model system a massive scalar field $\phi(x)$ with mass parameter m corresponding to that of a nucleon. Expanding the Einstein-Hilbert action to second order in metric deviations from Minkowski space-time, $g_{\mu\nu} = \eta_{\mu\nu} + \kappa h_{\mu\nu}$, we have:

$$S[h_{\mu\nu}, \phi] \approx S_S[\phi] + S_E[h_{\mu\nu}] + S_I[h_{\mu\nu}, \phi], \quad (4)$$

where $\kappa = \sqrt{32\pi G}$ (from now on we for the most part use natural units with $\hbar = c = 1$), and the system, environment, and interaction actions are respectively:

$$S_S = -\frac{1}{2}\int d^4x(\eta^{\mu\nu}\partial_\mu\phi\partial_\nu\phi + m^2\phi^2), \quad (5)$$

$$S_E = \int d^4x\Big(-\frac{1}{2}\partial^\rho h^{\mu\nu}\partial_\rho h_{\mu\nu} + \partial_\nu h^{\mu\nu}\partial^\rho h_{\mu\rho} - \partial_\mu h\partial_\nu h^{\mu\nu} + \frac{1}{2}\partial^\mu h\partial_\mu h\Big), \quad (6)$$

$$S_I = \int d^4x\Big(\frac{\kappa}{2}T^{\mu\nu}(\phi)h_{\mu\nu} + \frac{\kappa^2}{4}U^{\mu\nu\rho\sigma}(\phi)h_{\mu\nu}h_{\rho\sigma}\Big), \quad (7)$$

where $T_{\mu\nu}(\phi) = \partial_\mu\phi\partial_\nu\phi - (1/2)\eta_{\mu\nu}\partial_\rho\phi\partial^\rho\phi - (1/2)\eta_{\mu\nu}m^2\phi^2$ is the scalar field energy-momentum tensor and the explicit form of the quadratic in ϕ tensor $U_{\mu\nu\rho\sigma}(\phi)$ can be found in Ref. [38].

The closed time path integral approach [40] gives the following formal expression for the scalar matter system density matrix:

$$\rho_S[\phi, \phi', t] = \int d\phi_0 d\phi_0' \int_{\phi_0}^{\phi}[d\phi^+]\int_{\phi_0'}^{\phi'}[d\phi^-]\rho_S[\phi_0, \phi_0', 0] \times e^{\{i(S_S[\phi_+]-S_S[\phi^-]+S_{\rm IF}[\phi^+,\phi^-])\}}, \quad (8)$$

where $S_{\rm IF}$ is the Feynman-Vernon influence action that gives the effect of the thermal graviton environment on the scalar matter system. Evaluating $S_{\rm IF}$ to lowest, quadratic order in κ with harmonic gauge fixing term inserted in S_E, we obtain from Eq. (8) the following Born-approximated master equation for the scalar system:

$$\begin{aligned}\partial_t\rho_S(t) = &-i[H_S, \rho_S(t)] - \int_0^t d\tau\int d\mathbf{r}d\mathbf{r}'\{N(\mathbf{r}-\mathbf{r}', \tau)\\ &\times(2[T_{\mu\nu}(\mathbf{r}), [T^{\mu\nu}(\mathbf{r}', -\tau), \rho_S(t)]]\\ &-[T_\mu{}^\mu(\mathbf{r}), [T_\nu{}^\nu(\mathbf{r}', -\tau), \rho_S(t)]])\\ &- iD(\mathbf{r}-\mathbf{r}', \tau)(2[T_{\mu\nu}(\mathbf{r}), \{T^{\mu\nu}(\mathbf{r}', -\tau), \rho_S(t)\}]\\ &-[T_\mu{}^\mu(\mathbf{r}), \{T_\nu{}^\nu(\mathbf{r}', -\tau), \rho_S(t)\}])\},\end{aligned} \quad (9)$$

where H_S is the free scalar field Hamiltonian and the noise and dissipation kernels are respectively:

$$\begin{aligned}N(\mathbf{r}, t) &= \Big(\frac{\kappa}{4}\Big)^2\int\frac{d\mathbf{k}}{(2\pi)^3}\frac{e^{i\mathbf{k}\cdot\mathbf{r}}}{k}\cos(kt)[1+2n(k)],\\ D(\mathbf{r}, t) &= \Big(\frac{\kappa}{4}\Big)^2\int\frac{d\mathbf{k}}{(2\pi)^3}\frac{e^{i\mathbf{k}\cdot\mathbf{r}}}{k}\sin(kt),\end{aligned} \quad (10)$$

with $n(k)$ the thermal Bose-Einstein occupation number at temperature T.

While the master equation (9) can in principle be used to investigate the decoherence dynamics of quite general, relativistic scalar field matter states, we shall restrict ourselves to scalar matter states that model ordinary, nonrelativistic stationary macroscopic material objects. The following class of coherent states provides the basis for such a model:

$$|\alpha\rangle = \exp\Big[-\frac{1}{2}\int d\mathbf{k}|\alpha(\mathbf{k})|^2 + \int d\mathbf{k}\,\alpha a^\dagger(\mathbf{k})\Big]|0\rangle, \quad (11)$$

where

$$\alpha(\mathbf{k}) = \varphi_0 R^3\sqrt{\frac{\omega_m(k)}{2}}e^{-i\mathbf{k}\cdot\mathbf{r}_0-(kR)^2/2}, \quad (12)$$

with $\omega_m(k) = \sqrt{m^2+k^2}$. These states satisfy

$$\langle\alpha|\phi(\mathbf{r})|\alpha\rangle = \varphi_0 e^{-(\mathbf{r}-\mathbf{r}_0)^2/(2R^2)}, \quad \langle\alpha|\dot\phi(\mathbf{r})|\alpha\rangle = 0, \quad (13)$$

and thus describe Gaussian matter "balls" of radius R with the stationary center at $\mathbf{r}_0$, and total energy content depending on the amplitude parameter φ_0. If we furthermore consider ball radii R much larger than the nucleon's reduced Compton wavelength $\lambda_C = \hbar/(mc) \approx 10^{-16}$ m, then their rest mass energy $E = (\pi^3 m^2\varphi_0^2 R^3)/2$ is the dominant energy content and they approximately maintain their Gaussian profile (13) with little spatial spreading over the time scale of the initial transient (see below); for simplicity we will neglect this spreading. The noise term part of the master equation (9), which is responsible for decoherence, then simplifies to

$$\begin{aligned}\partial_t\rho_S[\phi, \phi', t] = \cdots - \int_0^t d\tau\int d\mathbf{r}d\mathbf{r}'N(\mathbf{r}-\mathbf{r}', \tau)\\ \times\Big[\frac{1}{2}m^2(\phi(\mathbf{r}))^2 - \frac{1}{2}m^2(\phi'(\mathbf{r}))^2\Big]\\ \times\Big[\frac{1}{2}m^2(\phi(\mathbf{r}'))^2 - \frac{1}{2}m^2(\phi'(\mathbf{r}'))^2\Big]\\ \times\rho_S[\phi, \phi', t],\end{aligned} \quad (14)$$

where we have used the fact that the energy density component $T_{00}(\phi) \approx (1/2)m^2\phi^2$ of the energy-momentum tensor terms in Eq. (9) dominates in the nonrelativistic, stationary limit, and we have also expressed the master equation in the field coordinate basis.

Let us now assume that, by some means, a superposition of two Gaussian ball states, each with distinct parameters $(\varphi_0, \mathbf{r}_0, R)$ and $(\tilde\varphi_0, \tilde{\mathbf{r}}_0, \tilde R)$, has been prepared at time $t = 0$:

$$\rho_S[\phi, \phi', 0] = \langle\phi|\Psi\rangle\langle\Psi|\phi'\rangle, \tag{15}$$

where

$$\langle\phi|\Psi\rangle = \frac{1}{\sqrt{2}}(\langle\phi|\alpha\rangle + \langle\phi|\tilde{\alpha}\rangle), \tag{16}$$

with the ball states in the field coordinate basis taking the form

$$\begin{aligned}\langle\phi|\alpha\rangle &= \exp\Big[-\frac{1}{2}\int d\mathbf{r}\sqrt{m^2+\nabla^2}(\phi(\mathbf{r}) \\ &\quad - \varphi_0 e^{-(\mathbf{r}-\mathbf{r_0})^2/(2R^2)})^2\Big] \\ &\approx \exp\Big[-\frac{m}{2}\int d\mathbf{r}(\phi(\mathbf{r}) - \varphi_0 e^{-(\mathbf{r}-\mathbf{r_0})^2/(2R^2)})^2\Big] \end{aligned} \tag{17}$$

and a similar expression for $\langle\phi|\tilde{\alpha}\rangle$ with parameters $(\tilde{\varphi}_0, \tilde{\mathbf{r}}_0, \tilde{R})$. The simpler approximate form in Eq. (17) follows from the condition $R \gg \lambda_C$. Evaluating the noise term in (14) for the off-diagonal, interference part of the density matrix with $\phi(\mathbf{r}) = \varphi_0 e^{-(\mathbf{r}-\mathbf{r_0})^2/(2R^2)}$ and $\phi'(\mathbf{r}) = \tilde{\varphi}_0 e^{-(\mathbf{r}-\tilde{\mathbf{r}}_0)^2/(2\tilde{R}^2)}$, we have

$$\begin{aligned}\partial_t \rho_S[\phi, \phi', t] = \cdots - \frac{T}{2\pi}\Big(\frac{\kappa}{4}\Big)^2\Big(\int dr\Big[\frac{1}{2}m^2(\phi(\mathbf{r}))^2 \\ - \frac{1}{2}m^2(\phi'(\mathbf{r}))^2\Big]\Big)^2\rho_S[\phi, \phi', t], \end{aligned} \tag{18}$$

where we neglect initial transients, corresponding to having t large compared to the time required for a graviton to traverse the matter state spatial extent, i.e., $ct \gg \max(\| \mathbf{r}_0 - \tilde{\mathbf{r}}_0 \|, R, \tilde{R})$—the Markovian approximation—and we also assume that $k_B T \gg \hbar/t$—the high temperature limit. From Eq. (18), we immediately see that the off-diagonal interference part of the density matrix decays only provided the two ball states in the superposition have distinct energies $E \neq \tilde{E}$; spatial superpositions with $\mathbf{r}_0 \neq \mathbf{r}'_0$ do not decohere if the respective energies are identical. Equation (3) immediately follows from (18). More precisely, we have for the decoherence rate in the Born-Markov approximation:

$$\Gamma_{\text{decohere}} = \frac{k_B T}{\hbar}\Big(\frac{E - \tilde{E}}{E_P}\Big)^2. \tag{19}$$

Discussion.—The decoherence rate formula (19) is sufficiently basic that one might expect it to be of more general validity beyond the specific scalar field model used above to derive it. Let us in particular assume that (19) applies to ordinary, stationary matter systems, such as a small chunk of crystalline solid or a trapped cold atom cloud in the laboratory, and that for simplicity the matter system comprises model two state (excited and ground) atoms with energy level separation $\sim$1 eV. For a cosmic gravitational wave background with temperature $T \sim 1$ K [41], we have for the gravitationally induced decoherence rate of an initial superposition of ground and excited states of a single atom: $\Gamma_{\text{decohere}} \sim 10^{-45}$ secs^{-1}. For a matter system comprising an Avogadro's number of atoms $\sim$1 gram in a quantum superposition where all of the atoms are either in their ground state or all in their excited state, then we have $\Gamma_{\text{decohere}} \sim 10^2$ sec^{-1}. For a system with mass $\sim$1 kg in such a superposition state, the gravitationally induced decoherence rate is $\Gamma_{\text{decohere}} \sim 10^8$ sec^{-1}. Thus, even leaving aside the technical challenges due to the presence of everyday environments in preparing such macroscopic matter superposition states, the cosmic gravitational background itself will unavoidably induce their rapid decoherence, leaving the matter system in a classical mixture of either its ground or its excited state.

How does our effective field theory approach to gravitationally induced decoherence and the resulting decoherence rate prediction (19) relate to other work [10–34] considering the role of gravity in the emergence of classicality? Two approaches can be identified: (a) the "intrinsic" or "fundamental decoherence" approach [31], where the standard Schrödinger evolution of a quantum matter system is modified by a wave function collapse process that is linked to an inherent "fuzziness" of space-time structure [11–13,15,16,18,20,24,28,29,31,33,34]; (b) the "quantum decoherence" approach [31], where standard quantum mechanics is applied to a model matter system plus gravity environment [19,21–23,25,27,32]. References [21,27] are closest to our approach, quantizing gravity in the weak, linearized metric perturbations about Minkowski space-time approximation. However, in contrast to our approach, Refs. [21,27] model the matter sector as comprising one or more point particles (as opposed to a scalar field) in the nonrelativistic limit and the resulting decoherence predictions depend on the free particle kinetic energy and not on their relativistic rest mass energy.

A possible way to understand how gravity gives rise to decoherence as predicted by (19), is to first consider the simpler situation of the matter ball superposition state in a static, weak gravitational potential $V(\mathbf{r})$: $g_{00} \approx -(1+2V/c^2)$, $g_{ij} = \delta_{ij}$. Following the analysis in Ref. [42] (Sec. IX) of the classic COW neutron interferometry experiment [43], the interference term is approximately:

$$\langle\tilde{\alpha}(t)|\alpha(t)\rangle \sim \exp[i(S - \tilde{S})/\hbar], \tag{20}$$

where S is the classical action of the ball, expressed in terms of its rest energy E and proper time τ along its worldline:

$$S = -\int_0^t E d\tau = -\int_0^t E\Big(-g_{\mu\nu}\frac{dx^\mu}{dt'}\frac{dx^\nu}{dt'}\Big)^{1/2}dt'. \tag{21}$$

Supposing that the ball is stationary in the laboratory frame gives $S \approx -Et - EV(\mathbf{r}_0)t/c^2$ and the interference term (20) simplifies to

$$\langle\tilde{\alpha}(t)|\alpha(t)\rangle \sim \exp[-i(E - \tilde{E})t/\hbar + i\theta], \tag{22}$$

where $\theta = -[EV(\mathbf{r}_0) - \tilde{E}V(\tilde{\mathbf{r}}_0)]t/(c^2\hbar)$ is the gravitationally induced phase shift difference between the two ball states in the superposition. From Eqs. (20)–(22), we can interpret the phase shift θ as due in part to the difference in rest energies and in part to the difference in proper times elapsed (gravitational redshift). Now, it should be possible to analogously account for the thermal gravitational wave environment by an appropriately chosen random phase shift normal distribution [44], i.e., by making the replacement $e^{i\theta} \to \langle e^{i\theta}\rangle = e^{i\langle\theta\rangle - (1/2)\langle\delta\theta^2\rangle}$ in (22). We therefore can interpret the gravitationally induced decoherence process as "dephasing," i.e., a growing phase difference uncertainty $\langle\delta\theta^2\rangle$ between the two ball states that suppresses the interference term, due in part to fluctuations in the elapsed proper time difference for the two ball states.

As effective field calculations go, the above $O(\kappa^2)$, Born-Markov derivation of the gravitationally induced decoherence rate is pretty straightforward; the present analysis should be viewed as a point of departure, showing the promise of the effective field theory approach [36,39] for analyzing gravitationally induced decoherence. The calculations might be extended in several directions beyond the master equation (9), including (a) going to $O(\kappa^4)$, so as to account for damping and decoherence due to graviton emission or absorption by the matter system, (b) investigating gravitationally induced decoherence for relativistic matter systems in curved space-time backgrounds, with application for example to the formation of cosmic matter structure in the early Universe [45,46], and (c) investigating the low temperature limit to determine whether gravity vacuum fluctuations can induce decoherence [21–23,25,32] and comparison with the predictions from the various vacuum fluctuation induced spontaneous collapse models [11,12,14–16,18,20,24,28]. It will also be interesting to try to establish whether a resulting decohered, mixed matter state can in principle be distinguished from a collapse model yielding the same matter state outcomes. Reference [33] postulates that such indistinguishability or "undecidability" allows for the interpretation of an actual matter state outcome or event, although now with the advantage that the effective field theory method can provide quantitative predictions for such outcomes.

I would like to thank J. Ankerhold, R. R. Caldwell, J. F. Donoghue, and R. Onofrio for very helpful discussions. This work was supported by the Carl Zeiss Foundation and the National Science Foundation (NSF) under Grants No. DMR-0804477 and No. DMR-1104790.

*miles.p.blencowe@dartmouth.edu

[1] A. O. Caldeira and A. J. Leggett, Ann. Phys. (N.Y.) **149**, 374 (1983).
[2] E. Joos and H. D. Zeh, Z. Phys. B **59**, 223 (1985).
[3] W. H. Zurek, Phys. Today **44**, 36 (1991).
[4] G. D. Cole, I. Wilson-Rae, K. Werbach, M. R. Vanner, and M. Aspelmeyer, Nat. Commun. **2**, 231 (2011).
[5] L. G. Remus and M. P. Blencowe, Phys. Rev. B **86**, 205419 (2012).
[6] T. C. Li, S. Kheifets, and M. G. Raizen, Nat. Phys. **7**, 527 (2011).
[7] O. Romero-Isart, A. C. Pflanzer, M. L. Juan, R. Quidant, N. Kiesel, M. Aspelmeyer, and J. I. Cirac, Phys. Rev. A **83**, 013803 (2011).
[8] O. Romero-Isart, L. Clemente, C. Navau, A. Sanchez, and J. I. Cirac, Phys. Rev. Lett. **109**, 147205 (2012).
[9] M. Cirio, G. K. Brennen, and J. Twamley, Phys. Rev. Lett. **109**, 147206 (2012).
[10] R. P. Feynman, F. B. Morinigo, W. G. Wagner, and B. Hatfield, *Feynman Lectures on Gravitation* (Westview Press, Boulder, 2003).
[11] F. Karolyhazy, A. Frenkel, and B. Lukacs, in *Quantum Concepts in Space and Time*, edited by R. Penrose and C. J. Isham (Oxford University Press, Oxford, 1986).
[12] L. Diósi, Phys. Lett. **120A**, 377 (1987).
[13] J. Ellis, S. Mohanty, and D. V. Nanopoulos, Phys. Lett. B **221**, 113 (1989).
[14] R. Penrose, *The Emperor's New Mind* (Oxford University Press, Oxford, 1989).
[15] G. C. Ghirardi, R. Grassi, and R. Rimini, Phys. Rev. A **42**, 1057 (1990).
[16] G. J. Milburn, Phys. Rev. A **44**, 5401 (1991).
[17] M. Blencowe, Ann. Phys. (N.Y.) **211**, 87 (1991).
[18] R. Penrose, Gen. Relativ. Gravit. **28**, 581 (1996).
[19] L. Stodolsky, Acta Phys. Pol. B **27**, 1915 (1996).
[20] P. Pearle and E. Squires, Found. Phys. **26**, 291 (1996).
[21] C. Anastopoulos, Phys. Rev. D **54**, 1600 (1996).
[22] B. S. Kay, Classical Quantum Gravity **15**, L89 (1998).
[23] L. J. Garay, Phys. Rev. D **58**, 124015 (1998).
[24] J. Anandan, Found. Phys. **29**, 333 (1999).
[25] W. L. Power and I. C. Percival, Proc. R. Soc. A **456**, 955 (2000).
[26] G. Amelino-Camelia, Phys. Rev. D **62**, 024015 (2000).
[27] B. Lamine, R. Hervé, A. Lambrecht, and S. Reynaud, Phys. Rev. Lett. **96**, 050405 (2006).
[28] S. L. Adler, J. Phys. A **40**, 755 (2007).
[29] R. Gambini, R. A. Porto, and J. Pullin, Gen. Relativ. Gravit. **39**, 1143 (2007).
[30] C. Anastopoulos and B. L. Hu, J. Phys. Conf. Ser. **67**, 012012 (2007).
[31] C. Anastopoulos and B. L. Hu, Classical Quantum Gravity **25**, 154003 (2008).
[32] H.-P. Breuer, E. Göklü, and C. Lämmerzahl, Classical Quantum Gravity **26**, 105012 (2009).
[33] R. Gambini, L. P. Garcia Pintos, and J. Pullin, Found. Phys. **40**, 93 (2010).
[34] O. Romero-Isart, Phys. Rev. A **84**, 052121 (2011).
[35] B. Allen, Phys. Rev. D **37**, 2078 (1988).
[36] J. F. Donoghue, Phys. Rev. D **50**, 3874 (1994).
[37] A. Campos and B. L. Hu, Phys. Rev. D **58**, 125021 (1998).
[38] D. Arteaga, R. Parentani, and E. Verdaguer, Phys. Rev. D **70**, 044019 (2004).
[39] C. P. Burgess, Living Rev. Relativity **7**, 5 (2004).
[40] E. Calzetta and B. L. Hu, *Nonequilibrium Quantum Field Theory* (Cambridge University Press, Cambridge, England, 2008).

[41] E. W. Kolb and M. S. Turner, in *The Early Universe* (Addison-Wesley, Reading, MA, 1990), p. 76.
[42] D. M. Greenberger, Rev. Mod. Phys. **55**, 875 (1983).
[43] R. Colella, A. W. Overhauser, and S. A. Werner, Phys. Rev. Lett. **34**, 1472 (1975).
[44] A. Stern, Y. Aharonov, and Y. Imry, Phys. Rev. A **41**, 3436 (1990).
[45] A. Perez, H. Sahlmann, and D. Sudarsky, Classical Quantum Gravity **23**, 2317 (2006).
[46] A. De Unánue and D. Sudarsky, Phys. Rev. D **78**, 043510 (2008).

Centre-of-mass motion in multi-particle Schrödinger-Newton dynamics

Domenico Giulini[1,2] **and André Großardt**[1,3]

[1] Center of Applied Space Technology and Microgravity
University of Bremen, Am Fallturm 1, D-28359 Bremen, Germany
[2] Institute for Theoretical Physics
Leibniz University Hannover, Appelstr. 2, D-30167 Hannover, Germany
[3] Department of Physics
University of Trieste, Strada Costiera 11, I-34151 Miramare-Trieste, Italy

E-mail: giulini@itp.uni-hannover.de, andre.grossardt@ts.infn.it

Abstract. We investigate the implication of the non-linear and non-local multi-particle Schrödinger-Newton equation for the motion of the mass centre of an extended multi-particle object, giving self-contained and comprehensible derivations. In particular, we discuss two opposite limiting cases. In the first case, the width of the centre-of-mass wave packet is assumed much larger than the actual extent of the object, in the second case it is assumed much smaller. Both cases result in non-linear deviations from ordinary free Schrödinger evolution for the centre of mass. On a general conceptual level we include some discussion in order to clarify the physical basis and intention for studying the Schrödinger-Newton equation.

PACS numbers: 03.65.-w, 04.60.-m

AMS classification scheme numbers: 35Q40

1. Introduction

How does a quantum system in a non-classical state gravitate? There is no unanimously accepted answer to this seemingly obvious question. If we assume that gravity is fundamentally quantum, as most physicists assume, the fairest answer is simply that we don't know. If gravity stays fundamentally classical, a perhaps less likely but not altogether outrageous possibility [1, 2], we also don't know; but we can guess. One such guess is that semi-classical gravity stays valid, beyond the realm it would be meant for if gravity were quantum [1, 2]. Semi-classical gravity in that extended sense is the theory which we wish to pursue in this paper. Since eventually we are aiming for the characterisation of experimentally testable consequences of such gravitational self-interaction through matter-wave interferometry, we focus attention on the centre-of-mass motion.

Note that by "quantum system" we refer to the possibility for the system to assume states which have no classical counterpart, like superpositions of spatially localised

states. We are not primarily interested in matter under extreme conditions (energy, pressure, etc.). Rather we are interested in ordinary laboratory matter described by non-relativistic Quantum Mechanics, whose states will source a classical gravitational field according to semi-classical equations. Eventually we are interested in the question concerning the range of validity of such equations. Since we do not exclude the possibility that gravity might stay classical at the most fundamental level, we explicitly leave open the possibility that these equations stay valid even for strongly fluctuating states of matter.

Now, if we assume that a one-particle state ψ gravitates like a classical mass density $\widetilde{\rho}(\mathbf{x}) = m|\psi(\mathbf{x})|^2$, we immediately get the coupled equations (neglecting other external potentials for simplicity)

$$\mathrm{i}\hbar\partial_t\psi(t;\mathbf{x}) \;=\; \left(-\frac{\hbar^2}{2m}\Delta + V_{\mathrm{g}}(t;\mathbf{x})\right)\,\psi(t;\mathbf{x})\,, \tag{1a}$$

$$\Delta V_{\mathrm{g}}(t;\mathbf{x}) \;=\; 4\pi\,G\,m^2\,|\psi(t;\mathbf{x})|^2\,. \tag{1b}$$

These equations are known as the (one-particle) *Schrödinger-Newton system*. This system can be transformed into a single, non-liner and non-local equation for ψ by first solving (1b) with boundary condition that ϕ be zero at spatial infinity, which leads to

$$V_{\mathrm{g}}(t;\mathbf{x}) = -Gm^2\int\frac{|\psi(t;\mathbf{x}')|^2}{\|\mathbf{x}-\mathbf{x}'\|}\,\mathrm{d}^3\mathbf{x}'\,. \tag{2}$$

Inserting (2) into (1a) results in the one-particle *Schrödinger-Newton equation*:

$$\mathrm{i}\hbar\partial_t\psi(t;\mathbf{x}) \;=\; \left(-\frac{\hbar^2}{2m}\Delta - Gm^2\int\frac{|\psi(t;\mathbf{x}')|^2}{\|\mathbf{x}-\mathbf{x}'\|}\,\mathrm{d}^3\mathbf{x}'\right)\,\psi(t;\mathbf{x})\,. \tag{3}$$

Concerning the theoretical foundation of (3), the non-linear self interaction should essentially be seen as a falsifiable hypothesis on the gravitational interaction of matter fields, where the reach of this hypothesis delicately depends on the kind of "fields" it is supposed to cover. For example, (3) has been shown to follow in a suitable non-relativistic limit from the Einstein–Klein-Gordon or Einstein-Dirac systems [3], i. e., systems where the energy-momentum tensor $T_{\mu\nu}$ on the right-hand side of Einstein's equations,

$$R_{\mu\nu} - \tfrac{1}{2}g_{\mu\nu}R = \frac{8\pi G}{c^4}\,T_{\mu\nu}\,, \tag{4}$$

is built from classical Klein-Gordon or classical Dirac fields. Such an expression for $T_{\mu\nu}$ results from the expectation value $\langle\psi|\hat{T}_{\mu\nu}|\psi\rangle$ in Quantum-Field Theory, where ψ labels the amplitude (wave function) of a one-particle state, $\hat{T}_{\mu\nu}$ is the operator-valued energy-momentum tensor which has been suitably regularised.‡ The non-relativistic

‡ Defining a suitably regularised energy-momentum operator of a quantum field in curved space-time is a non-trivial issue; see, e. g., [4].

limit is then simply the (regularised) mass density operator whose expectation value in a one-particle state is $m|\psi|^2$; see e. g. [5].

Now, if we believe that there exists an underlying quantum theory of gravity of which the semi-classical Einstein equation (4) with $T_{\mu\nu}$ replaced by $\langle\psi|\hat{T}_{\mu\nu}|\psi\rangle$ is only an approximation, then this will clearly only make sense in situations where the source-field for gravity, which is an operator, may be replaced by its mean-field approximation. This is the case in many-particle situations, i. e., where ψ is a many-particle amplitude, and then only in the limit as the particle number tends to infinity. From that perspective it would make little sense to use one-particle expectation values on the right hand side of Einstein's equation, for their associated classical gravitational field according to (4) will not be any reasonable approximation of the (strongly fluctuating) fundamentally quantum gravitational field. This has been rightfully stressed recently [5, 6].

On the other hand, if we consider the possibility that gravity stays fundamentally classical, as we wish to do so here, then we are led to contemplate the strict (and not just approximate) sourcing of gravitational fields by expectation values rather than operators. In this case we *do* get non-linear self-interactions due to gravity in the equations, even for the one-particle amplitudes. Note that it would clearly not be proper to regard these amplitudes as classical fields and once more (second) quantise them. This is an important conceptual point that seems to have caused some confusion recently. We will therefore briefly return to this issue at the end of section 2. Also recall that the often alleged existing evidences, experimental [7] or conceptual [8], are generally found inconclusive, e. g., [9, 10, 11].

Taken as a new hypothesis for the gravitational interaction of matter, the Schrödinger-Newton equation has attracted much attention in recent years. First of all, it raises the challenge to experimentally probe the consequences of the non-linear gravitational self-interaction term [12]. More fundamentally, the verification of the existence of this semi-classical self-interaction could shed new light on the holy grail of theoretical physics: Quantum Gravity and its alleged necessity; compare [2]. And even though the original numerical estimates made in [12] were too optimistic by many orders of magnitude, there is now consensus as to the prediction of (3) concerning gravity-induced inhibition of quantum-mechanical dispersion [13].

However, concerning the current and planned interference experiments, it must be stressed that they are made with extended objects, like large molecules or tiny "nano-spheres" [14], and that the so-called "large superpositions" concern only the centre-of-mass part of the overall multi-particle wave-function. But even if we assume the elementary constituents in isolation to obey (3), there is still no obvious reason why the centre of mass of a compound object would obey a similar equation. These equations are non-linear and "separating off" degrees of freedom is not as obvious a procedure as in the linear case. The study of this issue is the central concern of this paper. For this we start afresh from a multi-particle version of the Schrödinger-Newton equation.

2. The many-particle Schrödinger-Newton equation

In this paper we consider the $(N+1)$-particle Schrödinger-Newton equation for a function $\Psi : \mathbb{R}^{1+3(N+1)} \to \mathbb{C}$, where $3(N+1)$ arguments correspond to the 3 coordinates each of $(N+1)$ particles of masses $m_0, m_1, \cdots, m_N$, and one argument is given by the (Newtonian absolute) time t. In presence of non-gravitational 2-body interactions represented by potentials $V_{ab}\big(\|\mathbf{x}_a - \mathbf{x}_b\|\big)$, where $V_{ab} = V_{ba}$, for the pair labelled by (ab), the $(N+1)$-particle Schrödinger-Newton equation reads in full glory

$$\begin{aligned} \mathrm{i}\hbar\partial_t \Psi(t;\mathbf{x}_0,\cdots,\mathbf{x}_N) = \Big(&-\sum_{a=0}^{N} \frac{\hbar^2}{2m_a}\Delta_a + \sum_{a=0}^{N}\sum_{b>a}^{N} V_{ab}\big(\|\mathbf{x}_a-\mathbf{x}_b\|\big) \\ &- G\sum_{a=0}^{N}\sum_{b=0}^{N} m_a m_b \left\{\int \prod_{c=0}^{N} \mathrm{d}^3\mathbf{x}'_c\right\} \frac{|\Psi(t;\mathbf{x}'_0,\cdots,\mathbf{x}'_N)|^2}{\|\mathbf{x}_a-\mathbf{x}'_b\|}\Big)\Psi(t;\mathbf{x}_0,\cdots\mathbf{x}_N)\,. \end{aligned} \tag{5}$$

Here and in the sequel, we write

$$\mathrm{d}^3\mathbf{x}_c := \mathrm{d}x^1_c \wedge \mathrm{d}x^2_c \wedge \mathrm{d}x^3_c \quad \text{and} \quad \prod_{c=0}^{N} \mathrm{d}^3\mathbf{x}_c := \mathrm{d}^3\mathbf{x}_0 \wedge \cdots \wedge \mathrm{d}^3\mathbf{x}_N\,. \tag{6}$$

The second, non-linear and non-local potential term is meant to represent the gravitational interaction according to a suggestion first made in [15]. The structure of this term seems rather complicated, but the intuition behind it is fairly simple:

Assumption 1 *Each particle represents a mass distribution in physical space that is proportional to its marginal distribution derived from $\Psi(t;\mathbf{x}_0,\cdots,\mathbf{x}_N)$. More precisely, the mass distribution represented by the b-th particle is*

$$\begin{aligned} \widetilde{\rho}_b(t;\mathbf{x}) &= m_b \left\{\int \prod_{\substack{c=0\\c\neq b}}^{N} \mathrm{d}^3\mathbf{x}_c\right\} |\Psi(t;\mathbf{x}_0,\cdots,\mathbf{x}_{b-1},\mathbf{x},\mathbf{x}_{b+1},\cdots,\mathbf{x}_N)|^2 \\ &= m_b \left\{\int \prod_{c=0}^{N} \mathrm{d}^3\mathbf{x}_c\right\} \delta^{(3)}(\mathbf{x}-\mathbf{x}_b)\,|\Psi(t;\mathbf{x}_0,\cdots,\mathbf{x}_N)|^2 \end{aligned} \tag{7}$$

Assumption 2 *The total gravitational potential Φ at $\mathbf{x}$ in physical space is that generated by the sum of the mass distributions* (7) *according to Newtonian gravity. More precisely, the Newtonian gravitational potential is given by*

$$\Phi(t;\mathbf{x}) = -G\int \mathrm{d}^3\mathbf{x}' \frac{\sum_{b=0}^{N}\widetilde{\rho}_b(t;\mathbf{x}')}{\|\mathbf{x}-\mathbf{x}'\|} \tag{8}$$

Assumption 3 *The gravitational contribution $V_{\mathrm{g}}(\mathbf{x}_0,\cdots,\mathbf{x}_N)$ that enters the Hamiltonian in the multi-particle Schrödinger equation*

$$\begin{aligned} \mathrm{i}\hbar\partial_t \psi(t;\mathbf{x}_0,\cdots,\mathbf{x}_N) = \Big(&-\sum_{a=0}^{N}\frac{\hbar^2}{2m_a}\Delta_a + V_{\mathrm{other}}(t;\mathbf{x}_0,\cdots,\mathbf{x}_N) \\ &+ V_{\mathrm{g}}(t;\mathbf{x}_0,\cdots,\mathbf{x}_N)\Big)\Psi(t;\mathbf{x}_0,\cdots,\mathbf{x}_N)\,. \end{aligned} \tag{9}$$

is the sum of the gravitational potential energies of $(N+1)$ *point-particles (sic!) of masses* m_a *situated at positions* $\mathbf{x}_a$*. More precisely, the total gravitational contribution to the Hamiltonian is*

$$V_{\rm g}(t;\mathbf{x}_0,\cdots,\mathbf{x}_N)=\sum_{a=0}^{N} m_a\Phi(t;\mathbf{x}_a) \tag{10}$$

where Φ *is given by* (8)*.*

Taken together, all three assumptions result in a gravitational contribution to the Hamiltonian of

$$V_{\rm g}(t;\mathbf{x}_0,\cdots,\mathbf{x}_N)=-G\sum_{a=0}^{N}\sum_{b=0}^{N} m_a m_b\left\{\int\prod_{c=0}^{N}\mathrm{d}^3\mathbf{x}'_c\right\}\frac{|\Psi(t;\mathbf{x}'_0,\cdots,\mathbf{x}'_N)|^2}{\|\mathbf{x}_a-\mathbf{x}'_b\|} \tag{11}$$

just as in (5). We note that (5) can be derived from a Lagrangian

$$L=T-U \tag{12}$$

where the kinetic part§, T, is

$$\begin{aligned} T=&\frac{\mathrm{i}\hbar}{2}\left\{\int\prod_{a=0}^{N}\mathrm{d}^3\mathbf{x}_a\right\}\left(\bar\Psi\partial_t\Psi-\Psi\partial_t\bar\Psi\right)\\ &+\hbar^2\left\{\int\prod_{a=0}^{N}\mathrm{d}^3\mathbf{x}_a\right\}\sum_{b=0}^{N}\frac{1}{m_b}\nabla_b\bar\Psi\cdot\nabla_b\Psi\,. \end{aligned} \tag{13}$$

Here all functions are taken at the same argument $(t;\mathbf{x}_0,\cdots,\mathbf{x}_N)$, which we suppressed. The potential part, U, consists of a sum of two terms. The first term represents possibly existent 2-body interactions, like, e. g., electrostatic energy:

$$U^{\text{local 2-body}}=\left\{\int\prod_{c=0}^{N}\mathrm{d}^3\mathbf{x}_c\right\}\sum_{a=0}^{N}\sum_{b>a}^{N}V_{ab}(t;\mathbf{x}_0,\cdots,\mathbf{x}_N)\,|\Psi(t;\mathbf{x}_0,\cdots,\mathbf{x}_N)|^2 \tag{14}$$

The second contribution is that of gravity:

$$\begin{aligned} U^{\rm grav}=&-\frac{G}{2}\left\{\int\prod_{c=0}^{N}\mathrm{d}^3\mathbf{x}_c\right\}\left\{\int\prod_{d=0}^{N}\mathrm{d}^3\mathbf{x}'_d\right\}\sum_{a=0}^{N}\sum_{b=0}^{N}m_a m_b\\ &\times\frac{|\Psi(t;\mathbf{x}_0,\cdots,\mathbf{x}_N)|^2|\Psi(t;\mathbf{x}'_0,\cdots,\mathbf{x}'_N)|^2}{\|\mathbf{x}_a-\mathbf{x}'_b\|}\\ =&-\frac{G}{2}\sum_{a=0}^{N}\sum_{b=0}^{N}\int\mathrm{d}^3\mathbf{x}\int\mathrm{d}^3\mathbf{x}'\quad\frac{\widetilde\rho_a(\mathbf{x})\,\widetilde\rho_b(\mathbf{x}')}{\|\mathbf{x}-\mathbf{x}'\|} \end{aligned} \tag{15}$$

§ In classical field theory it would be physically more natural to regard the second part of the kinetic term $\propto|\nabla\Psi|^2$ as part of the potential energy. In Quantum Mechanics, however, it represents the kinetic energy of the particles.

The last line shows that the gravitational energy is just the usual binding energy of $(N+1)$ lumps of matter distributed in physical space according to (7). Note that the sum not only contains the energies for the mutual interactions between the lumps, but also the self-energy of each lump. The latter are represented by the diagonal terms in the double sum, i. e. the terms where $a = b$. These self-energy contributions would diverge for pointlike mass distributions, i. e. if $\widetilde{\rho}_a(\mathbf{x}) = m_a \delta^{(3)}(\mathbf{x} - \mathbf{x}_a)$, as in the case of electrostatic interaction (see below). Here, however, the hypotheses underlying the three assumptions above imply that gravitationally the particles interact differently, resulting in finite self-energies. Because of these self-energies we already obtain a modification of the ordinary Schrödinger equation in the one-particle case, which is just given by (3). Explicit expressions for the double integrals over $\widetilde{\rho}_a(\mathbf{x})\widetilde{\rho}_b(\mathbf{x}')/\|\mathbf{x}-\mathbf{x}'\|$ can, e. g., be found in [16] for some special cases where $\widetilde{\rho}_a$ and $\widetilde{\rho}_b$ are spherically symmetric.

Finally we wish to come back to the fundamental issue already touched upon in the introduction, namely of how to relate the interaction term (15) to known physics as currently understood. As already emphasised in the context of (3), i. e. for just one particle, the gravitational interaction contains self-energy contributions. In the multi-particle scheme they just correspond to the diagonal terms $a = b$ in (15). These terms are certainly finite for locally bounded $\widetilde{\rho}_a$.

This would clearly not be the case in a standard quantum field-theoretic treatment, like QED, outside the mean-field limit. In non-relativistic Quantum Field Theory the interaction Hamiltonian would be a double integral over $\Psi^\dagger(\mathbf{x})\Psi(\mathbf{x})\Psi^\dagger(\mathbf{x}')\Psi(\mathbf{x}')/\|\mathbf{x}-\mathbf{x}'\|$, where Ψ is the (non-relativistic) field operator. (See, e. g., chpater 11 of [17] for a textbook account of non-relativistic QFT.) This term will lead to divergent self energies, which one renormalises through normal ordering, and pointwise Coulomb interactions of pairs. This is just the known and accepted strategy followed in deriving the multi-particle Schrödinger equation for charged point-particles from QED. This procedure has a long history. In fact, it can already be found in the Appendix of Heisenberg's 1929 Chicago lectures [18] on Quantum Mechanics.

It has therefore been frequently complained that the Schrödinger-Newton equation does *not* follow from "known physics" [19, 20, 5, 6]. This is true, of course. But note that this does not imply the sharper argument according to which the Schrödinger-Newton equation even contradicts known physics. Such sharper arguments usually beg the question by assuming some form of quantum gravity to exist. But this hypothetical theory is not yet part of "known physics" either, and may never be! Similarly, by rough analogy of the classical fields in gravity and electromagnetism, the Schrödinger-Newton equation is sometimes argued to contradict known physics because the analogous non-linear "Schrödinger-Coulomb" equation yields obvious nonsense, like a grossly distorted energy spectrum for hydrogen. In fact, this has already been observed in 1927 by Schrödinger who wondered about this factual contradiction with what he described as a natural demand (self coupling) from a classical field-theoretic point of view [21]. Heisenberg in his 1929 lectures also makes this observation which he takes as irrefutable evidence for the need to (second) quantise the Schrödinger field, thereby turning a non-

linear "classical" field theory into a linear quantum version of it.

To say it once more: all this is only an argument against the Schrödinger-Newton equation provided we assume an underlying theory of quantum gravity to exist and whose effective low energy approximation can be dealt with in full analogy to, say, QED. But our attitude here is different! What we have is a hypothesis that is essentially based on the assumption that gravity behaves differently as regards its coupling to matter and, in particular, its need for quantisation. The interesting aspect of this is that it gives rise to potentially observable consequences that render this hypothesis falsifiable.

3. Centre-of-mass coordinates

Instead of the $(N+1)$ positions $\mathbf{x}_a$, $a = 0, \cdots, N$, in absolute space, we introduce the centre of mass and N positions relative to it. We write

$$M := \sum_{a=0}^{N} m_a \tag{16}$$

for the total mass and adopt the convention that greek indices $\alpha, \beta, \cdots$ take values in $\{1, \cdots, N\}$, in contrast to latin indices $a, b, \cdots$, which we already agreed to take values in $\{0, 1, \cdots, N\}$. The centre-of-mass and the relative coordinates of the N particles labelled by $1, \cdots, N$ are given by (thereby distinguishing the particle labelled by 0)

$$\mathbf{c} \;:=\; \frac{1}{M}\sum_{a=0}^{N} m_a\,\mathbf{x}_a = \frac{m_0}{M}\mathbf{x}_0 + \sum_{\beta=1}^{N}\frac{m_\beta}{M}\mathbf{x}_\beta\,, \tag{17a}$$

$$\mathbf{r}_\alpha \;:=\; \mathbf{x}_\alpha - \mathbf{c} = -\frac{m_0}{M}\,\mathbf{x}_0 + \sum_{\beta=1}^{N}\Big(\delta_{\alpha\beta} - \frac{m_\beta}{M}\Big)\,\mathbf{x}_\beta \tag{17b}$$

The inverse transformation is obtained by simply solving (17) for $\mathbf{c}$ and $\mathbf{r}_\alpha$:

$$\mathbf{x}_0 = \mathbf{c} - \sum_{\beta=1}^{N}\frac{m_\beta}{m_0}\,\mathbf{r}_\beta\,, \tag{18a}$$

$$\mathbf{x}_\alpha = \mathbf{c} + \mathbf{r}_\alpha\,. \tag{18b}$$

All this may be written in a self-explanatory $(1+N)$ split matrix form

$$\begin{pmatrix}\mathbf{c}\\ \mathbf{r}_\alpha\end{pmatrix} = \begin{pmatrix}\frac{m_0}{M} & \frac{m_\beta}{M}\\ -\frac{m_0}{M} & \delta_{\alpha\beta} - \frac{m_\beta}{M}\end{pmatrix}\begin{pmatrix}\mathbf{x}_0\\ \mathbf{x}_\beta\end{pmatrix}\,, \tag{19}$$

$$\begin{pmatrix}\mathbf{x}_0\\ \mathbf{x}_\alpha\end{pmatrix} = \begin{pmatrix}1 & -\frac{m_\beta}{m_0}\\ 1 & \delta_{\alpha\beta}\end{pmatrix}\begin{pmatrix}\mathbf{c}\\ \mathbf{r}_\beta\end{pmatrix}\,. \tag{20}$$

For the wedge product of the $(N+1)$ 1-forms $\mathrm{d}x^1_a$ for $a = 0, 1, \cdots, N$ we easily get

from (18)

$$\begin{aligned} \mathrm{d}x^1_0 \wedge \cdots \wedge \mathrm{d}x^1_N &= \left(\mathrm{d}c^1 - \sum_{\beta=1}^{N} \frac{m_\beta}{m_0} \mathrm{d}r^1_\beta\right) \wedge \left(\mathrm{d}c^1 + \mathrm{d}r^1_1\right) \wedge \cdots \wedge \left(\mathrm{d}c^1 + \mathrm{d}r^1_N\right) \\ &= \frac{M}{m_0}\left(\mathrm{d}c^1 \wedge \mathrm{d}r^1_1 \wedge \cdots \wedge \mathrm{d}r^1_N\right) . \end{aligned} \tag{21}$$

Hence, writing $\mathrm{d}^3\mathbf{x}_\alpha := \mathrm{d}x^1_\alpha \wedge \mathrm{d}x^2_\alpha \wedge \mathrm{d}x^3_\alpha$ and $\prod_{\alpha=1}^{N}$ for the N-fold wedge product, we have

$$\prod_{a=0}^{N} \mathrm{d}^3\mathbf{x}_a = \left(\frac{M}{m_0}\right)^3 \left(\mathrm{d}^3\mathbf{c} \wedge \prod_{\alpha=1}^{N} \mathrm{d}^3\mathbf{r}_\alpha\right) . \tag{22}$$

Note that the sign changes that may appear in rearranging the wedge products on both sides coincide and hence cancel. From (22) we can just read off the determinant of the Jacobian matrix for the transformation (18):

$$\left|\frac{\partial(\mathbf{x}_0, \mathbf{x}_\alpha)}{\partial(\mathbf{c}, \mathbf{r}_\beta)}\right| := \det\left\{\frac{\partial(\mathbf{x}_0, \mathbf{x}_\alpha)}{\partial(\mathbf{c}, \mathbf{r}_\beta)}\right\} = \left(\frac{M}{m_0}\right)^3 . \tag{23}$$

Equation (18) also allows to simply rewrite the kinetic-energy metric

$$G = \sum_{a=0}^{N}\sum_{b=0}^{N} G_{ab}\, \mathrm{d}\mathbf{x}_a \otimes \mathrm{d}\mathbf{x}_b := \sum_{a=0}^{N} m_a\, \mathrm{d}\mathbf{x}_a \otimes \mathrm{d}\mathbf{x}_a \tag{24}$$

in terms of the new coordinates: It is given by

$$\begin{aligned} G = m_0 &\left(\mathrm{d}\mathbf{c} - \sum_{\alpha=1}^{N} \frac{m_\alpha}{m_0} \mathrm{d}\mathbf{r}_\alpha\right) \otimes \left(\mathrm{d}\mathbf{c} - \sum_{\beta=1}^{N} \frac{m_\beta}{m_0} \mathrm{d}\mathbf{r}_\beta\right) \\ &+ \sum_{\alpha=1}^{N} m_\alpha\left(\mathrm{d}\mathbf{c} + \mathrm{d}\mathbf{r}_\alpha\right) \otimes \left(\mathrm{d}\mathbf{c} + \mathrm{d}\mathbf{r}_\alpha\right) \\ = M\, \mathrm{d}\mathbf{c} \otimes \mathrm{d}\mathbf{c} &+ \sum_{\alpha=1}^{N}\sum_{\beta=1}^{N} H_{\alpha\beta}\, \mathrm{d}\mathbf{r}_\alpha \otimes \mathrm{d}\mathbf{r}_\beta . \end{aligned} \tag{25}$$

The first thing to note is that there are no off-diagonal terms, i. e. terms involving tensor products between $\mathrm{d}\mathbf{c}$ and $\mathrm{d}\mathbf{r}_\alpha$. This means that the degrees of freedom labelled by our $\mathbf{r}_a$ coordinates are perpendicular (with respect to the kinetic-energy metric) to the centre-of-mass motion. The restriction of the kinetic-energy metric to the relative coordinates has the components

$$H_{\alpha\beta} = \left(\frac{m_\alpha m_\beta}{m_0} + m_\alpha \delta_{\alpha\beta}\right) . \tag{26}$$

The determinant of $\{H_{\alpha\beta}\}$ follows from taking the determinant of the transformation formula for the kinetic-energy metric (taking due account of the 3-fold multiplicities hidden in the inner products in $\mathbb{R}^3$)

$$\left(\det\{G_{ab}\}\right)^3 \times \left|\frac{\partial(\mathbf{x}_0, \mathbf{x}_\alpha)}{\partial(\mathbf{c}, \mathbf{r}_\beta)}\right|^2 = M^3 \times \left(\det\{H_{\alpha\beta}\}\right)^3 \tag{27}$$

which, using (23) and $\det\{G_{ab}\} = \prod_{a=0}^{N}(m_a/2)$, results in

$$\det\{H_{\alpha\beta}\} = \frac{M}{m_0^2}\prod_{a=0}^{N} m_a\,. \tag{28}$$

Finally we consider the inverse of the kinetic-energy metric:

$$G^{-1} = \sum_{a=0}^{N}\sum_{b=0}^{N} G^{ab}\frac{\partial}{\partial \mathbf{x}_a}\otimes\frac{\partial}{\partial \mathbf{x}_b} = \sum_{a=0}^{N}\frac{1}{m_a}\frac{\partial}{\partial \mathbf{x}_a}\otimes\frac{\partial}{\partial \mathbf{x}_a} \tag{29}$$

Using (17) we have

$$\frac{\partial}{\partial \mathbf{x}_0} = \frac{m_0}{M}\left(\frac{\partial}{\partial \mathbf{c}} - \sum_{\alpha=1}^{N}\frac{\partial}{\partial \mathbf{r}_\alpha}\right), \tag{30a}$$

$$\frac{\partial}{\partial \mathbf{x}_\alpha} = \frac{\partial}{\partial \mathbf{r}_\alpha} + \frac{m_\alpha}{M}\left(\frac{\partial}{\partial \mathbf{c}} - \sum_{\beta=1}^{N}\frac{\partial}{\partial \mathbf{r}_\beta}\right). \tag{30b}$$

Inserting this into (29) we obtain the form

$$G^{-1} = \frac{1}{M}\frac{\partial}{\partial \mathbf{c}}\otimes\frac{\partial}{\partial \mathbf{c}} + \sum_{\alpha=1}^{N}\sum_{\beta=1}^{N} H^{\alpha\beta}\frac{\partial}{\partial \mathbf{r}_\alpha}\otimes\frac{\partial}{\partial \mathbf{r}_\beta}\,, \tag{31}$$

where $\{H^{\alpha\beta}\}$ is the inverse matrix to $\{H_{\alpha\beta}\}$, which turns out to be surprisingly simple:

$$H^{\alpha\beta} = \left(m_\alpha^{-1}\,\delta_{\alpha\beta} - M^{-1}\right). \tag{32}$$

In fact, the relation $\sum_{\beta=1}^{N} H_{\alpha\beta}H^{\beta\gamma} = \delta_\alpha^\gamma$ is easily checked from the given expressions.

Note that the kinetic part in (5) is just $(-\hbar^2/2)$ times the Laplacian on $\mathbb{R}^{3(N+1)}$ with respect to the kinetic-energy metric. Since $\det(G)$ and $\det(H)$ are constant, this Laplacian is just:

$$\begin{aligned}\Delta_G &= \sum_{a=0}^{N}\sum_{b=0}^{N} G^{ab}\frac{\partial}{\partial \mathbf{x}_a}\cdot\frac{\partial}{\partial \mathbf{x}_b} = \sum_{a=0}^{N}\frac{1}{m_a}\frac{\partial}{\partial \mathbf{x}_a}\cdot\frac{\partial}{\partial \mathbf{x}_a}\\ &= \frac{1}{M}\frac{\partial}{\partial \mathbf{c}}\cdot\frac{\partial}{\partial \mathbf{c}} + \sum_{\alpha=1}^{N}\sum_{\beta=1}^{N} H^{\alpha\beta}\frac{\partial}{\partial \mathbf{r}_\alpha}\cdot\frac{\partial}{\partial \mathbf{r}_\beta}\\ &=: \Delta_c + \Delta_r\,.\end{aligned} \tag{33}$$

Here Δ_c is the part just involving the three centre-of-mass coordinates $\mathbf{c}$ and Δ_r the part involving the derivatives with respect to the $3N$ relative coordinates $\mathbf{r}_\alpha$. Note that there are no terms that mix the derivatives with repect to $\mathbf{c}$ and $\mathbf{r}_\alpha$, but that Δ_r mixes any two derivatives with respect to $\mathbf{r}_\alpha$ due to the second term on the right-hand side of (32). Clearly, a further linear redefinition of the relative coordinates $\mathbf{r}_\alpha$ could be employed to diagonalise $H_{\alpha\beta}$ and $H^{\alpha\beta}$, but that we will not need here.

4. Schrödinger-Newton effect on the centre of mass

Having introduced the centre-of-mass coordinates, one can consider the possibility that the wave-function separates into a centre-of-mass and a relative part,‖

$$\Psi(t;\mathbf{x}_0,\cdots,\mathbf{x}_N)=\left(\frac{m_0}{M}\right)^{3/2}\psi(t;\mathbf{c})\,\chi(t;\mathbf{r}_1,\cdots,\mathbf{r}_N)\,. \tag{34}$$

In order to obtain an independent equation for just the centre-of-mass dynamics one is, however, left with the necessity to show that equation (5) also separates for this ansatz. This is true for the kinetic term, as shown in (33), and it is also obvious for the non-gravitational contribution V_{ab} which depends on the relative distances, and therefore the relative coordinates, only.

As long as non-gravitational interactions are present these are presumably much stronger than any gravitational effects. Hence, the latter can be ignored for the *relative* motion, which leads to a usually complicated but well-known equation: the ordinary, linear Schrödinger equation whose solution becomes manifest in the inner structure of the present lump of matter.

However, while separating the linear multi-particle Schrödinger equation in the absence of external forces (i. e. equation (5) with the gravitational constant G set to zero) yields a free Schrödinger equation for the evolution of the centre of mass, the $(N+1)$-particle Schrödinger-Newton equation (5) will comprise contributions of the gravitational potential to the centre-of-mass motion. The reason for these to appear is the non-locality of the integral term in the equation (and not the mere existence of the diagonal term $a=b$ as one could naively assume).

Let us take a closer look at the gravitational potential (11). Using the results from the previous section, in centre-of-mass coordinates it reads:

$$\begin{aligned}V_{\mathrm{g}}(t;\mathbf{c},\mathbf{r}_1,\cdots,\mathbf{r}_N)=-G\int \mathrm{d}^3\mathbf{c}'|\psi(t;\mathbf{c}')|^2\left\{\int\prod_{\gamma=1}^{N}\mathrm{d}^3\mathbf{r}'_\gamma\right\}\\ \times\Bigg[m_0^2\frac{|\chi(t;\mathbf{r}'_1,\cdots,\mathbf{r}'_N)|^2}{\|\mathbf{c}-\mathbf{c}'-\sum_{\delta=1}^{N}\frac{m_\delta}{m_0}\left(\mathbf{r}_\delta-\mathbf{r}'_\delta\right)\|}\\ +m_0\sum_{\alpha=1}^{N}m_\alpha\frac{|\chi(t;\mathbf{r}'_1,\cdots,\mathbf{r}'_N)|^2}{\|\mathbf{c}-\mathbf{c}'-\sum_{\delta=1}^{N}\frac{m_\delta}{m_0}\mathbf{r}_\delta-\mathbf{r}'_\alpha\|}\\ +m_0\sum_{\alpha=1}^{N}m_\alpha\frac{|\chi(t;\mathbf{r}'_1,\cdots,\mathbf{r}'_N)|^2}{\|\mathbf{c}-\mathbf{c}'+\mathbf{r}_\alpha+\sum_{\delta=1}^{N}\frac{m_\delta}{m_0}\mathbf{r}'_\delta\|}\\ +\sum_{\alpha=1}^{N}\sum_{\beta=1}^{N}m_\alpha m_\beta\frac{|\chi(t;\mathbf{r}'_1,\cdots,\mathbf{r}'_N)|^2}{\|\mathbf{c}-\mathbf{c}'+\mathbf{r}_\alpha-\mathbf{r}'_\beta\|}\Bigg]\,.\end{aligned} \tag{35}$$

The m_0 dependent terms in the second, third, and fourth line are more intricate than those in the last line; but they are only $(2N+1)$ out of $(N+1)^2$ terms and therefore

‖ Here we include the square-root of the inverse of the Jacobian determinant (23) to allow for simultaneous normalisation to $\|\Psi\|=\|\psi\|=\|\chi\|=1$, which we imply in the following.

can be neglected for large N.¶ In this "large N"-approximation only the last double-sum in (35) survives. All $\mathbf{r}'_\gamma$ integrations except that where $\gamma = \beta$ can be carried out (obtaining the β-th marginal distributions for $|\chi(t;\mathbf{r}'_1,\cdots,\mathbf{r}'_N)|^2$). Because of the remaining integration over $\mathbf{r}'_\beta$ we may rename the integration variable $\mathbf{r}'_\beta \to \mathbf{r}'$, thereby removing its fictitious dependence on β. All this leads to the expression

$$V_{\mathrm{g}}(t;\mathbf{c},\mathbf{r}_1,\cdots,\mathbf{r}_N) = -G\sum_{\alpha=1}^{N} m_\alpha \int \mathrm{d}^3\mathbf{c}' \int \mathrm{d}^3\mathbf{r}' \frac{|\psi(t;\mathbf{c}')|^2\rho_c(\mathbf{r}')}{\|\mathbf{c}-\mathbf{c}'+\mathbf{r}_\alpha-\mathbf{r}'\|}\,, \tag{36}$$

where we defined

$$\rho_c(t;\mathbf{r}) := \sum_{\beta=1}^{N} m_\beta \left\{ \int \prod_{\substack{\gamma=1\\ \gamma\neq\beta}}^{N} \mathrm{d}^3\mathbf{r}_\gamma \right\} \; |\chi(t;\mathbf{r}_1,\cdots,\mathbf{r}_{\beta-1},\mathbf{r},\mathbf{r}_{\beta+1},\cdots,\mathbf{r}_N)|^2\,. \tag{37}$$

This "relative" mass distribution is built analogously to (7) from the marginal distributions, here involving only the relative coordinates of all but the zeroth particle. In the large N approximation this omission of m_0 should be neglected and $\rho_c(t;\mathbf{r})$ should be identified as the mass distribution relative to the centre of mass. Given a (stationary) solution χ of the Schrödinger equation for the relative motion, ρ_c is then simply the mass density of the present lump of matter (e. g. a molecule) relative to the centre of mass. Although for the following discussion the time-dependence of ρ_c makes no difference, we will omit it. This may be justified by an adiabatic approximation, since the typical frequencies involved in the relative motions are much higher than the frequencies involved in the centre-of-mass motion.

Note that the only approximation that entered the derivation of (36) so far is that of large N. For the typical situations we want to consider, where N is large indeed, this will be harmless. However, the analytic form taken by the gravitational potential in (36) is not yet sufficiently simple to allow for a separation into centre-of-mass and relative motion. In order to perform such a separation we have to get rid of the $\mathbf{r}_\alpha$-dependence. This can be achieved if further approximations are made, as we shall explain now.

5. Approximation schemes

5.1. Wide wave-functions

As long as the centre-of-mass wave-function is much wider than the extent of the considered object one can assume that it does not change much over the distance $\mathbf{r}_\alpha$, i. e. $|\psi(t;\mathbf{c}'+\mathbf{r}_\alpha)| \approx |\psi(t;\mathbf{c}')|$. Substituting $\mathbf{c}'$ by $\mathbf{c}'+\mathbf{r}_\alpha$ in (36) then yields the following potential, depending only on the centre-of-mass coordinate:

$$V_{\mathrm{g}}^{(A)}(t;\mathbf{c}) \approx -GM \int \mathrm{d}^3\mathbf{c}' \int \mathrm{d}^3\mathbf{r}' \, \frac{|\psi(t;\mathbf{c}')|^2\rho_c(\mathbf{r}')}{\|\mathbf{c}-\mathbf{c}'-\mathbf{r}'\|}\,. \tag{38}$$

¶ To be more distinct, assign the label "0" to that particle for which the absolute value of the sum of all $(2N+1)$ terms involving m_0 is the smallest. Then these terms can be estimated against all the others and the error made by their negligence is of the order $1/N$.

As a result, the equation for the centre of mass is now indeed of type (1) with $V_{\rm g} = V_{\rm g}^{(A)}$ being given by M times the convolution of $|\psi|^2$ with the Newtonian gravitational potential for the mass-density ρ_c. Case A has been further analysed in [22].

5.2. Born-Oppenheimer-Type approximation

An alternative way to get rid of the dependence of (36) on the relative coordinates, i. e., the $\mathbf{r}'_\alpha$-dependence on the right-hand side, is to just replace $V_{\rm g}$ with its expectation value in the state χ of the relative-motion.[+] This procedure corresponds to the Born-Oppenheimer approximation in molecular physics where the electronic degrees of freedom are averaged over in order to solve the dynamics of the nuclei. The justification for this procedure in molecular physics derives from the much smaller timescales for the motion of the fast and lighter electrons as compared to the slow and heavier nuclei. Hence the latter essentially move only according to the averaged potential sourced by the electrons. In case of the Schrödinger-Newton equation the justification is formally similar, even though it is clear that there is no real material object attached to the centre of mass. What matters is that the relative interactions (based on electrodynamic forces) are much stronger than the gravitational ones, so that the characteristic frequencies of the former greatly exceed those of the latter; compare, e. g., the discussion in [23].

Now, the expectation value is easily calculated:

$$\begin{aligned} V_{\rm g}^{(B)}(t;\mathbf{c}) &= \left\{\int \prod_{\beta=1}^{N} \mathrm{d}^3\mathbf{r}''_\beta\right\} |\chi(\mathbf{r}''_1,\cdots,\mathbf{r}''_N)|^2\; V_{\rm g}(t;\mathbf{c},\mathbf{r}''_1,\cdots,\mathbf{r}''_N) \\ &= -G\sum_{\alpha=1}^{N} m_\alpha \int \mathrm{d}^3\mathbf{c}' \int \mathrm{d}^3\mathbf{r}' \left\{\int \prod_{\beta=1}^{N} \mathrm{d}^3\mathbf{r}''_\beta\right\} \\ &\qquad\qquad \times \frac{|\psi(t;\mathbf{c}')|^2 \rho_c(\mathbf{r}') |\chi(\mathbf{r}''_1,\cdots,\mathbf{r}''_N)|^2}{\|\mathbf{c}-\mathbf{c}'-\mathbf{r}'+\mathbf{r}''_\alpha\|} \\ &= -G\int \mathrm{d}^3\mathbf{c}' \int \mathrm{d}^3\mathbf{r}' \int \mathrm{d}^3\mathbf{r}''\; \frac{|\psi(t;\mathbf{c}')|^2 \rho_c(\mathbf{r}')\rho_c(\mathbf{r}'')}{\|\mathbf{c}-\mathbf{c}'-\mathbf{r}'+\mathbf{r}''\|}\,. \end{aligned} \tag{39}$$

Note that this expression involves one more $\mathbb{R}^3$ integrations than (38).

In [22] we studied two simple models for the matter density ρ_c: a solid and a hollow sphere. The solid-sphere suffers from some peculiar divergence issues which we explain in Appendix B and is also mathematically slightly more difficult to handle than the hollow sphere whose radial mass distribution is just a δ-function. We therefore use the hollow sphere as a model to compare the two approximation ansätze given above.

While in [12, 2, 13, 22] the expression "collapse mass" was used in a rather loosely defined manner, here we define as critical mass the mass value for which at $t = 0$ the second order time derivative of the second moment $Q(t) = \int \mathrm{d}^3\mathbf{c}\,|\mathbf{c}|^2|\psi(t;\mathbf{c})|^2$ vanishes, i. e. $\ddot{Q}(t=0) = 0$. (Note that for a real-valued initial wave-packet the first order time derivative always vanishes.) For the one-particle Schrödinger-Newton equation and a

[+] We are grateful to Mohammad Bahrami for this idea.

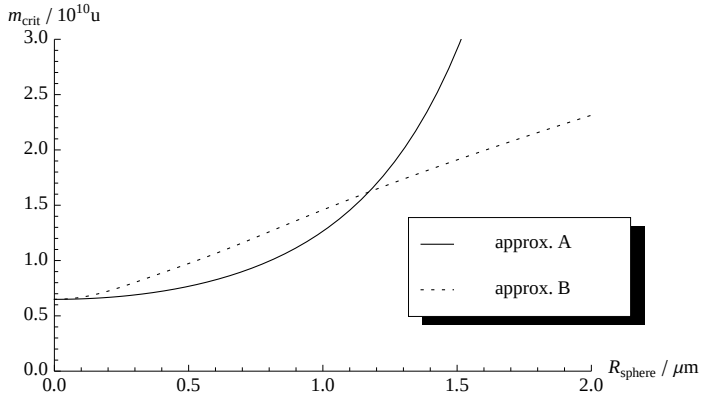

Figure 1. Critical mass for a hollow sphere as indicated by the behaviour of the second moment. We used a wave-packet width of $0.5\,\mu$m.

Gaussian wave packet of $0.5\,\mu$m width this yields a critical mass of $6.5 \times 10^9\,$u which fits very well with the numerical results obtained in [13].

For the hollow sphere we then obtain the analytic expression

$$m_{\mathrm{crit}} = \left(\sqrt{\frac{\pi}{2}}\,\frac{3\hbar^2}{G\,a\,f(R/a)}\right)^{1/3} \approx 5.153 \times 10^9\,\mathrm{u}\,\left((a/\mu\mathrm{m}) \times f\left(\frac{R}{a}\right)\right)^{-1/3} \tag{40}$$

for the critical mass. This expression is derived in Appendix A. The function f is constantly 1 in case of the one-particle Schrödinger-Newton equation and shows an exponential dependence on R in case of the wide wave-function approximation. In case of the Born-Oppenheimer approximation f is a rather complicated function that can be found in the appendix.

The resulting critical mass for a width of the centre-of-mass wave-function of $0.5\,\mu$m is plotted as a function of the hollow-sphere radius in figure 1. The curve that the figure shows for the wide wave-function approximation coincides well with the results we obtained in the purely numerical analysis in [22]. For the Born-Oppenheimer-Type approximation the plot shows a radius dependence of the collapse mass that is almost linear. This is in agreement with the result by Diósi [15] who estimates the width of the ground state for a *solid* sphere to be proportional to $(R/M)^{3/4}$.

5.3. Narrow wave-functions in the Born-Oppenheimer scheme

With the Born-Oppenheimer-Type approximation scheme just derived we now possess a tool with which we can consider the opposite geometric situation than that in Case A, namely for widths of the centre-of-mass wave-function ψ which are much smaller than the extensions (diameters of the support) of the matter distribution ρ_c, i. e., for well localised mass centres inside the bulk of matter.

Let us recall that in Newtonian gravitational physics the overall gravitational self-energy of a mass distribution $\widetilde{\rho}$ is given by

$$U_{\mathrm{g}}(\widetilde{\rho}) := -\frac{G}{2}\int \mathrm{d}^3\mathbf{x}\int \mathrm{d}^3\mathbf{x}'\,\frac{\widetilde{\rho}(\mathbf{x})\widetilde{\rho}(\mathbf{x}')}{\|\mathbf{x}-\mathbf{x}'\|}\,. \tag{41}$$

If $\widetilde{\rho} = \rho + \rho'$, we have by the simple quadratic dependence on $\widetilde{\rho}$

$$U_{\mathrm{g}}(\rho + \rho') := U_{\mathrm{g}}(\rho) + U_{\mathrm{g}}(\rho') + I_{\mathrm{g}}(\rho, \rho')\,, \tag{42}$$

where

$$I_{\mathrm{g}}(\rho, \rho') := -G \int \mathrm{d}^3\mathbf{x} \int \mathrm{d}^3\mathbf{x}' \, \frac{\rho(\mathbf{x})\rho'(\mathbf{x}')}{\|\mathbf{x} - \mathbf{x}'\|}\,. \tag{43}$$

represents the mutual gravitational *interaction* of the matter represented by ρ with that represented by ρ'. In the special case $\rho' = T_{\mathbf{d}}\rho$, where $T_{\mathbf{d}}$ denotes the operation of translation by the vector $\mathbf{d}$,

$$\big(T_{\mathbf{d}}\rho\big)(\mathbf{x}) := \rho(\mathbf{x} - \mathbf{d})\,, \tag{44}$$

we set

$$I_\rho(\mathbf{d}) := I_{\mathrm{g}}(\rho, T_{\mathbf{d}}\rho)\,. \tag{45}$$

It is immediate from (43) that $I_\rho : \mathbb{R}^3 \to \mathbb{R}$ has a zero derivative at the origin $\mathbf{0} \in \mathbb{R}^3$,

$$I'_\rho(\mathbf{0}) = 0\,, \tag{46}$$

and that it satisfies the following equivariance

$$I_\rho(R\mathbf{d}) = I_{\rho\circ R}(\mathbf{d}) \tag{47}$$

for any orthogonal 3×3 matrix R. The latter implies the rather obvious result that the function $\mathbf{d} \mapsto I_\rho(\mathbf{d})$ is rotationally invariant if ρ is a rotationally invariant distribution, i. e., the interaction energy depends only on the modulus of the shift, not its direction.

For example, given that ρ is the matter density of a homogeneous sphere of radius R and mass M,

$$\rho(\mathbf{x}) = \begin{cases} \frac{3M}{4\pi R^3} & \text{for } \|\mathbf{x}\| \le R \\ 0 & \text{for } \|\mathbf{x}\| > R\,, \end{cases} \tag{48}$$

the gravitational interaction energy is between two such identical distributions a distance $d := \|\mathbf{d}\|$ apart is

$$I_\rho(d) = -\frac{GM^2}{R} \times \begin{cases} \frac{6}{5} - 2\left(\frac{d}{2R}\right)^2 + \frac{3}{2}\left(\frac{d}{2R}\right)^3 - \frac{1}{5}\left(\frac{d}{2R}\right)^5 & \text{for } d \le 2R\,, \\ \frac{R}{d} & \text{for } d \ge 2R\,. \end{cases} \tag{49}$$

The second line is obvious, whereas the first line follows, e. g., from specialising the more general formula (42) of [16] to equal radii ($R_p = R_t$) and making the appropriate redefinitions in order to translate their electrostatic to our gravitational case. This formula also appears in [24].

Using the definitions (43) and (45), we can rewrite the right-hand side of (39) as convolution of $|\psi|^2$ with I_{ρ_c}:

$$V_{\mathrm{g}}^{(B)}(t;\mathbf{c}) = \int \mathrm{d}^3\mathbf{c}'\, I_{\rho_c}(\mathbf{c}-\mathbf{c}')\,|\psi(t;\mathbf{c}')|^2\,. \tag{50}$$

Since in equation (3) this potential is multiplied with $\psi(t,\mathbf{c})$, we see that only those values of $I_{\rho_c}(\mathbf{c}-\mathbf{c}')$ will contribute where $|\psi(t;\mathbf{c}')|^2\psi(t;\mathbf{c})$ appreciably differs from zero. Hence if ψ is concentrated in a region of diameter D then we need to know $I_{\rho_c}(\mathbf{c}-\mathbf{c}')$ only for $\|\mathbf{c}-\mathbf{c}'\| < D$. Assuming D to be small we expand I_{ρ_c} in a Taylor series. Because of (46) there is no linear term, so that up to and including the quadratic terms we have (using that $|\psi(t;\mathbf{c}')|^2$ is normalised with respect to the measure $\mathrm{d}^3\mathbf{c}'$)

$$V_{\mathrm{g}}^{(B)}(t;\mathbf{c}) \approx I_{\rho_c}(\mathbf{0}) + \tfrac{1}{2}I''_{\rho_c}(\mathbf{0})\cdot\Big(\mathbf{c}\otimes\mathbf{c} - 2\,\mathbf{c}\otimes\langle\mathbf{c}\rangle + \langle\mathbf{c}\otimes\mathbf{c}\rangle\Big)\,. \tag{51}$$

Here $I''_{\rho_c}(\mathbf{0})$ denotes the second derivative of the function $I_{\rho_c}:\mathbb{R}^3\to\mathbb{R}$ at $\mathbf{0}\in\mathbb{R}$ (which is a symmetric bilinear form on $\mathbb{R}^3$) and $\langle\,\cdot\,\rangle$ denotes the expectation value with respect to ψ. We stress that the non-linearity in ψ is now entirely encoded into this state dependence of the expectation values which appear in the potential. If, for simplicity, we only consider centre-of-mass motions in one dimension, the latter being coordinatised by $c\in\mathbb{R}$, then (51) simplifies to

$$\begin{aligned} V_{\mathrm{g}}^{(B)}(t;c) \;&\approx\; I_{\rho_c}(0) + \tfrac{1}{2}I''_{\rho_c}(0)\Big(c^2 - 2c\,\langle c\rangle + \langle c^2\rangle\Big) && \text{(52a)}\\ &=\; I_{\rho_c}(0) + \tfrac{1}{2}I''_{\rho_c}(0)\big(c-\langle c\rangle\big)^2 + \tfrac{1}{2}I''_{\rho_c}(0)\big(\langle c^2\rangle - \langle c\rangle^2\big)\,. && \text{(52b)}\end{aligned}$$

The first term, $I_{\rho_c}(0)$, just adds a constant to the potential which can be absorbed by adding $-(\mathrm{i}/\hbar)I_{\rho_c}(0)t$ to the phase ψ. The second term is the crucial one and has been shown in [23] to give rise to interesting and potentially observable for Gaussian states.

More precisely, consider a one-dimensional non-linear Schrödinger evolution of the form (1a) with V_{g} given by the second term in (52) and an additional external harmonic potential for the centre of mass, then we get the following non-linear Schrödinger-Newton equation for the centre-of-mass wave-function,

$$\mathrm{i}\hbar\partial_t\psi(t;c) = \left(-\frac{\hbar^2}{2M}\frac{\partial^2}{\partial c^2} + \tfrac{1}{2}M\omega_c^2c^2 + \tfrac{1}{2}M\omega_{\mathrm{SN}}^2\big(c-\langle c\rangle\big)^2\right)\psi(t;c)\,, \tag{53}$$

where $\omega_{\mathrm{SN}} := \sqrt{I''_{\rho_c}(0)/M}$ is called the Schrödinger-Newton frequency. This equation has been considered in [23], where the last term on the right-hand side of (52b) has been neglected for a priori no good reason. Note that $\langle c^2\rangle$ and $\langle c\rangle^2$ contain the wave function and hence are therefore not constant (in time). Now, in the context of [23] the consequences of interest were the evolution equations for the first and second moments in the canonical phase-space variables, and it shows that for them only spatial derivatives of the potential contribute. As a consequence, the term in question makes no difference. The relevant steps in the computation are displayed in Appendix C.

Based on the observation that equation (53) evolves Gaussian states into Gaussian states, it has then been shown that the covariance ellipse of the Gaussian state rotates at frequency $\omega_q := \sqrt{\omega_c^2 + \omega_{\mathrm{SN}}^2}$ whereas the centre of the ellipse orbits the origin in phase with frequency ω_c. This asynchrony results from a difference between first- and second-moment evolution and is a genuine effect of self gravity. It has been suggested that it may be observable via the output spectra of optomechanical systems [23].

6. Conclusions and outlook

Although the many-particle Schrödinger-Newton equation (5) does not exactly separate into centre-of-mass and relative motion, we could show that for some well-motivated approximations such a separation is possible. As long as the extent of an object is negligible in comparison to the uncertainty in localisation of its centre of mass the one-particle equation (3) is a good model in both approximation schemes considered.

In the opposite case of a well localised object, i. e. one that has a narrow wave-function compared to its extent, the gravitational potential takes the form (52) which yields a closed system of equations for the first and second moments and therefore the effects described in [23]. The non-linear Schrödinger equation resulting from the potential (52) is also considered in [24], where it is used for comparison of Schrödinger-Newton dynamics with models of quantum state reduction and decoherence.

The modification (38) provides a valid correction of the one-particle Schrödinger-Newton equation for objects of finite but small radii. This equation was considered in [25] and studied numerically in [22]. It remains unclear for which ratio of the object's extent to the width of the wave-function the Born-Oppenheimer-Type approximation (39) starts to be superior to the wide wave-function approximation. It may even be the better approximation throughout the whole range of possible object sizes and wave-functions since a Born-Oppenheimer like approximation is implicitly assumed also for the wide wave-function when the mass density is taken to be that of a solid object.

In passing we make the final technical remark that the analysis of the critical mass for the hollow sphere shows that this mass increases linearly with the radius R of the sphere. Given a fixed mass, this implies that the width of the stationary solution increases like $R^{3/4}$, a relation already found by Diósi [15].

The interface between Quantum Mechanics and gravity theory remains one of the most interesting and profound challenges with hopefully revealing experimental consequences, which we are only beginning to explore. In this context one should also mention that non-linear one-particle Schrödinger equations are of course also considered for Einstein-Bose condensates, in which case inclusion of self gravity adds a Schrödinger-Newton term in addition to that non-linear term obtained from the effective potential within the Hartree-Fock approximation (Gross-Pitaevskii-Newton equation). Such equations are derivable for particle numbers $N \to \infty$ without further hypotheses and may open up the possibility to test self-gravity effects on large quantum systems.

Recent experiments have demonstrated the high potential of atom interferometry on freely falling Einstein-Bose condensates [26] and it seems an interesting question whether this may be used to see self-gravity effects on such systems.

Acknowledgements

We gratefully acknowledge funding and support through the Center for Quantum Engineering and Space-Time Research (QUEST) at the Leibniz University Hannover and the Center of Applied Space Technology and Microgravity (ZARM) at the University of Bremen. AG is supported by the John Templeton foundation (grant 39530).

Appendix A. Comparison of approximations for spherically symmetric mass distributions

For both the wide wave-function approximation (38) and the Born-Oppenheimer-Type approximation (39) one must solve integrals of the type

$$I(\mathbf{a}) = \int \mathrm{d}^3\mathbf{r}\, \frac{\rho_c(\mathbf{r})}{\|\mathbf{r}-\mathbf{a}\|}\,. \tag{A.1}$$

In a spherically symmetric situation these take the form

$$\begin{aligned} I(a) &= \int_0^\infty r^2\,\mathrm{d}r \int_{-1}^1 \mathrm{d}\cos\theta \int_0^{2\pi} \mathrm{d}\varphi\, \frac{\rho_c(r)}{\sqrt{r^2+a^2-2ra\cos\theta}} \\ &= \frac{4\pi}{a}\int_0^a \mathrm{d}r\, r^2\,\rho_c(r) + 4\pi\int_a^\infty \mathrm{d}r\, r\,\rho_c(r)\,, \end{aligned} \tag{A.2}$$

where we write a for the absolute value $|\mathbf{a}|$, etc. If now we assume that ρ_c is the mass density of a hollow sphere of radius R, i. e.

$$\rho_c(r) = \frac{M}{4\pi\, r^2}\,\delta(r-R)\,, \tag{A.3}$$

these integrals simplify to

$$I_R(a) = \begin{cases} \frac{M}{R} & \text{if } a < R \\ \frac{M}{a} & \text{if } a \geq R \end{cases}\,. \tag{A.4}$$

With this the wide wave-function approximation (38) results in

$$V_{\mathrm{g}}^{(A)}(t;c;R) = -GM\int \mathrm{d}^3\mathbf{c}'\,|\psi(t;\mathbf{c}')|^2\, I_R(\|\mathbf{c}-\mathbf{c}'\|)\,. \tag{A.5}$$

On the other hand, the Born-Oppenheimer approximation (39) leads to

$$V_{\mathrm{g}}^{(B)}(t;c;R) = -G\int \mathrm{d}^3\mathbf{c}'\,|\psi(t;\mathbf{c}')|^2 \int \mathrm{d}^3\mathbf{r}'\,\rho_c(\mathbf{r}')\, I_R(\|\mathbf{c}-\mathbf{c}'-\mathbf{r}'\|)\,. \tag{A.6}$$

In order to be able to obtain an analytical result we consider the initial Gaussian wave packet

$$\psi(t=0;\mathbf{c}) = (\pi a^2)^{-3/4}\,\exp\left(-\frac{c^2}{2a^2}\right)\,, \tag{A.7}$$

for which these potentials take the form

$$\begin{aligned} V_A^0(c;R) = -\frac{GM^2}{2}\Bigg\{ & \frac{a}{\sqrt{\pi}\,c\,R}\left[\exp\left(-\frac{(c+R)^2}{a^2}\right) - \exp\left(-\frac{(c-R)^2}{a^2}\right)\right] \\ & + \frac{1}{c}\left[\operatorname{erf}\left(\frac{c+R}{a}\right) + \operatorname{erf}\left(\frac{c-R}{a}\right)\right] \\ & + \frac{1}{R}\left[\operatorname{erf}\left(\frac{c+R}{a}\right) - \operatorname{erf}\left(\frac{c-R}{a}\right)\right]\Bigg\} \end{aligned} \tag{A.8}$$

$$\begin{aligned} V_B^0(c;R) = -\frac{GM^2}{2}\Bigg\{ & \frac{a}{\sqrt{\pi}\,c}\left(\frac{1}{R} + \frac{8R}{3a^2}\right)\exp\left(-\frac{(c+2R)^2}{a^2}\right) \\ & + \frac{a}{\sqrt{\pi}\,R}\left(\frac{1}{2c} - \frac{1}{4R}\right)\left[\exp\left(-\frac{(c+2R)^2}{a^2}\right) - \exp\left(-\frac{(c-2R)^2}{a^2}\right)\right] \\ & + \frac{1}{c}\left[\operatorname{erf}\left(\frac{c+2R}{a}\right) + \operatorname{erf}\left(\frac{c-2R}{a}\right)\right] \\ & + \frac{1}{R}\left(1 - \frac{c}{4R} - \frac{a^2}{8cR}\right)\left[\operatorname{erf}\left(\frac{c+2R}{a}\right) - \operatorname{erf}\left(\frac{c-2R}{a}\right)\right]\Bigg\}. \end{aligned} \tag{A.9}$$

Note that both potentials agree in the limits

$$\lim_{R\to 0} V_{A,B}^0(c;R) = -\frac{GM^2}{c}\operatorname{erf}\left(\frac{c}{a}\right) \quad \text{and} \quad \lim_{R\to\infty} V_{A,B}^0(c;R) = 0\,. \tag{A.10}$$

As a measure to compare these potentials with each other and the one-particle Schrödinger-Newton equation we use the second moment $Q(t) = \int \mathrm{d}^3\mathbf{c}\,|\mathbf{c}|^2|\psi(t;\mathbf{c})|^2$. For a real wave packet its first order time derivative can be shown to vanish. Therefore the sign of the second order time derivative $\ddot{Q}$ at $t = 0$ determines if a wave packet initially shrinks or increases in width. In general the second order time derivative is

$$\ddot{Q}(t) = \int \mathrm{d}^3\mathbf{c}\left(\frac{2\hbar^2}{M^2}|\nabla\psi(t;\mathbf{c})|^2 + \frac{2}{M}V_{\mathrm{g}}(t;\mathbf{c})\left(3\,|\psi(t;\mathbf{c})|^2 + \mathbf{c}\cdot\nabla|\psi(t;\mathbf{c})|^2\right)\right) \tag{A.11}$$

which for the spherically symmetric gaussian state (A.7) takes the form

$$\ddot{Q}(t=0) = \frac{3\hbar^2}{M^2a^2} + \frac{8}{\sqrt{\pi}\,M\,a^5}\int_0^\infty \mathrm{d}c\,\exp\left(-\frac{c^2}{a^2}\right)\,V^0(c)\,\left(3a^2c^2 - 2c^4\right) \tag{A.12}$$

$$= \frac{3\hbar^2}{M^2a^2} - \sqrt{\frac{2}{\pi}}\frac{G\,M}{a}\,f\left(\frac{R}{a}\right)\,. \tag{A.13}$$

The critical mass defined by $\ddot{Q}(t=0)=0$ is then given by

$$m_{\mathrm{crit}} = \left(\sqrt{\frac{\pi}{2}}\,\frac{3\hbar^2}{G\,a\,f(R/a)}\right)^{1/3} \approx 5.153\times 10^9\,\mathrm{u}\,\left((a/\mu\mathrm{m})\times f\left(\frac{R}{a}\right)\right)^{-1/3}. \quad \text{(A.14)}$$

The function f is $f\equiv 1$ for the one-particle Schrödinger-Newton equation. For the hollow sphere potential in the wide wave-function and Born-Oppenheimer-Type approximations, (A.8) and (A.9), respectively, this function can be calculated as

$$f_A\left(\frac{R}{a}\right) = \exp\left(-\frac{R^2}{2a^2}\right) \quad \text{(A.15)}$$

$$\begin{aligned} f_B\left(\frac{R}{a}\right) = {} & \frac{2}{3}\sqrt{\frac{2}{\pi}}\exp\left(-\frac{4R^2}{a^2}\right)\frac{R}{a}\left(1-\left(\frac{2R}{a}\right)^2\right) \\ & +\exp\left(-\frac{2R^2}{a^2}\right)\left(1-\mathrm{erf}\left(\sqrt{2}\frac{R}{a}\right)\right)\left(1+\frac{1}{3}\left(\frac{2R}{a}\right)^4\right) \\ & +\frac{a^2}{2R^2}\left(\frac{1}{\sqrt{2}}\mathrm{erf}\left(2\frac{R}{a}\right)-\exp\left(-\frac{2R^2}{a^2}\right)\mathrm{erf}\left(\sqrt{2}\frac{R}{a}\right)\right). \end{aligned} \quad \text{(A.16)}$$

Appendix B. Divergence of the solid-sphere potential in the wide wave-function approximation

Given a spherically symmetric situation the wide wave-function approximation (38) takes the form

$$V(c) = (|\psi|^2 * \Phi)(c) = 4\pi\int_0^\infty \mathrm{d}c'\; c'^2\,|\psi(c')|^2\,\Phi(|c-c'|)\,, \quad \text{(B.1)}$$

where for the potential Φ we want to consider the following three cases:

- Coulomb potential (i. e. the case of the Schrödinger-Newton equation (3)):

$$\Phi_c(c) = -\frac{1}{c}\,, \quad \text{(B.2)}$$

- hollow sphere of radius R:

$$\Phi_h(c) = \begin{cases} -\frac{1}{R} & \text{if } c<R \\ \Phi_c(c) & \text{if } c\geq R \end{cases}, \quad \text{(B.3)}$$

- solid sphere of radius R:

$$\Phi_s(c) = \begin{cases} -\frac{3}{2R}+\frac{c^2}{2R^3} & \text{if } c<R \\ \Phi_c(c) & \text{if } c\geq R \end{cases}. \quad \text{(B.4)}$$

First we want to study the behaviour of $V_0 = V(c=0)$ for a Gaussian wave packet $|\psi(c)|^2 = \frac{1}{4\pi}\exp(-c^2)$. For convenience we omit all pre-factors. Equation (B.1) then reads:

$$V_0 = \int_0^\infty \mathrm{d}c\, c^2\, \exp(-c^2)\, \Phi(c) \tag{B.5}$$

$$= \int_0^R \mathrm{d}c\, c^2\, \exp(-c^2)\, \Phi(c) + \int_R^\infty \mathrm{d}c\, c^2\, \exp(-c^2)\, \Phi_c(c) \tag{B.6}$$

$$= \int_0^R \mathrm{d}c\, c^2\, \exp(-c^2)\, \Phi(c) - \frac{\exp(-R^2)}{2}\,. \tag{B.7}$$

For the three different potentials one obtains

$$\begin{aligned} V_{0,c} &= \int_0^R \mathrm{d}c\, c^2\, \exp(-c^2)\, \Phi_c(c) - \frac{\exp(-R^2)}{2} \\ &= -\frac{1}{2} + \frac{\exp(-R^2)}{2} - \frac{\exp(-R^2)}{2} \\ &= -\frac{1}{2} \end{aligned} \tag{B.8}$$

$$\begin{aligned} V_{0,h} &= \int_0^R \mathrm{d}c\, c^2\, \exp(-c^2)\, \Phi_h(c) - \frac{\exp(-R^2)}{2} \\ &= \frac{\exp(-R^2)}{2} - \frac{\sqrt{\pi}}{4R}\mathrm{erf}(R) - \frac{\exp(-R^2)}{2} \\ &= -\frac{\sqrt{\pi}}{4R}\mathrm{erf}(R) \end{aligned} \tag{B.9}$$

$$\begin{aligned} V_{0,s} &= \frac{3}{2}\int_0^R \mathrm{d}c\, c^2\, \exp(-c^2)\, \Phi_h(c) \\ &\quad + \frac{1}{2R^3}\int_0^R \mathrm{d}c\, c^4 \exp(-c^2) - \frac{\exp(-R^2)}{2} \\ &= -\frac{3\sqrt{\pi}}{8R}\mathrm{erf}(R) - \frac{3}{8R^2}\exp(-R^2) - \frac{3\sqrt{\pi}}{16R^2}\mathrm{erf}(R) \end{aligned} \tag{B.10}$$

In the limit $R \to 0$ the function $\mathrm{erf}(R)/R$ converges to $2/\sqrt{\pi}$. Thus, (B.9) converges to $-1/2$ and yields the same value as one gets for Φ_c. For (B.10) both the second and third term diverge but the sum of both terms converges and altogether $V_{0,s}$ also converges to the value of $-1/2$. So everything seems fine.

But now consider the behaviour of $V(c)$ in a small neighbourhood of $c = 0$, i. e. $V_\varepsilon = V(c = \varepsilon)$. For the hollow sphere this changes nothing of course, since the potential is constant within radius R. The potentials Φ_c and Φ_s can be expanded around $\varepsilon = 0$ and yield

$$\Phi_c(c+\varepsilon) = \Phi_c(c) + \varepsilon\,\frac{1}{c^2} + \mathcal{O}(\varepsilon^2) \tag{B.11}$$

$$\Phi_s(c+\varepsilon) = \Phi_s(c) + \varepsilon\,\frac{c}{R^3} + \mathcal{O}(\varepsilon^2)\,. \tag{B.12}$$

This gives the additional contributions

$$V_{\varepsilon,c} = V_{0,c} + \varepsilon \int_0^R \mathrm{d}c\ \exp(-c^2) \tag{B.13}$$

$$= V_{0,c} + \varepsilon\, \frac{\sqrt{\pi}}{2}\, \mathrm{erf}(R) \tag{B.14}$$

$$V_{\varepsilon,s} = V_{0,s} + \frac{\varepsilon}{R^3} \int_0^R \mathrm{d}c\ c^3\ \exp(-c^2) \tag{B.15}$$

$$= V_{0,s} - \varepsilon\, \frac{1+R^2}{2}\, \exp(-R^2) + \frac{\varepsilon}{2R^3} \tag{B.16}$$

to the potentials. For the Coulomb potential everything is fine since $\mathrm{erf}(R) \to 0$ for $R \to 0$. Hence, both the Coulomb and the hollow sphere potential obtain no further contributions at this order and it can be easily checked that this also holds for all higher orders in ε.

For the solid sphere potential, however, things are not fine at all. Not only does the term proportional to $\exp(-R^2)$ in the limit $R \to 0$ yield a contribution $-\varepsilon/2$ which already makes it differ from the Coulomb potential. The last term is even worse because it diverges in this limit. Therefore, we cannot take this model seriously for small radii of the solid sphere and we are better off taking the hollow sphere potential as a toy model for the density of a molecule.

Appendix C. Evolution equations for first and second moments in the narrow wave-function limit

Here we will explicitly derive the self-contained system of evolution equations for the first and second moments given in [23]. It has been noted there that since this system is closed, Gaussian states will remain Gaussian under evolution. We will show that the difference of our equation (52) to equation (53) given in [23] has no influence on this set of equations.

For this we consider the Schrödinger equation

$$\mathrm{i}\dot{\psi} = \frac{p^2}{2M}\psi + H_1\psi\,, \tag{C.1}$$

where

$$H_1 = \frac{k}{2}\mathbf{x^2} - k_{\mathrm{SN}}\mathbf{x}\cdot\langle\mathbf{x}\rangle + \alpha\langle\mathbf{x}\rangle^2 + \beta\langle\mathbf{x}^2\rangle$$
$$p_i = -\mathrm{i}\partial_i$$
$$k = k_{\mathrm{CM}} + k_{\mathrm{SN}} = M\omega_{\mathrm{CM}}^2 + M\omega_{\mathrm{SN}}^2\,.$$

In principle, in the case of equation (52) we have $\alpha = 0$, $\beta = k_{\mathrm{SN}}/2$, while in the case of equation (53) $\alpha = k_{\mathrm{SN}}/2$, $\beta = 0$. But note that

$$\partial_i\langle\mathbf{x}\rangle_j = 0 \tag{C.2a}$$

$$\partial_i\langle\mathbf{x}^2\rangle = 0\,. \tag{C.2b}$$

Therefore, independent of the choice of α and β the derivatives of H_1 are

$$\partial_i H_1 = k x_i - k_{\mathrm{SN}} \langle \mathbf{x} \rangle_i \tag{C.3a}$$
$$\Delta H_1 = 3k\,. \tag{C.3b}$$

We will see that H_1 will enter into the evolution equations for the first and second moments only through these derivatives. Thus, for the different equations (52) and (53) we obtain the same evolution equations for the first and second moments, which are:

$$\partial_t \langle \mathbf{x} \rangle_i = \int \mathrm{d}^3x\, x_i \left(\psi^* \dot{\psi} + \psi \dot{\psi}^* \right) = \frac{\mathrm{i}}{2M} \int \mathrm{d}^3x\, x_i \left(\psi^* \Delta\psi - \psi \Delta\psi^* \right) \tag{C.4a}$$
$$= \frac{\mathrm{i}}{2M} \int \mathrm{d}^3x \left(-(\partial_j \psi) \partial_j (x_i \psi^*) + (\partial_j \psi^*) \partial_j (x_i \psi) \right) \tag{C.4b}$$
$$= \frac{\mathrm{i}}{2M} \int \mathrm{d}^3x \left(-\psi^* \partial_i \psi + \psi \partial_i \psi^* \right) = \frac{1}{M} \int \mathrm{d}^3x\, \psi^* (-\mathrm{i}\partial_i) \psi \tag{C.4c}$$
$$= \frac{\langle \mathbf{p} \rangle_i}{M} \tag{C.4d}$$

$$\partial_t \langle \mathbf{p} \rangle_i = -\mathrm{i} \int \mathrm{d}^3x \left(\dot{\psi}^* \partial_i \psi + \psi^* \partial_i \dot{\psi} \right) \tag{C.5a}$$
$$= \frac{1}{2M} \int \mathrm{d}^3x \left(-(\Delta\psi^*) \partial_i \psi + \psi^* \partial_i \Delta\psi \right) - \langle \partial_i H_1 \rangle \tag{C.5b}$$
$$= \frac{1}{2M} \int \mathrm{d}^3x \left((\partial_j \psi^*) \partial_i \partial_j \psi + \psi^* \partial_i \Delta\psi \right) - \langle \partial_i H_1 \rangle \tag{C.5c}$$
$$= \frac{1}{2M} \int \mathrm{d}^3x \left(-\psi^* \partial_i \Delta\psi + \psi^* \partial_i \Delta\psi \right) - \langle \partial_i H_1 \rangle \tag{C.5d}$$
$$= -k \langle \mathbf{x} \rangle_i + k_{\mathrm{SN}} \langle \mathbf{x} \rangle_i \tag{C.5e}$$
$$= -k_{\mathrm{CM}} \langle \mathbf{x} \rangle_i \tag{C.5f}$$

$$\partial_t \langle \mathbf{x}^2 \rangle = \int \mathrm{d}^3x\, \mathbf{x}^2 \left(\psi^* \dot{\psi} + \psi \dot{\psi}^* \right) = \frac{\mathrm{i}}{2M} \int \mathrm{d}^3x\, \mathbf{x}^2 \left(\psi^* \Delta\psi - \psi \Delta\psi^* \right) \tag{C.6a}$$
$$= \frac{\mathrm{i}}{2M} \int \mathrm{d}^3x \left(-(\partial_j \psi) \partial_j (x_i x_i \psi^*) + (\partial_j \psi^*) \partial_j (x_i x_i \psi) \right) \tag{C.6b}$$
$$= \frac{\mathrm{i}}{M} \int \mathrm{d}^3x \left(-x_i \psi^* \partial_i \psi + x_i \psi \partial_i \psi^* \right) \tag{C.6c}$$
$$= \frac{1}{M} \int \mathrm{d}^3x \left(\psi^* x_i (-\mathrm{i}\partial_i) \psi + \psi^* (-\mathrm{i}\partial_i)(x_i \psi) \right) \tag{C.6d}$$
$$= \frac{1}{M} \left(\langle \mathbf{x} \cdot \mathbf{p} \rangle + \langle \mathbf{p} \cdot \mathbf{x} \rangle \right) \tag{C.6e}$$

$$\partial_t\langle\mathbf{p}^2\rangle = -\int \mathrm{d}^3x \left(\dot{\psi}^*\Delta\psi + \psi^*\Delta\dot{\psi}\right) = \frac{\mathrm{i}}{2M}\int \mathrm{d}^3x\,((\Delta\psi^*)\Delta\psi - \psi^*\Delta\Delta\psi) + 2\mathrm{i}\int \mathrm{d}^3x\,\psi^*(\partial_i H_1)\partial_i\psi + \mathrm{i}\langle\Delta H_1\rangle \tag{C.7a}$$

$$= 2\mathrm{i}\int \mathrm{d}^3x\,\psi^*\left(kx_i - k_{\mathrm{SN}}\langle\mathbf{x}\rangle_i\right)\partial_i\psi + 3\mathrm{i}k \tag{C.7b}$$

$$= -2k\int \mathrm{d}^3x\,\psi^* x_i(-\mathrm{i}\partial_i)\psi + 2k_{\mathrm{SN}}\langle\mathbf{x}\rangle_i\int \mathrm{d}^3x\,\psi^*(-\mathrm{i}\partial_i)\psi + 3\mathrm{i}k \tag{C.7c}$$

$$= -2k\langle\mathbf{x}\cdot\mathbf{p}\rangle + 2k_{\mathrm{SN}}\langle\mathbf{x}\rangle\cdot\langle\mathbf{p}\rangle + k\langle\mathbf{x}\cdot\mathbf{p}\rangle - k\langle\mathbf{p}\cdot\mathbf{x}\rangle \tag{C.7d}$$

$$= -k\left(\langle\mathbf{x}\cdot\mathbf{p}\rangle + \langle\mathbf{p}\cdot\mathbf{x}\rangle\right) + 2k_{\mathrm{SN}}\langle\mathbf{x}\rangle\cdot\langle\mathbf{p}\rangle \tag{C.7e}$$

$$\partial_t\langle\mathbf{x}\cdot\mathbf{p}\rangle = \partial_t\langle\mathbf{p}\cdot\mathbf{x}\rangle = \int \mathrm{d}^3x \left(\dot{\psi}^* x_i(-\mathrm{i}\partial_i)\psi + \psi^* x_i(-\mathrm{i}\partial_i)\dot{\psi}\right) \tag{C.8a}$$

$$= -\frac{1}{2M}\int \mathrm{d}^3x\,x_i\left((\Delta\psi^*)\partial_i\psi - \psi^*\partial_i\Delta\psi\right) - \langle x_i\partial_i H_1\rangle \tag{C.8b}$$

$$= \frac{1}{2M}\int \mathrm{d}^3x\,(\partial_j\psi^*)\partial_j(x_i\partial_i\psi) + \frac{1}{2M}\int \mathrm{d}^3x\,x_i\psi^*\partial_i\Delta\psi - \langle x_i\partial_i H_1\rangle \tag{C.8c}$$

$$= \frac{1}{2M}\int \mathrm{d}^3x\,((\partial_i\psi^*)\partial_i\psi + x_i(\partial_j\psi^*)\partial_i\partial_j\psi + x_i\psi^*\partial_i\Delta\psi) - \langle x_i\partial_i H_1\rangle \tag{C.8d}$$

$$= \frac{1}{2M}\int \mathrm{d}^3x\,(-\psi^*\Delta\psi - \psi^*\partial_j(x_i\partial_i\partial_j\psi) + x_i\psi^*\partial_i\Delta\psi) - \langle x_i\partial_i H_1\rangle \tag{C.8e}$$

$$= -\frac{1}{M}\int \mathrm{d}^3x\,\psi^*\Delta\psi - \langle x_i\partial_i H_1\rangle \tag{C.8f}$$

$$= \frac{\langle\mathbf{p}^2\rangle}{M} - k\langle\mathbf{x}^2\rangle + k_{\mathrm{SN}}\langle\mathbf{x}\rangle^2 \tag{C.8g}$$

The same evolution equations are obtained by operators $\mathbf{x}$ and $\mathbf{p}$ that in the Heisenberg picture fulfil

$$\partial_t\mathbf{x} = \frac{\mathbf{p}}{M} \tag{C.9a}$$

$$\partial_t\mathbf{p} = -k_{\mathrm{CM}}\mathbf{x} - k_{\mathrm{SN}}(\mathbf{x} - \langle\mathbf{x}\rangle)\,. \tag{C.9b}$$

This was used in [23] to describe the effect of the Schrödinger-Newton equation on Gaussian states.

References

[1] Rosenfeld L 1963 *Nuclear Physics* **40** 353–356

[2] Carlip S 2008 *Classical and Quantum Gravity* **25** 154010 (6 pages)

[3] Giulini D and Großardt A 2012 *Classical and Quantum Gravity* **29** 215010 (25 pages)

[4] Wald R M 1994 *Quantum Field Theory in Curved Spacetime and Black Hole Thermodynamics* Chicago Lectures in Physics (Chicago: The University of Chicago Press)

[5] Anastopoulos C and Hu B L 2014 Problems with the Newton-Schrödinger equations arXiv:1403.4921
[6] Anastopoulos C and Hu B L 2014 Newton-Schrödinger equations are not derivable from General Relativity + Quantum Field Theory arXiv:1402.3813
[7] Page D N and Geilker C 1981 *Physical Review Letters* **47** 979–982
[8] Eppely K and Hannah E 1977 *Foundations of Physics* **7** 51–68
[9] Mattingly J 2005 Is quantum gravity necessary? *Einstein Studies Volume 11. The Universe of General Relativity* Einstein Studies ed Kox A J and Eisenstaedt J (Boston: Birkhäuser) chap 17, pp 327–338
[10] Mattingly J 2006 *Physical Review D* **73** 064025 (8 pages)
[11] Albers M, Kiefer C and Reginatto M 2008 *Physical Review D* **78** 064051 (17 pages)
[12] Salzman P J and Carlip S A possible experimental test of quantized gravity arXiv:gr-qc/0606120 based on the Ph.D. thesis of P. Salzman: "Investigation of the Time Dependent Schrödinger-Newton Equation", Univ. of California at Davis, 2005
[13] Giulini D and Großardt A 2011 *Classical and Quantum Gravity* **28** 195026 (17 pages)
[14] Hornberger K, Gerlich S, Haslinger P, Nimmrichter S and Arndt M 2012 *Reviews of Modern Physics* **84** 157–173
[15] Diósi L 1984 *Physics Letters A* **105** 199–202
[16] Iwe H 182 *Zeitschrift für Physik A: Atoms and Nuclei* **304** 347–361
[17] Grawert G 1977 *Quantenmechanik* 3rd ed (Wiesbaden, Germany: Akademische Verlagsgesellschaft)
[18] Heisenberg W 1949 *The Physical Principles of the Quantum Theory* (Mineola, New York: Dover Publications). Lectures delivered 1929 at the Univerity of Chicago
[19] Christian J 1997 *Physical Review D* **56** 4844–4877
[20] Adler S L 2007 *Journal of Physics A: Mathematical and Theoretical* **40** 755–763
[21] Schrödinger E 1927 *Annalen der Physik (Vierte Folge)* **82** 265–272
[22] Giulini D and Großardt A 2013 *Classical and Quantum Gravity* **30** 155018 (9 pages)
[23] Yang H, Miao H, Lee D S, Helou B and Chen Y 2013 *Physical Review Letters* **110** 170401 (5 pages)
[24] Colin S, Durt T and Willox R 2014 Crucial tests of macrorealist and semi-classical gravity models with freely falling mesoscopic nanospheres arXiv:1402.5653 [quant-ph]
[25] Jääskeläinen M 2012 *Physical Review A* **86** 052105 (5 pages)
[26] Müntinga H, Ahlers H, Krutzik M, Wenzlawski A, Arnold S, Becker D, Bongs K, Dittus H, Duncker H, Gaaloul N, Gherasim C, Giese E, Grzeschik C, Hänsch T W, Hellmig O, Herr W, Herrmann S, Kajari E, Kleinert S, Lämmerzahl C, Lewoczko-Adamczyk W, Malcolm J, Meyer N, Nolte R, Peters A, Popp M, Reichel J, Roura A, Rudolph J, Schiemangk M, Schneider M, Seidel S T, Sengstock K, Tamma V, Valenzuela T, Vogel A, Walser R, Wendrich T, Windpassinger P, Zeller W, van Zoest T, Ertmer W, Schleich W P and Rasel E M 2013 *Physical Review Letters* **110** 093602 (5 pages)

Large Quantum Superpositions and Interference of Massive Nanometer-Sized Objects

O. Romero-Isart,[1] A. C. Pflanzer,[1] F. Blaser,[2] R. Kaltenbaek,[2] N. Kiesel,[2] M. Aspelmeyer,[2] and J. I. Cirac[1]

[1]*Max-Planck-Institut für Quantenoptik, Hans-Kopfermann-Strasse 1, D-85748, Garching, Germany*

[2]*Vienna Center for Quantum Science and Technology, Faculty of Physics, University of Vienna, Boltzmanngasse 5, A-1090 Vienna, Austria*

(Received 21 March 2011; published 7 July 2011)

We propose a method to prepare and verify spatial quantum superpositions of a nanometer-sized object separated by distances of the order of its size. This method provides unprecedented bounds for objective collapse models of the wave function by merging techniques and insights from cavity quantum optomechanics and matter-wave interferometry. An analysis and simulation of the experiment is performed taking into account standard sources of decoherence. We provide an operational parameter regime using present-day and planned technology.

DOI: 10.1103/PhysRevLett.107.020405 PACS numbers: 03.65.Ta, 03.75.−b, 42.50.Pq

Quantum superpositions of a massive object at two spatial locations are allowed by quantum mechanics. This puzzling prediction has been observed in seminal matter-wave interferometry experiments with electrons, neutrons, atoms and dimers, van der Waals clusters, and even complex molecules (e.g., C_{70}, $C_{60}F_{48}$) [1]. Preparing quantum superpositions of even larger objects is considered to be extremely challenging due to the decoherence caused by interaction with the environment [2]. However, succeeding in this task would allow completely new tests of quantum mechanics: this includes experiments in a hitherto unachieved parameter regime where collapse theories predict quantum mechanics to fail [3,4], or even more general tests of quantum theory against full classes of macrorealistic theories [5]. Moreover, these states would be so fragile to environmental interactions that one could exploit this ultrahigh sensitivity to design a new generation of sensors. Pushing large objects to the quantum regime is also the aim of cavity quantum optomechanics [6]. Similarly to laser cooling of atoms, the radiation pressure of light is exploited to cool and coherently manipulate the mechanical motion of some degree of freedom (e.g., the center of mass) of a massive object and even to create quantum superpositions of harmonic vibrational states [7,8].

In this Letter, we present a method to prepare spatial quantum superpositions of massive objects (with masses of $\sim 10^7$ amu) based on cavity quantum optomechanics and show how it can be used to test wave function collapse models. This builds upon the recent proposal of using an optically levitating nanodielectric as a cavity quantum optomechanical system [8–11]. The main idea is to trap a dielectric sphere in the standing wave field of an optical cavity. The mechanical motion of the sphere's center of mass along the cavity axis is predicted to be a high-quality mechanical oscillator due to the absence of clamping losses. This facilitates laser cooling to its motional ground state (see also experiments on feedback cooling of an optically levitated microsphere [12]). In addition, a cooled levitating object offers the possibility to be released by switching off the trap [10], creating in this way a scenario similar to matter-wave interferometry experiments. Here, we will use precisely this feature both to coherently expand the wave function over a large spatial region and to enhance the nonlinear coupling that is required to prepare large quantum superpositions.

More specifically, the linear and quadratic coupling in cavity optomechanics after displacing the cavity field (see, e.g., Sec. V.A.1 and Appendix B.2 in [10]) is given by

$$\hat{H}_{\mathrm{OM}} = -\hbar g(\hat{a} + \hat{a}^\dagger)\tilde{x} + \hbar g_q(\hat{a} + \hat{a}^\dagger)\tilde{x}^2, \qquad (1)$$

where $\hat{a}(\hat{a}^\dagger)$ is the annihilation (creation) operator of a cavity photon, $\tilde{x} = \hat{x}/x_0$ is the dimensionless position operator of the mechanical resonator, with $x_0 = [\hbar/(2m\omega_t)]^{1/2}$ its zero point motion, m the mass, and ω_t the mechanical frequency. The photon-enhanced linear optomechanical coupling is given by g and the typical quadratic coupling by $g_q = k_c x_0 g$, where $k_c = 2\pi/\lambda_c$ is the wave number of the cavity mode. When the equilibrium position is at the node (antinode) of the standing wave, $g \neq 0$ and $g_q = 0$ ($g = 0$ and $g_q \neq 0$). A fundamental figure of merit of the cavity-mechanical system is the cooperativity parameter defined as $\mathcal{C}_l = g^2/(\kappa\Gamma)$ for the linear coupling, and $\mathcal{C}_q = g_q^2/(\kappa\Gamma) = \mathcal{C}_l(k_c x_0)^2$ for the quadratic one. Here, κ is the decay rate of the cavity field and Γ the decoherence rate of the mechanical motion. Ground-state cooling requires $\mathcal{C}_l \gtrsim 1$, whereas nonlinear effects, such as energy quantization detection [13] or preparation of non-Gaussian states without using hybrid systems or single photon resources, require $\mathcal{C}_q \gtrsim 1$. The latter is a very demanding condition due to the strong reduction given by $(k_c x_0)^2 \ll 1$. In this Letter we propose to achieve this challenging regime by expanding the wave function to a given size $\langle \hat{x}^2 \rangle \sim \sigma^2 \gg x_0$, such that

$$\bar{\mathcal{C}}_q = \frac{\bar{g}_q^2}{\kappa\bar{\Gamma}} = \mathcal{C}_l(k_c\sigma)^2, \qquad (2)$$

where $\bar{g}_q$ and $\bar{\Gamma}$ are defined below. Thus, for sufficiently

large σ and $\mathcal{C}_l$, the nonlinear regime $\bar{\mathcal{C}}_q \gtrsim 1$ can be attained. This technique is also applicable to other setups where the mechanical frequency can be varied and hence the wave function of the mechanical oscillator expanded [14,15].

We discuss now the different stages of the protocol using levitated nanospheres [8–11] trapped within an optical cavity [Fig. 1(a)]. The optomechanical coupling is given by $g = x_0\sqrt{n_{\rm ph}}\epsilon_c k_c^2 cV/(4V_c)$, where $\epsilon_c \equiv 3\,{\rm Re}[(\epsilon_r - 1)/(\epsilon_r + 2)]$ depends on the relative dielectric constant ϵ_r, c is the vacuum speed of light, V the volume for a sphere of radius R and mass m, V_c the cavity volume, and $n_{\rm ph}$ the cavity photon number in the steady state. The decoherence rate of the center of mass motion is dominated by light scattering and is given by $\Gamma = \Lambda_{\rm sc} x_0^2$, with a localization rate $\Lambda_{\rm sc} = \epsilon_c^2 n_{\rm ph} c V^2 k_c^6/(6\pi V_c)$ [9,10]. The decay rate of the cavity also has a contribution due to light scattering given by $\kappa_{\rm sc} = \epsilon_c^2 V^2 k_c^4 c/(16\pi V_c)$. Sideband cooling of the center of mass motion allows the preparation of thermal states to a final number occupation given by $\bar{n} \approx [\kappa/(4\omega_t)]^2 + \mathcal{C}_l^{-1}$ [16], where backaction heating contributes with $\mathcal{C}_l \sim c/(k_c^2 V_c \kappa)$ for a levitated object at very low pressures. Moderate cooling along the other directions is applied to keep the trap stable at low pressures and reduce the position fluctuations during the time of flight. After cooling, the harmonic trap is switched off, the object falls [see Fig. 1(b)], and the state evolves freely according to

$$\dot{\hat{\rho}} = \frac{i}{2m\hbar}[\hat{p}, \hat{p}^2] - \Lambda[\hat{x}, [\hat{x}, \hat{\rho}]]. \tag{3}$$

The position-localization dissipation part of this master equation describes standard decoherence processes such as scattering of air molecules and emission, absorption, and scattering of black body radiation [2] with the total localization rate $\Lambda_{\rm sd}$ given below. Decoherence due to light scattering is absent during the time of flight since the lasers are switched off. Since both the initial state and the master equation Eq. (3) are Gaussian, the evolved density matrix can be fully determined by computing the moments $\langle \hat{x}^2(t)\rangle$, $\langle \hat{p}^2(t)\rangle$, and $\langle \hat{x}(t)\hat{p}(t)\rangle$, where $\langle \hat{x}^2(0)\rangle = (2\bar{n}+1)x_0^2$, and $\langle \hat{p}^2(0)\rangle = (2\bar{n}+1)\hbar^2/(4x_0^2)$. The spatial coherence length ξ_l, obtained by noticing that $\langle -x/2|\hat{\rho}|x/2\rangle \propto \exp[-x^2/\xi_l^2]$, is given by $\xi_l^2 = 8\langle \hat{x}^2\rangle\langle \mathcal{P}\rangle^2$, where $\langle \mathcal{P}\rangle$ is the mean value of the parity operator.

After an expansion of duration t_1, a second cavity is used to implement an optomechanical double slit [Fig. 1(c)]. To this end, the setup is aligned such that the object passes through a small high-finesse optical cavity at an antinode of the cavity mode. Simultaneously, a pulse of length $\tau \approx 2\pi/\kappa$ is fed into the cavity such that a short interaction is triggered. Note that during this interaction, standard decoherence and, in particular, light scattering decohere the state of the system with a rate given by $\bar{\Gamma} = \Lambda_{\rm sc}\langle \hat{x}^2(t_1)\rangle$. This can be taken into account by adding the corresponding contribution of time τ to the moments of the Gaussian state before the measurement.

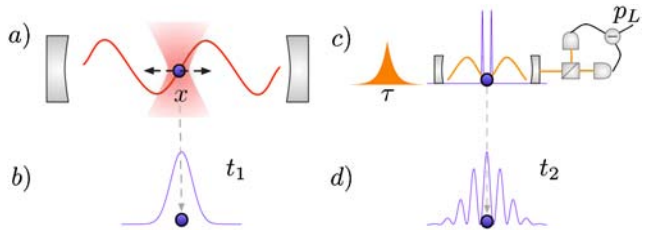

FIG. 1 (color online). Schematic representation of the proposal. (a) The optically trapped object is laser cooled using a high-finesse optical cavity. (b) The trap is switched off and the wave function expands during some time t_1. (c) The object enters into a second small cavity where a pulsed (of time τ) interaction is performed using the quadratic optomechanical coupling. The homodyne measurement of the output phase measures $\hat{x}^2$ and prepares a quantum superposition state conditional of the outcome result p_L. (d) The particle falls during a time t_2 until its center of mass position is measured, which after repetition unveils an interference pattern for each p_L.

Linear pulsed optomechanics has been discussed recently for tomography and cooling applications [17]. Here, we extend these results to the case of the quadratic coupling (see also [18]). The interaction Hamiltonian, in the displaced frame and in the rotating frame with the resonant laser frequency, is given by $\hat{H} = \hat{p}^2/(2m) + \hbar\bar{g}_q\sqrt{n_{\rm ph}}\tilde{x}^2 + \hbar\bar{g}_q(\hat{a}^\dagger + \hat{a})\tilde{x}^2$. A key remark is that, at this stage, the dimensionless position operator is defined as $\tilde{x} = \hat{x}/\sigma(t_1)$ [hereafter we define $\sigma^2 \equiv \sigma^2(t_1) = x_0^2 + \hbar^2 t_1^2/(4x_0^2 m^2)$]. Then $\bar{g}_q \equiv g_q(\sigma/x_0)^2$ is the quadratic optomechanical coupling enhanced by the enlarged wave function. Note that, as mentioned above, the kinetic term can be neglected since $\tau\langle \hat{p}^2\rangle/(2m\hbar) \approx \omega_t\tau/4 \ll 1$ for short cavities where $\kappa \gg \omega_t$. The squared position measurement is performed by measuring the integrated output quadrature of the light field $\hat{p}_L \equiv \int_0^\tau dt[\hat{a}_{\rm out}^\dagger(t) + \hat{a}_{\rm out}(t)]/\sqrt{\tau}$. Using the input-output formalism, $\hat{a}_{\rm out}(t) + \hat{a}_{\rm in}(t) = \sqrt{2\kappa}(\hat{a} + \sqrt{n_{\rm ph}})$, one obtains that $\langle \hat{p}_L\rangle = \chi\langle \tilde{x}^2\rangle$ and $\langle \hat{p}_L^2 - \langle \hat{p}_L\rangle^2\rangle = 1/2 + \chi^2\langle \tilde{x}^4 - \langle \tilde{x}^2\rangle^2\rangle$ (we assume a coherent drive such that the optical input phase noise is $1/2$). Therefore, the measurement strength of the squared position measurement is defined as $\chi = 2\sqrt{\bar{\mathcal{C}}_q}$ (the physical parameters are chosen such that $\tau \approx 1/\bar{\Gamma} \approx 2\pi/\kappa$, see below). Note that the measurement strength is intimately related to the enhanced nonlinear cooperativity [see Eq. (2)]. The generalized measurement operator for the measurement outcome p_L of the integrated optical phase $\hat{p}_L$ is given by

$$\hat{\mathcal{M}} = \exp[-i\phi\tilde{x}^2 - (p_L - \chi\tilde{x}^2)^2], \tag{4}$$

where $\phi = \bar{g}_q\sqrt{n_{\rm ph}}\tau$ is the phase accumulated during the interaction with the classical field. The density matrix after the measurement is described by $\hat{\rho}(t_2 + \tau) = \hat{\mathcal{M}}\,\hat{\rho}\,\hat{\mathcal{M}}^\dagger/{\rm tr}[\hat{\mathcal{M}}\,\hat{\rho}\,\hat{\mathcal{M}}^\dagger]$. The action of the measurement operator, Eq. (4), is to prepare a superposition of two wave

packets separated by a distance $d = 2\sigma\sqrt{p_L/\chi}$, and a width given by approximately $\sigma_2 \sim \sigma/(4\sqrt{p_L\chi}) = \sigma^2/(2d\chi)$. This can be intuitively understood as a consequence of the projective nature of the pulsed measurement [17]: for the ideal case, this measurement prepares the system in an eigenstate of the $\hat{x}^2$ operator, which for a pure initial state with even parity is of the type $|x\rangle + |-x\rangle$, i.e., a coherent spatial superposition. The separation of the wave packets, d, determined by the outcome of the measurement, represents the effective slit separation. In order to prepare (with high probability) and resolve the peaks of the superposition state, one requires $\sigma > d > 2\sigma_2$. This sets up an upper bound $d^{\mathrm{a}}_{\mathrm{max}} \equiv \sigma$ and a lower bound $d_{\mathrm{min}} \equiv \sigma\sqrt{2/\chi}$ for d. A second upper bound is provided by the decoherence during the expansion of the wave function; we demand $d < d^{b}_{\mathrm{max}} \equiv \xi_l$. Finally, the total number of photons n_{ph} used in the pulse and the time of flight t_1 is fixed by enforcing that ϕ compensates the complex phase accumulated during the time of flight, which is given by $\sim\langle\hat{x}(t_1)\hat{p}(t_1) + \hat{p}(t_1)\hat{x}(t_1)\rangle/(4\hbar)$, as well as by fulfilling the condition $\tau \approx 1/\bar{\Gamma} \approx 2\pi/\kappa$. This corresponds to choosing $n_{\mathrm{ph}} \approx (2\bar{n}+1)/[32\pi\mathcal{C}_l(k_c x_0)^2]$ and $t_1^2 \approx 16\kappa\mathcal{C}_l k_c^2/[\omega^2(2\bar{n}+1)^2\Lambda_{\mathrm{sc}}/n_{\mathrm{ph}}]$.

After the preparation of the superposition state by the pulsed interaction, the particle falls freely during another time of flight of duration t_2. An interference pattern in the mean value of the position is formed with fringes separated by a distance $x_f = 2\pi\hbar t_2/(md)$. The final step of the protocol is thus to perform a position measurement of the center of mass [Fig. 2(d)]. This requires a resolution $\delta x < x_f$, providing a third upper bound for d, $d^{c}_{\mathrm{max}} \equiv 2\pi\hbar t_2/(m\delta x)$. Note that sufficiently long time $t_2 \sim m\sigma^2/(\hbar\chi)$ is needed to guarantee the overlap of the two wave packets. The effect of standard decoherence on the visibility of the interference pattern can be obtained by solving the evolution of the position distribution for a non-Gaussian state under the evolution of Eq. (3). This is given by the closed expression [19]

$$\langle x|\hat{\rho}(t)|x\rangle = \int_{-\infty}^{\infty} dy \frac{e^{-y^2/\sigma_b^2(t)}}{\sigma_b(t)\sqrt{\pi}} \langle x+y|\hat{\rho}_{\Lambda=0}(t)|x+y\rangle, \quad (5)$$

where $\hat{\rho}_{\Lambda=0}(t)$ is the state obtained with the evolution due to the Schrödinger equation only, that is, with $\Lambda = 0$. As observed in (5), the effect of decoherence is to blur the position distribution with a blurring coefficient given by $\sigma_b(t) = 2\hbar m^{-1}\sqrt{t_2^3\Lambda/3}$. Therefore, the fringes separated by a distance x_f will be visible provided $x_f > \sigma_b(t_2)/2$, which provides the fourth upper bound $d^{d}_{\mathrm{max}} \equiv \pi\sqrt{3/(t_2\Lambda_{\mathrm{sd}})}/2$. Putting everything together, the operational regime for the experiment modeled here is given by $d_{\mathrm{min}} < d < \min\{d^{a}_{\mathrm{max}}, d^{b}_{\mathrm{max}}, d^{c}_{\mathrm{max}}, d^{d}_{\mathrm{max}}\}$.

We now address the experimental conditions required for this experiment. The localization rate for black body radiation Λ_{bb} has contributions due to scattering $\Lambda_{\mathrm{bb,sc}} \propto R^6 T_e^9\,\mathrm{Re}[(\epsilon_{\mathrm{bb}}-1)/(\epsilon_{\mathrm{bb}}+2)]^2$, and emission (absorption) of blackbody radiation $\Lambda_{\mathrm{bb},e(a)} \propto R^3 T_{i(e)}^6\,\mathrm{Im}[(\epsilon_{\mathrm{bb}}-1)/(\epsilon_{\mathrm{bb}}+2)]$ (see [2,9] for the exact expressions). ϵ_{bb} is the average relative permittivity, which is assumed to be constant across the relevant blackbody spectrum, and $T_{i(e)}$ is the internal (environmental) temperature. T_i at very low pressure can be computed using the balance between the emitted blackbody power and the light absorption during the optical cooling and trapping [9]. Second, decoherence due to air molecules is described by the master equation Eq. (3) [20], with the parameter given by [2] $\Lambda_{\mathrm{air}} = 8\sqrt{2\pi}m_a\bar{v}PR^2/(3\sqrt{3}\hbar^2)$, where P is the air pressure, m_a is the mass of the air molecules, and $\bar{v}$ their thermal velocity. The total standard decoherence rate is thus given by $\Lambda_{\mathrm{sd}} = \Lambda_{\mathrm{bb}} + \Lambda_{\mathrm{air}}$. The overall performance of this challenging experiment is mainly limited by the quality of the cavity used in the measurement and the vacuum and temperature conditions required for the environment. In particular, very good vacuum conditions are needed to keep the coherence of these fragile states. Note however that pressures down to 10^{-17} Torr at cryogenic temperatures of $T = 4.5$ K were reported in [22]. Extremely good

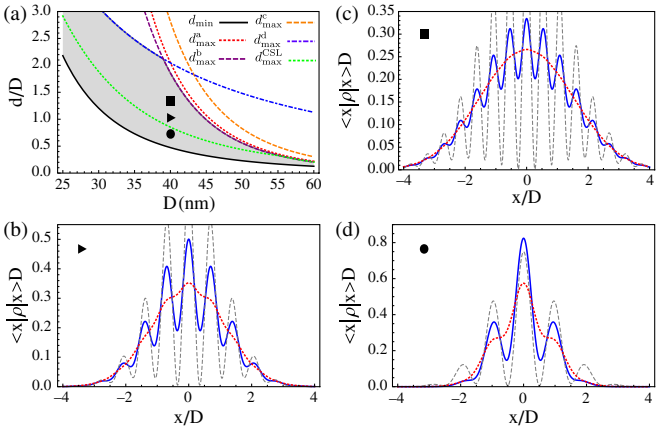

FIG. 2 (color online). (a) The operational parameter regime for the optomechanical double slit distance d and the diameter of the sphere D is plotted (see legend for the lower and upper bounds). The simulation of the interference pattern is computed for a sphere of 40 nm and (b) $d = D$ (triangle), (c) $d = 1.3D$ (square), and (d) $d = 0.7D$ (circle) in units of D. The solid blue (dashed grey) line is the simulated interference pattern with (without) standard decoherence. The dotted red line is the interference pattern in the presence of the CSL model with $\lambda = 10^4\lambda_0$ s^{-1} (the upper bound $d^{\mathrm{CSL}}_{\mathrm{max}}$ in the operational parameter plot provided by the CSL model is also shown—see legend). Experimental parameters for the environmental conditions are $P = 10^{-16}$ Torr, $T_e = 4.5$ K, $\mathrm{Im}[(\epsilon_{\mathrm{bb}}-1)(\epsilon_{\mathrm{bb}}+2)] = 0.1$, $\mathrm{Re}[\epsilon_{\mathrm{bb}}] = 2.3$, $\bar{n} = 0.1$; for the cavity, they are $\mathcal{F} = 1.3\times10^5$, length 2 μm, waist $= 1.5$ μm, $\lambda_c = 1064$ nm; and for a silica sphere, $\epsilon_r = 2.1 + i2.5\times10^{-10}$, density $= 2201$ kg/m^3, $\omega_t/2\pi = 135$ kHz, and $\delta x = 10$ nm. Using this, for a sphere of 40 nm and $d = D$, one obtains $\kappa/2\pi = \tau^{-1} = 2.8\times10^8$ Hz, $\mathcal{C}_l = 1500$, $n_{\mathrm{ph}} = 272$, $T_i = 206$ K, $t_1 = 3.3$ ms, $t_2 = 125$ ms, and $\sigma/x_0 = 2928$.

cavities are needed in order to obtain a large cooperativity $\mathcal{C}_i$; for instance, consider fiber-based Fabry-Perot cavities of length of 2 μm and finesse $\mathcal{F} \approx 1.3 \times 10^5$ as discussed in [23]. In Fig. 2 the operational parameter regime is shown for different sphere sizes and superposition distances with the particular set of experimental parameters given in the caption. The interference pattern simulated by solving the master equation numerically, which describes the evolution of the state during the experiment, is also plotted. Spheres of $\sim$40 nm with a mass of $\sim 10^7$ amu can be prepared in a superposition of locations separated by a distance equal to their diameter. In principle, the scheme can be applied to even larger objects albeit with further constraints on the experimental parameters.

To conclude, we shall discuss the application of using this experiment to test theories beyond quantum mechanics that provide an objective collapse of the wave function for sufficiently large objects. In particular, we focus on the paradigmatic model associated to Ghirardi-Rimini-Weber-Pearle (see [4] and references therein) denoted as the continuous spontaneous localization model (CSL). This theory is derived by adding a nonlinear stochastic term to the Schrödinger equation. The model recovers all the phenomenology of quantum mechanics for elementary particles but predicts a fast localization (collapse) of the wave function for larger objects. This comes at the price of introducing two phenomenological constants given by $\alpha^{-1/2} \approx 10^{-7}$ m (related to the localization extension) and $\lambda_0 \approx 2.2 \times 10^{-17}$ s^{-1} (related to the intensity of the localization). For a spherical body [24], the CSL model can be cast into a master equation of the form of Eq. (3) with $\Lambda_{\mathrm{CSL}} = m^2 \lambda_0 \alpha f(\sqrt{\alpha} R)/(2m_0^2)$, where m_0 is the mass of a nucleon, and the function $f(x)$ defined in [24] has the following limits: $f(1) \approx 0.62$, $f(x \ll 1) = 1$, and $f(x \gg 1) \approx 6x^{-4}$. Recently, Adler [25] reexamined the CSL theory and, by considering the collapse of the wave function at the latent image formation level, predicted a significantly larger value for λ_0, namely, $\lambda_A = 2 \times 10^{9\pm2} \lambda_0$. This prediction cannot be tested by current experiments [3]. In Fig. 2 we show however that a possible CSL process would have a strong impact on our experiment already for $\lambda = 10^4 \lambda_0$ (see the upper bound $d_{\mathrm{max}}^{\mathrm{CSL}}$ provided by the blurring of the interference pattern). The effect is also clearly visible in the simulation of the interference pattern. Thus, the experiment proposed here puts unprecedented bounds for one of the most studied collapse models and even challenges the recent theoretical prediction given by Adler (see also [26]). Finally we note that our scheme allows us to prepare superpositions of macroscopically distinct spatial states of a massive object. In combination with the specific time-of-flight evolution this may provide a rigorous experimental test of some of the crucial assumptions of macrorealism [5].

We are grateful to M. D. Lukin, E. M. Kessler, and F. Pastawski for stimulating discussions. We acknowledge the support of Alexander von Humboldt Stiftung, ENB (Project QCCC), Caixa Manresa, EU (AQUTE, MINOS, Q-ESSENCE, Marie Curie), FWF (START, FOQUS), ÖAW (APART), ERC (StG QOM), and FQXi .

[1] C. Davisson and L. H. Germer, Nature (London) **119**, 558 (1927); H. v. J. Halban and P. Halban, C.R. Hebd. Seances Acad. Sci. **203**, 73 (1936); I. Estermann and O. Stern, Z. Phys. **61**, 95 (1930); W. Schöllkopf and J. P. Toennies, Science **266**, 1345 (1994); M. Arndt *et al.*, Nature (London) **401**, 680 (1999); B. Brezger *et al.*, Phys. Rev. Lett. **88**, 100404 (2002); L. Hackermüller *et al.*, *ibid.* **91**, 090408 (2003).

[2] E. Joos *et al.*, *Decoherence and the Appearance of a Classical World in Quantum Theory* (Springer, New York, 2003); M. A. Schlosshauer, *Decoherence and the Quantum-to-Classical Transition* (Springer, New York, 2007).

[3] S. L. Adler and A. Bassi, Science **325**, 275 (2009).

[4] A. Bassi and G. C. Ghirardi, Phys. Rep. **379**, 257 (2003).

[5] A. J. Leggett and A. Garg, Phys. Rev. Lett. **54**, 857 (1985).

[6] T. Kippenberg and K. Vahala, Science **321**, 1172 (2008); F. Marquardt and S. M. Girvin, Physics **2**, 40 (2009); M. Aspelmeyer *et al.*, J. Opt. Soc. Am. B **27**, A189 (2010).

[7] W. Marshall *et al.*, Phys. Rev. Lett. **91**, 130401 (2003).

[8] O. Romero-Isart *et al.*, New J. Phys. **12**, 033 015 (2010).

[9] D. E. Chang *et al.*, Proc. Natl. Acad. Sci. U.S.A. **107**, 1005 (2010).

[10] O. Romero-Isart *et al.*, Phys. Rev. A **83**, 013803 (2011).

[11] P. F. Barker and M. N. Shneider, Phys. Rev. A **81**, 023826 (2010).

[12] A. Ashkin and J. M. Dziedzic, Appl. Phys. Lett. **30**, 202 (1977); T. Li, S. Kheifets, and M. G. Raizen, arXiv:1101.1283.

[13] J. D. Thompson *et al.*, Nature (London) **452**, 72 (2008); J. C. Sankey *et al.*, Nature Phys. **6**, 707 (2010).

[14] D. E. Chang *et al.*, arXiv:1101.0146.

[15] S. Singh *et al.*, Phys. Rev. Lett. **105**, 213602 (2010).

[16] I. Wilson-Rae *et al.*, Phys. Rev. Lett. **99**, 093901 (2007); F. Marquardt *et al.*, *ibid.* **99**, 093902 (2007); C. Genes *et al.*, Phys. Rev. A **77**, 033804 (2008).

[17] M. R. Vanner *et al.*, arXiv:1011.0879.

[18] K. Jacobs, L. Tian, and J. Finn, Phys. Rev. Lett. **102**, 057208 (2009).

[19] G. C. Ghirardi, A. Rimini, and T. Weber, Phys. Rev. D **34**, 470 (1986).

[20] This is valid for separations smaller than the de Broglie wavelength of the air molecules. For larger separations this master equation is a good approximation; see [21] and the infinite frequency limit of [19].

[21] M. R. Gallis and G. N. Fleming, Phys. Rev. A **42**, 38 (1990).

[22] G. Gabrielse *et al.*, Phys. Rev. Lett. **65**, 1317 (1990).

[23] D. Hunger *et al.*, New J. Phys. **12**, 065 038 (2010).

[24] B. Collett and P. Pearle, Found. Phys. **33**, 1495 (2003).

[25] S. L. Adler, J. Phys. A **40**, 2935 (2007).

[26] S. Nimmrichter *et al.*, Phys. Rev. A **83**, 043621 (2011).

nature COMMUNICATIONS

OPEN

ARTICLE

Received 13 Jun 2011 | Accepted 5 Sep 2011 | Published 18 Oct 2011

DOI: 10.1038/ncomms1498

Quantum interferometric visibility as a witness of general relativistic proper time

Magdalena Zych[1], Fabio Costa[1], Igor Pikovski[1] & Časlav Brukner[1,2]

Current attempts to probe general relativistic effects in quantum mechanics focus on precision measurements of phase shifts in matter–wave interferometry. Yet, phase shifts can always be explained as arising because of an Aharonov–Bohm effect, where a particle in a flat space–time is subject to an effective potential. Here we propose a quantum effect that cannot be explained without the general relativistic notion of proper time. We consider interference of a 'clock'—a particle with evolving internal degrees of freedom—that will not only display a phase shift, but also reduce the visibility of the interference pattern. According to general relativity, proper time flows at different rates in different regions of space–time. Therefore, because of quantum complementarity, the visibility will drop to the extent to which the path information becomes available from reading out the proper time from the 'clock'. Such a gravitationally induced decoherence would provide the first test of the genuine general relativistic notion of proper time in quantum mechanics.

[1] Faculty of Physics, University of Vienna, Boltzmanngasse 5, 1090 Vienna, Austria. [2] Institute for Quantum Optics and Quantum Information, Austrian Academy of Sciences, Boltzmanngasse 3, 1090 Vienna, Austria. Correspondence and requests for materials should be addressed to M.Z. (email: magdalena.zych@univie.ac.at).

In the theory of general relativity, time is not a global background parameter but flows at different rates depending on the space–time geometry. Although verified to high precision in various experiments[1], this prediction (as well as any other general relativistic effect) has never been tested in the regime where quantum effects become relevant. There is, in general, a fundamental interest in probing the interplay between gravity and quantum mechanics[2]. The reason is that the two theories are grounded on seemingly different premises and, although consistent predictions can be extrapolated for a large range of phenomena, a unified framework is still missing and fundamentally new physics is expected to appear at some scale.

One of the promising experimental directions is to reveal, through interferometric measurements, the phase acquired by a particle moving in a gravitational potential[3,4]. Typically considered is a Mach–Zehnder type interferometer (Fig. 1), placed in the Earth's gravitational field, where a particle travels in a coherent superposition along the two interferometric paths γ_1, γ_2 that have different proper lengths. The two amplitudes in the superposition acquire different, trajectory-dependent phases Φ_i, $i=1,2$. In addition, the particle acquires a controllable relative phase shift φ. Taking into account the action of the first beam splitter and denoting by $|r_i\rangle$ the mode associated with the respective path γ_i, the state inside the Mach–Zehnder setup $|\Psi_{MZ}\rangle$, just before it is recombined, can be written as

$$|\Psi_{MZ}\rangle = \frac{1}{\sqrt{2}}\left(ie^{-i\Phi_1}|r_1\rangle + e^{-i\Phi_2+i\varphi}|r_2\rangle\right). \qquad (1)$$

Finally, the particle can be registered by one of the two detectors $D_\pm$ with corresponding probabilities $P_\pm$:

$$P_\pm = \frac{1}{2} \pm \frac{1}{2}\cos(\Delta\Phi + \varphi), \qquad (2)$$

where $\Delta\Phi := \Phi_1 - \Phi_2$. The phase Φ_i is proportional to the action along the corresponding (semiclassical) trajectory γ_i on which the particle moves. For a free particle on an arbitrary space–time background, the action can be written in terms of the proper time τ that elapsed during the travel, $S_i = -mc^2\int_{\gamma_i} \mathrm{d}\tau$. This might suggest that the measurement of $\Delta\Phi$ is an experimental demonstration of the general relativistic time dilation.

There is, however, a conceptual issue in interpreting experiments measuring a gravitationally induced phase shift as tests of the relativistic time dilation. The action S_i above can be written in terms of an effective gravitational potential on a flat space–time. Thus, all the effects resulting from such an action are fully described by the Schödinger equation with the corresponding gravitational potential and where the time evolution is given with respect to the global time. Note that a particle in a field of arbitrary nature is subject to a Hamiltonian where the potential energy is proportional to the field's charge and a position-dependent potential. Therefore, even in a homogeneous field, the particle acquires a trajectory-dependent phase although the force acting on it is the same at any point—the phase arises only because of the potential. For a homogeneous electric field, this relative phase is known as the electric Aharonov–Bohm effect[5]. The case of Newtonian gravity is directly analogous—the role of the particle's electric charge and of the Coulomb potential are taken by the particle's mass and the Newtonian gravitational potential, respectively[6]. All quantum interferometric experiments performed to date (see for example, refs 7–9) are fully explainable by this gravitational analogue of the electric Aharonov–Bohm effect. Moreover, even if one includes non-Newtonian terms in the Hamiltonian, this dichotomy of interpretations is still present. Again, one can interpret the phase shift $\Delta\Phi$ as a type of an Aharanov–Bohm phase, which a particle moving in a flat space–time acquires because of an effective, non-Newtonian, gravitational potential (at least for an effective gravitational potential arising from the typically considered Kerr or Schwarzschild space–times).

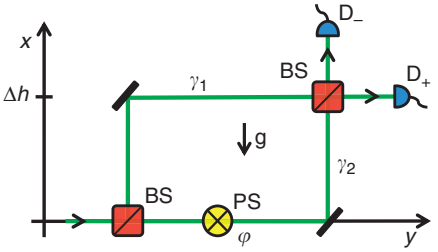

Figure 1 | Mach–Zehnder interferometer in the gravitational field. The setup considered in this work consists of two beam splitters (BS), a phase shifter (PS) and two detectors $D_\pm$. The PS gives a controllable phase difference φ between the two trajectories γ_1 and γ_2, which both lie in the $x-y$ plane. A homogeneous gravitational field (g) is oriented antiparallel to the x direction. The separation between the paths in the direction of the field is Δh. General relativity predicts that the amount of the elapsed proper time is different along the two paths. In our approach, we will consider interference of a particle (which is not in free fall) that has an evolving internal degree of freedom that acts as a 'clock'. Such an interference experiment will therefore not only display a phase shift, but also reduce the visibility of the interference pattern to the extent to which the path information becomes available from reading out the proper time of the 'clock'.

Here we predict a quantum effect that cannot be explained without the general relativistic notion of proper time and thus show how it is possible to unambiguously distinguish between the two interpretations discussed above. We consider a Mach–Zehnder interferometer placed in the gravitational potential and with a 'clock' used as an interfering particle. By 'clock' we mean some evolving internal degree of freedom of the particle. If there is a difference in proper time elapsed along the two trajectories, the 'clock' will evolve into different quantum states for the two paths of the interferometer. Because of quantum complementarity between interference and which-path information the interferometric visibility will decrease by an amount given by the which-way information accessible from the final state of the clock[10–12]. Such a reduction in the visibility is a direct consequence of the general relativistic time dilation, which follows from the Einstein equivalence principle. Seeing the Einstein equivalence principle as a corner stone of general relativity, observation of the predicted loss of the interference contrast would be the first confirmation of a genuine general relativistic effect in quantum mechanics.

One might sustain the view that the interference observed with particles without evolving degrees of freedom is a manifestation of some intrinsic oscillations associated with the particle and that such oscillations can still be seen as the ticking of a clock that keeps track of the particle's time. If any operational meaning was to be attributed to this clock, it would imply that which-way information is, in principle, accessible. One should then either assume that proper time is a quantum degree of freedom, in which case, there should be a drop in the interferometric visibility, or that the quantum complementarity relation (between which-path information and interferometric visibility) would be violated when general relativistic effects become relevant. Our proposed experiment allows to test these possibilities. The hypothesis that proper time is a degree of freedom has indeed been considered in various works[13–15].

The above considerations are also relevant in the context of the debate over ref. 16 (determination of the gravitational redshift by reinterpreting interferometric experiment[9] that measured the acceleration of free fall). It was pointed out in refs 17–20 that only states non-trivially evolving in time can be referred to as 'clocks'. In ref. 18, the interference in such a case was discussed, however, the role of the interferometric visibility as a witness of proper time in quantum mechanics and as a tool to test new hypotheses has not been previously considered.

In the present paper, we discuss an interferometric experiment in the gravitational field where the interfering particle can be operationally treated as a 'clock'. We predict that as a result of the quantum complementarity between interference and which-path information the general relativistic time dilation will cause the decrease in the interferometric visibility. The observation of such a reduction in the visibility would be the first confirmation of a genuinely general relativistic effect in quantum mechanics, in particular, it would unambiguously probe proper time as predicted by general relativity. The proposed experiment can also lead to a conclusive test of theories in which proper time is treated as a quantum degree of freedom.

Results

Which-way information from proper time. Consider an interferometric experiment with the setup as in Fig. 1, but in a situation where the particle in superposition has some internal degree of freedom that can evolve in time. In such a case, state (1) is no longer the full description of the system. Moreover, if this degree of freedom can be considered as a 'clock', according to the general relativistic notion of proper time it should evolve differently along the two arms of the interferometer in the presence of gravity. For a trajectory γ_i, let us call $|\tau_i\rangle$ the corresponding state of the 'clock'. The superposition (1) inside the interferometer now reads

$$|\Psi_{MZ}\rangle = \frac{1}{\sqrt{2}}\left(ie^{-i\Phi_1}|r_1\rangle|\tau_1\rangle + e^{-i\Phi_2+i\varphi}|r_2\rangle|\tau_2\rangle\right). \qquad (3)$$

In general, the state (3) is entangled and according to quantum mechanics interference in the path degrees of freedom should correspondingly be washed away. The reason is that one could measure the 'clock' degrees of freedom and in that way read out the accessible which-path information. Tracing out the 'clock' states in equation (3) gives the detection probabilities

$$P_{\pm} = \frac{1}{2} \pm \frac{1}{2}|\langle\tau_1|\tau_2\rangle|\cos(\Delta\Phi + \alpha + \varphi), \qquad (4)$$

where $\langle\tau_1|\tau_2\rangle = |\langle\tau_1|\tau_2\rangle|e^{i\alpha}$. When the ancillary phase shift φ is varied, the probabilities $P_{\pm}$ oscillate with the amplitude $\mathcal{V}$, called the visibility (contrast) of the interference pattern. Formally

$$\mathcal{V} := \frac{Max_{\varphi}P_{\pm} - Min_{\varphi}P_{\pm}}{Max_{\varphi}P_{\pm} + Min_{\varphi}P_{\pm}}.$$

Whereas without the 'clock' the expected contrast is always maximal (equation (2) yields $\mathcal{V}=1$), in the case of equation (4) it reads

$$\mathcal{V} = |\langle\tau_1|\tau_2\rangle|. \qquad (5)$$

The distinguishability $\mathcal{D}$ of the trajectories is the probability to correctly guess which path was taken in the two-way interferometer by measuring the degrees of freedom that serve as a which-way detector[12] (in mathematical terms it is the trace norm distance between the final states of the detectors associated with different paths). In our case, these are the 'clock' degrees of freedom and we obtain $\mathcal{D} = \sqrt{1-|\langle\tau_1|\tau_2\rangle|^2}$. The amount of the which-way information that is potentially available sets an absolute upper bound on the fringe visibility and we recover the well-known duality relation[10–12] in the form $\mathcal{V}^2 + \mathcal{D}^2 = 1$, as expected for pure states.

The above result demonstrates that general relativistic effects in quantum interferometric experiments can go beyond previously predicted corrections to the non-relativistic phase shift. When proper time is treated operationally we anticipate the gravitational time dilation to result in the reduction of the fringe contrast. This drop in the visibility is expected independently of how the proper time is measured and which system and interaction are used for the 'clock'. Moreover, when the information about the time elapsed is not physically accessible, the drop in the visibility will not occur. This indicates that the effect unambiguously arises because of the proper time as predicted by general relativity, in contrast to measurements of the phase shift alone. The gravitational phase shift occurs independently of whether the system can or cannot be operationally treated as a 'clock', just as the phase shift acquired by a system in the electromagnetic potential. Therefore, the notion of proper time is not probed in such experiments.

Massive quantum 'clock' in an external gravitational field. In the next paragraphs, we present how the above idea can be realized when the 'clock' degrees of freedom are implemented in internal states of a massive particle (neglecting the finite-size effects). Let $H_{\circlearrowright}$ be the Hamiltonian that describes the internal evolution. In the rest reference frame, the time coordinate corresponds to the proper time τ, and the evolution of the internal states is given by $i\hbar(\partial/\partial\tau) = H_{\circlearrowright}$. Changing coordinates to the laboratory frame, the evolution is given by $i\hbar(\partial/\partial t) = \dot{\tau}H_{\circlearrowright}$, where $\dot{\tau} = \mathrm{d}\tau/\mathrm{d}t$ describes how fast the proper time flows with respect to the coordinate time. For a general metric $g_{\mu\nu}$, it is given by $\dot{\tau} = \sqrt{-g_{\mu\nu}\dot{x}^{\mu}\dot{x}^{\nu}}$, where we use the signature $(-+++)$ and summation over repeated indices is understood. The energy–momentum tensor of a massive particle described by the action S can be defined as the functional derivative of S with respect to the metric, that is, $T^{\mu\nu} := \delta S/\delta g_{\mu\nu}$ (see, for example, ref. 21). Since the particle's energy E is defined as the T_{00} component, it reads $E = g_{0\mu}g_{0\nu}T^{\mu\nu}$. In the case of a free evolution in a space–time with a stationary metric (in coordinates such that $g_{0j}=0$ for $j=1,2,3$), we have

$$E = mc^2\frac{-g_{00}}{\sqrt{-g_{\mu\nu}\dot{x}^{\mu}\dot{x}^{\nu}}}, \qquad (6)$$

where m is the mass of the particle. Space–time geometry in the vicinity of Earth can be described by the Schwarzschild metric. In isotropic coordinates (x,θ,ϑ) and with $\mathrm{d}\Omega^2 \equiv \mathrm{d}\theta^2 + \sin^2\theta\,\mathrm{d}\vartheta^2$ it takes the form[21]

$$c^2\mathrm{d}\tau^2 = \frac{(1+\frac{\phi(x)}{2c^2})^2}{(1-\frac{\phi(x)}{2c^2})^2}c^2\mathrm{d}t^2 - \left(1-\frac{\phi(x)}{2c^2}\right)^4\left(\mathrm{d}x^2 + x^2\mathrm{d}\Omega^2\right),$$

where $\phi(x) = -GM/x$ is the Earth's gravitational potential (G denotes the gravitational constant and M is the mass of Earth). We consider the limit of a weak field and of slowly moving particles. In the final result, we therefore keep up to quadratic terms in the kinetic and potential energy. In this approximation, the metric components read[21]

$$g_{00} \simeq -\left(1+2\frac{\phi(x)}{c^2}+2\frac{\phi(x)^2}{c^4}\right),\ g_{ij} \simeq \frac{1}{c^2}\delta_{ij}\left(1-2\frac{\phi(x)}{c^2}\right),$$

so that

$$\dot{\tau} \simeq \sqrt{1+2\frac{\phi(x)}{c^2}+2\frac{\phi(x)^2}{c^4}-\left(\frac{\dot{x}}{c}\right)^2\left(1-2\frac{\phi(x)}{c^2}\right)}.$$

The total Hamiltonian in the laboratory frame is given by $H_{\mathrm{Lab}} = H_0 + \dot{\tau}H_{\circlearrowright}$, where the operator H_0 describes the dynamics of the external degrees of freedom of the particle and is obtained by canonically quantizing the energy (6), that is, the particle's coordinate x and kinematic momentum $p = m\dot{x}$ become operators satisfying the canonical commutation relation $([x,p] = i\hbar)$. Thus, approximating up to the second order also in the internal energy,

$H_{\rm Lab}$ reads

$$H_{\rm Lab} \simeq mc^2 + H_{\circlearrowright} + E_k^{GR} + \frac{\phi(x)}{c^2}\left(mc^2 + H_{\circlearrowright} + E_{\rm corr}^{GR}\right), \qquad (7)$$

where

$$E_k^{GR} = \frac{p^2}{2m}\left(1 + 3\left(\frac{p}{2mc}\right)^2 - \frac{1}{mc^2}H_{\circlearrowright}\right)$$

and

$$E_{\rm corr}^{GR} = \frac{1}{2}m\phi(x) - 3\frac{p^2}{2m}\ .$$

We consider a semiclassical approximation of the particle's motion in the interferometer. Therefore, all terms in $H_{\rm Lab}$, apart from the internal Hamiltonian $H_{\circlearrowright}$, appear as purely numerical functions defined along the fixed trajectories.

In a setup as in Figure 1, the particle follows in superposition two fixed non-geodesic paths γ_1, γ_2 in the homogeneous gravitational field. The acceleration and deceleration, which the particle undergoes in the x direction, is assumed to be the same for both trajectories, as well as the constant velocity along the y axis. This assures that the trajectories have different proper length, but there will be no time dilation between the paths stemming from special relativistic effects. The particle inside the interferometer will thus be described by the superposition $|\Psi_{MZ}\rangle = \frac{1}{\sqrt{2}}\left(i|\Psi_1\rangle + e^{i\varphi}|\Psi_2\rangle\right)$, where the states $|\Psi_i\rangle$ associated with the two paths γ_i are given by applying the Hamiltonian (7) to the initial state, which we denote by $|x^{\rm in}\rangle|\tau^{\rm in}\rangle$. Up to an overall phase, these states read

$$|\Psi_i\rangle = e^{-\frac{i}{\hbar}\int_{\gamma_i} {\rm d}t \frac{\phi(x)}{c^2}\left(mc^2 + H_{\circlearrowright} + E_{\rm corr}^{GR}\right)}|x^{\rm in}\rangle|\tau^{\rm in}\rangle. \qquad (8)$$

For a small size of the interferometer, the central gravitational potential $\phi(x)$ can be approximated to linear terms in the distance Δh between the paths:

$$\phi(R + \Delta h) = \phi(R) + g\Delta h + \mathcal{O}(\Delta h^2), \qquad (9)$$

where $g = GM/R^2$ denotes the value of the Earth's gravitational acceleration in the origin of the laboratory frame, which is at distance R from the centre of Earth.

For a particle having two internal states $|0\rangle$, $|1\rangle$ with corresponding energies E_0, E_1, the rest frame Hamiltonian of the internal degrees of freedom can be written as

$$H_{\circlearrowright} = E_0|0\rangle\langle 0| + E_1|1\rangle\langle 1| \qquad (10)$$

and if we choose the initial state of this internal degrees to be

$$|\tau^{\rm in}\rangle = \frac{1}{\sqrt{2}}(|0\rangle + |1\rangle) \qquad (11)$$

the detection probabilities read

$$P_{\pm}(\varphi, m, \Delta E, \Delta V, \Delta T) = \frac{1}{2} \pm \frac{1}{2}\cos\left(\frac{\Delta E \Delta V \Delta T}{2\hbar c^2}\right)\cos\left(\left(mc^2 + \langle H_{\circlearrowright}\rangle + \bar{E}_{\rm corr}^{GR}\right) + \frac{\Delta V \Delta T}{\hbar c^2} + \varphi\right), \qquad (12)$$

where ΔT is the time (as measured in the laboratory frame) for which the particle travels in the interferometer in a superposition of two trajectories at constant heights, $\Delta V := g\Delta h$ is the difference in the gravitational potential between the paths, $\bar{E}_{\rm corr}^{GR}$ represents the corrections $E_{\rm corr}^{GR}$ from equation (7) averaged over the two trajectories and $\Delta E := E_1 - E_0$. The expectation value $\langle H_{\circlearrowright}\rangle$ is taken with respect to the state (11). The corresponding visibility (5) is

$$\mathcal{V} = \left|\cos\left(\frac{\Delta E \Delta V \Delta T}{2\hbar c^2}\right)\right|. \qquad (13)$$

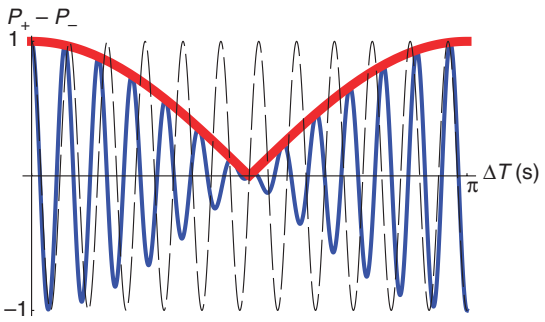

Figure 2 | Visibility of the interference pattern and the phase shift in the cases with and without the 'clock.' The plot of the difference between the probabilities $P_{\pm}(\varphi, m, \Delta E, \Delta V, \Delta T)$, equation (12), to find the particle in the output path of the Mach–Zehnder interferometer as a function of the time ΔT for which the particle travels in a superposition of two trajectories at constant heights (this corresponds to changing the length of the interferometric arms). The term proportional to the particle's mass is the phase originating from the Newtonian potential energy $m\Delta V$. General relativistic corrections stemming from external degrees of freedom are given by $\bar{E}_{\rm corr}^{GR}$, see for example, ref. 3. Without the 'clock' degrees of freedom, only these terms are present in the result (dashed, black line in the plot). In the situation with the 'clock' (blue line), we expect two new effects: the change of the interferometric visibility given by the absolute value of the first cosine (thick red line) and an extra phase shift proportional to the average internal energy of the 'clock'. The values for the energy gap ΔE and the gravitational potential difference ΔV between the interferometric paths are chosen such that $\Delta E \Delta V / 2\hbar c^2 = 1{\rm Hz}$. Whereas the phase shift alone can always be understood as an Aharonov–Bohm phase of an effective potential, the notion of general relativistic proper time is necessary to explain the decrease of the visibility.

The introduction of the 'clock' degrees of freedom results in two new quantum effects that cannot be explained without including general relativity: the change of the interferometric visibility and the extra phase shift proportional to the average internal energy (Fig. 2; equation (12)). The drop in the visibility is a consequence of a direct coupling of the particle's internal degrees of freedom to the potential in the effective Hamiltonian (7). Such a coupling is never found in Newtonian gravity, and it is the mathematical expression of the prediction that the 'clock' ticks at different rates when placed in different gravitational potentials. This coupling can directly be obtained from the Einstein equivalence principle. Recall that the latter postulates that accelerated reference frames are physically equivalent to those in the gravitational field of massive objects. When applied within special relativity, this exactly results in the prediction that initially synchronized clocks subject to different gravitational potentials will show different times when brought together. The proposed experiment probes the presence of such a gravitational time dilation effect for a quantum system—it directly shows whether the 'clock' would tick at different rates when taken along the two possible trajectories in the interferometer. On the other hand, to obtain the correct phase shift, it is sufficient to consider a semiclassical coupling of the average total energy of the system to the gravitational potential. With such a coupling, the time displayed by the 'clock' used in

the experiment will not depend on the path taken. This means that a gravitationally induced phase shift can probe general relativistic corrections to the Newtonian gravitational potential but is always consistent with having an operationally well-defined notion of global time, that is, with a flat space–time.

The effect described in our work follows directly from the Einstein equivalence principle, which is itself crucial for the formulation of general relativity as a metric theory[22]. Thus, the drop in the fringe contrast is not only genuinely quantum mechanical but also a genuine general relativistic effect that in particular unambiguously probes the general relativistic notion of proper time.

General 'clocks' and gravitational fields. Let us call $t_\perp$ the orthogonalization time of a quantum system, that is, the minimal time needed for a quantum state to evolve under a given Hamiltonian into an orthogonal one[23,24]. For the initial state (11) subject to the rest frame Hamiltonian $H_{\circlearrowleft}$ given by equation (10) we obtain

$$t_\perp = \frac{\pi\hbar}{\Delta E}. \tag{14}$$

A system with finite $t_\perp$ can be seen as a clock that ticks at a rate proportional to $t_\perp^{-1}$. Thus, the orthogonalization time gives also the precision of a considered 'clock'. From the expression for $\dot{\tau}$ in the approximation (9), it follows that the total time dilation $\Delta\tau$ between the trajectories is

$$\Delta\tau = \frac{\Delta V \Delta T}{c^2}. \tag{15}$$

We can, therefore, phrase the interferometric visibility $\mathcal{V}$ solely in terms of $t_\perp$ and $\Delta\tau$:

$$\mathcal{V} = \left|\cos\left(\frac{\Delta\tau}{t_\perp}\frac{\pi}{2}\right)\right|. \tag{16}$$

The total time dilation $\Delta\tau$ is a parameter capturing the relevant information about the paths, and $t_\perp$ grasps pertinent features of the 'clock'. It is only their ratio that matters for the fringe visibility. Equation (16) is a generalization of the result (13) to the case of an arbitrary initial state, 'clock' Hamiltonian and a non-homogeneous gravitational field: whenever the time dilation $\Delta\tau$ between the two trajectories through the Mach–Zehnder interferometer is equal to the orthogonalization time $t_\perp$ of the quantum mechanical system that is sent through the setup, the physically accessible proper time difference will result in the full loss of fringe contrast. There are several bounds on the orthogonalization time based on energy distribution moments[23,25,26]. Such bounds can through equation (16) give some estimates on the gravity-induced decoherence rates in more general situations. As an example, for mixed states one generally has[26]:

$$\frac{1}{t_\perp} \le \frac{2^{\frac{1}{\alpha}}}{\pi\hbar}\langle (H-E_{gr})^\alpha\rangle^{\frac{1}{\alpha}},$$

$\alpha > 0$ (provided the initial state is in the domain of $(H-E_{gr})^\alpha$) where H denotes the internal Hamiltonian and E_{gr} the energy of its ground state.

Discussion

Current approaches to test general relativistic effects in quantum mechanics mainly focus on high precision measurements of the phase induced by the gravitational potential. Although such experiments would probe the potential and thus could verify non-Newtonian corrections in the Hamiltonian, they would not constitute an unambiguous proof of the gravitational time dilation, because they are also explainable without this concept by the Aharonov–Bohm effect: a trajectory-dependent phase acquired by a particle moving in a flat space–time in the presence of a position-dependent potential.

In our proposed experiment, the effects arising from general relativistic proper time can be separated and probed independently from the Aharonov–Bohm type of effects. Unlike the phase shift, which occurs independently of whether the interfering particle can be treated as a 'clock', the change of the interferometric visibility (equation (13)) is a quantum effect that arises if and only if general relativistic proper time has a well defined operational meaning. Indeed, if one prepares the initial state $|\tau^{in}\rangle$ as an eigenstate of the internal energy Hamiltonian $H_{\circlearrowleft}$, only the phase of such a state would change during the time evolution and, according to equation (16), interferometric visibility would be maximal. This 'clock' would not 'tick' (it has orthogonalization time $t_\perp = \infty$) so the concept of proper time would have no operational meaning in this case. Moreover, reasoning that any (even just an abstract) frequency which can be ascribed to the particle allows considering proper time as a physical quantity would imply that interference should always be lost, as the which-path information is stored 'somewhere'. This once again shows that, in quantum mechanics, it makes no sense to speak about quantities without specifying how they are measured.

The interferometric experiment proposed in this work can also be used to test whether proper time is a new quantum degree of freedom. This idea was discussed in the context of, for example, the equivalence principle in refs 13,14 and a mass–proper time uncertainty relation[15]. The equations of motion for proper time treated dynamically, as put forward in refs 13–15, are in agreement with general relativity. Therefore, the predictions of equation (5) would also be valid, if the states $|\tau_i\rangle$, introduced in equation (3), stand for this new degree of freedom. Already performed experiments, like

Table 1 | Discussion of possible outcomes of the proposed interferometric experiment.

Experimental visibility	Possible explanation	Current experimental status
$\mathcal{V}_m = 0$	Proper time: quantum d.o.f., sharply defined	Disproved in, for example, refs 7,9
$0 < \mathcal{V}_m < \mathcal{V}_{QM}$	Proper time: quantum d.o.f. with uncertainty σ_τ	Consistent with current data for $\sigma_\tau > \lvert\Delta\tau\rvert/\sqrt{-8\ln(1-\Delta\mathcal{V})}$
$\mathcal{V}_m = \mathcal{V}_{QM}$	Proper time: not a quantum d.o.f. or has a very broad uncertainty	Consistent with current data
$\mathcal{V}_m > \mathcal{V}_{QM}$	Quantum interferometric complementarity does not hold when general relativistic effects become relevant	Not tested

The measured visibility $\mathcal{V}_m$ is compared with the quantum mechanical prediction $\mathcal{V}_{QM}$ given by equation (13). Depending on their relation, different conclusions can be drawn regarding the possibility that proper time is a quantum degree of freedom (d.o.f.). Assuming that the distribution of the proper time d.o.f. is a Gaussian of the width σ_τ, current interferometric experiments give bounds on possible σ_τ in terms of the proper time difference $\Delta\tau$ between the paths and the experimental error $\Delta\mathcal{V}$ of the visibility measurement.

Table 2 | Comparison of different systems for the experimental observation of the reduced interferometric visibility.

System	'Clock'	ω (Hz)	ΔhΔT (ms) achieved	ΔhΔT (ms) required
Atoms	Hyperfine states	10^{15}	10^{-5}	10
Electrons	Spin precession	10^{13}	10^{-6}	10^{3}
Molecules	Vibrational modes	10^{12}	10^{-8}	10^{4}
Neutrons	Spin precession	10^{10}	10^{-6}	10^{6}

Several possible systems are compared on the basis of theoretically required and already experimentally achieved parameters, which are relevant for our proposed experiment. For a 'clock' with a frequency $\omega = \Delta E/\hbar$, the required value of the parameter $\Delta h \Delta T$ (Δh being the separation between the interferometers arms and ΔT the time for which the particle travels in superposition at constant heights) for the full loss of the fringe visibility (see equation (13)), is given in the rightmost column. In our estimations, we assumed a constant gravitational acceleration $g = 10(m/s^2)$. See section Methods for further discussion on possible experimental implementations.

in refs 7,16, which measured a gravitational phase shift, immediately rule out the possibility that the state of proper time was sharply defined in those tests, in the sense of $\langle\tau_1|\tau_2\rangle = \delta(\tau_1 - \tau_2)$. However, such experiments can put a finite bound on the possible uncertainty in the state of proper time. The phase shift measured in those experiments can be phrased in terms of the difference in the proper time $\Delta\tau$ between the paths. Denote by $\Delta\mathcal{V}$ the experimental error with which the visibility of the interference pattern was measured in those tests. As a result, a Gaussian state of the proper time degree of freedom of width σ_τ such that $\sigma_\tau > |\Delta\tau|/\sqrt{-8\ln(1-\Delta\mathcal{V})}$, is consistent with the experimental data. An estimate of the proper time uncertainty can be based on the Heisenberg uncertainty principle for canonical variables and the equation of motion for the proper time. In such an analysis, the rest mass m can be considered as a canonically conjugated momentum to the proper time variable τ, that is, one assumes $[\tau, mc^2] = i\hbar$ [13–15]. In Table 1, we discuss what can be inferred about proper time as a quantum degree of freedom from an experiment in which the measured visibility would be $\mathcal{V}_m$ and where $\mathcal{V}_{QM}$ is the visibility predicted by quantum mechanics, as given by equation (13).

In conclusion, we predicted a quantum effect in interferometric experiments that, for the first time, allows probing general relativistic proper time in an unambiguous way. In the presence of a gravitational potential, we showed that a loss in the interferometric visibility occurs, if the time dilation is physically accessible from the state of the interfered particle. This requires that the particle is a 'clock' measuring proper time along the trajectories, therefore revealing the which-way information. Our predictions can be experimentally verified by implementing the 'clock' in some internal degrees of freedom of the particle (see Methods). The proposed experiment can also lead to a conclusive test of theories in which proper time is treated as a quantum degree of freedom. As a final remark, we note that decoherence due to the gravitational time dilation may have further importance in considering the quantum to classical transition and in attempts to observe collective quantum phenomena in extended, complex quantum systems because the orthogonalization time may become small enough in such situations to make the predicted decoherence effect prominent.

Methods

Systems for the implementation of the interferometric setup. Here we briefly discuss various systems for the possible implementation of the interferometric setup. Interferometry with many different massive quantum systems has been achieved, for example, with neutrons[7,8], atoms[16,27], electrons[28,29] and molecules[30,31]. In our framework, further access to an internal degree of freedom is paramount, as to initialize the 'clock' which measures the proper time along the interferometric path. Therefore, the experimental requirements are more challenging. To observe full loss of the interferometric visibility, the proper time difference in the two interferometric arms needs to be $\Delta\tau = t_\perp$. For a two level system, the revival of the visibility due to the indistinguishability of the proper time in the two arms occurs when $\Delta\tau = 2t_\perp$.

The best current atomic clocks operate at optical frequencies ω around 10^{15} Hz. For such systems, we have $t_\perp = \pi/\omega$, and one would therefore require an atomic superposition with $\Delta h \Delta T \sim 10$ ms to see full disappearance of the interferometric visibility. For example, the spatial separation would need to be of the order of 1 m, maintained for about 10 s. Achieving and maintaining such large superpositions of atoms still remains a challenge, but recent rapid experimental progress indicates that this interferometric setup could be conceivable in the near future. For neutrons, a separation of $\Delta h \sim 10^{-2}$ m with a coherence time of $t \sim 10^{-4}$ s has been achieved[8]. To implement our 'clock' in neutron interferometry, one can use spin precession in a strong, homogeneous magnetic field. However, such a 'clock' could reach frequencies up to $\omega \sim 10^9$ Hz (for a magnetic field strength of order of $10T$ (ref. 32)), which is still a few orders of magnitude lower than necessary for the observation of full decoherence owing to a proper time difference. Improvements in the coherence time and the size of the interferometer would still be necessary. Other systems, such as molecules, could be used as well and Table 2 summarizes the requirements for various setups (note again that the particles are assumed to travel at fixed height during the time ΔT).

The effect we predict can be measured even without achieving full orthogonalization of the 'clocks'. Note that even for $\Delta\tau \ll t_\perp$ the small reduction of visibility can already be sufficient to prove the accessibility of which-path information due to the proper time difference. With current parameters in atom interferometry, an accuracy of the measurement of the visibility of $\Delta\mathcal{V} = 10^{-6}$ would have to be achieved for the experimental confirmation of our predictions. A very good precision measurement of the interferometric visibility and a precise knowledge about other decoherence effects would therefore make the requirements for the other parameters less stringent.

References

1. Hafele, J. C. & Keating, R. E. Around-the-world atomic clocks: predicted relativistic time gains. *Science* **177,** 166–168 (1972).
2. Chiao, R. Y., Minter, S. J., Wegter-McNelly, K. & Martinez, L. A. Quantum incompressibility of a falling Rydberg atom, and a gravitationally-induced charge separation effect in superconducting systems. *Found. Phys.*1–19, DOI: 10.1007/s10701-010-9531-2 (2011).
3. Wajima, S., Kasai, M. & Futamase, T. Post-Newtonian effects of gravity on quantum interferometry. *Phys. Rev. D* **55,** 1964–1970 (1997).
4. Dimopoulos, S., Graham, P. W., Hogan, J. M. & Kasevich, M. A. General relativistic effects in atom interferometry. *Phys. Rev. D* **78,** 042003 (2008).
5. Aharonov, Y. & Bohm, D. Significance of electromagnetic potentials in the quantum theory. *Phys. Rev.* **115,** 485–491 (1959).
6. Ho, V. B. & Morgan, M. J. An experiment to test the gravitational Aharonov-Bohm effect. *Aust. J. Phys.* **47,** 245–253 (1994).
7. Colella, R., Overhauser, A. W. & Werner, S. A. Observation of gravitationally induced quantum interference. *Phys. Rev. Lett.* **34,** 1472–1474 (1975).
8. Zawisky, M., Baron, M., Loidl, R. & Rauch, H. Testing the world's largest monolithic perfect crystal neutron interferometer. *Nucl. Instrum. Methods Phys. Res. A* **481,** 406–413 (2002).
9. Peters, A., Chung, K. Y. & Chu, S. Measurement of gravitational acceleration by dropping atoms. *Nature* **400,** 849–852 (1999).
10. Wootters, W. K. & Zurek, W. H. Complementarity in the double-slit experiment: Quantum nonseparability and a quantitative statement of Bohr's principle. *Phys. Rev. D* **19,** 473–484 (1979).
11. Greenberger, D. M. & Yasin, A. Simultaneous wave and particle knowledge in a neutron interferometer. *Phys. Lett. A* **128,** 391–394 (1988).
12. Englert, B. G. Fringe visibility and which-way information: An inequality. *Phys. Rev. Lett.* **77,** 2154–2157 (1996).
13. Greenberger, D. M. Theory of particles with variable mass. I. Formalism. *J. Math. Phys.* **11,** 2329 (1970).
14. Greenberger, D. M. Theory of particles with variable mass. II. Some physical consequences. *J. Math. Phys.* **11,** 2341 (1970).
15. Kudaka, S. & Matsumoto, S. Uncertainty principle for proper time and mass. *J. Math. Phys.* **40,** 1237 (1999).
16. Müller, H., Peters, A. & Chu, S. A precision measurement of the gravitational redshift by the interference of matter waves. *Nature* **463,** 926–929 (2010).
17. Wolf, P. *et al.* Atom gravimeters and gravitational redshift. *Nature* **467,** E1 (2010).
18. Sinha, S. & Samuel, J. Atom interferometers and the gravitational redshift. *Class. Quantum Grav.* **28,** 145018 (2011).

19. Giulini, D. Equivalence principle, quantum mechanics, and atom-interferometric tests. arXiv:1105.0749v1 (2011).
20. Wolf, P. *et al.* Does an atom interferometer test the gravitational redshift at the Compton frequency? *Class. Quantum Grav.* **28**, 145017 (2011).
21. Weinberg, S. *Gravitation and Cosmology*, (John Wiley & Sons, 1972).
22. Will, C. M. *Theory and Experiment in Gravitational Physics*, (Cambridge University Press, 1993).
23. Mandelstam, L. & Tamm, I. The uncertainty relation between energy and time in non-relativistic quantum mechanics. *Journ. Phys. (USSR)* **9,** 249 (1945).
24. Fleming, G. N. A unitarity bound on the evolution of nonstationary states. *Nuovo Cim. A* **16,** 232–240 (1973).
25. Margolus, N. & Levitin, L. B. The maximum speed of dynamical evolution. *Physica D* **120,** 188–195 (1998).
26. Zielinski, B. & Zych, M. Generalization of the Margolus-Levitin bound. *Phys. Rev. A* **74,** 034301 (2006).
27. Müller, H., Chiow, S., Herrmann, S. & Chu, S. Atom interferometers with scalable enclosed area. *Phys. Rev. Lett.* **102,** 240403 (2009).
28. Neder, I., Heiblum, M., Mahalu, D. & Umansky, V. Entanglement, dephasing, and phase recovery via cross-correlation measurements of electrons. *Phys. Rev. Lett.* **98,** 036803 (2007).
29. Ji, Y. *et al.* An electronic Mach-Zehnder interferometer. *Nature* **422,** 415–418 (2003).
30. Arndt, M. *et al.* Wave-particle duality of C 60 molecules. *Nature* **401,** 680–682 (1999).
31. Gerlich, S. *et al.* Quantum interference of large organic molecules. *Nat. Commun.* 2:263 doi: 10.1038/ncomms1263 (2011).
32. Miller, J. R. The NHMFL 45-T hybrid magnet system: past, present, and future. *IEEE Trans. Appl. Supercond.* **13,** 1385–1390 (2003).

Acknowledgements

We thank M. Arndt, B. Dakic, S. Gerlich, D. M. Greenberger, H. Müller, S. Nimmrichter, A. Peters, and P. Wolf for insightful discussions. The research was funded by the Austrian Science Fund (FWF) projects: W1210, P19570-N16 and SFB-FOQUS, the Foundational Questions Institute (FQXi) and the European Commission Project Q-ESSENCE (No. 248095). F.C., I.P. and M.Z. are members of the FWF Doctoral Program CoQuS.

Author contributions

M.Z., F.C., I.P. and Č.B. contributed to all aspects of the research with the leading input from M.Z.

Additional information

Competing financial interests: The authors declare no competing financial interests.

How to cite this article: Zych, M. *et al.* Quantum interferometric visibility as a witness of general relativistic proper time. *Nat. Commun.* 2:505 doi: 10.1038/ncomms1498 (2011).